

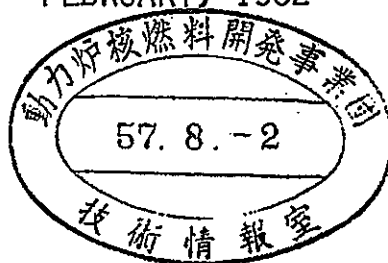
T  
SJ 201 82 - 03

NOT FOR PUBLICATION

本資料は2001年7月31日付けで  
登録区分変更する。 [技術展開部技術協力課]

SUPPLEMENT TO  
RADIATION SHIELDING ANALYSES OF JOYO-(A)

FEBRUARY, 1982



POWER REACTOR AND NUCLEAR FUEL DEVELOPMENT CORPORATION  
TOSHIBA CORPORATION

本資料は、核燃料サイクル開発機構の開発業務を進めるために作成されたものです。したがって、その利用は限られた範囲としており、その取扱には十分な注意を払ってください。この資料の全部または一部を複写・複製・転載あるいは引用する場合、特別の許可を必要としますので、下記にお問い合わせください。

〒319-1184 茨城県那珂郡東海村大字村松4番地49  
核燃料サイクル開発機構  
技術展開部 技術協力課

Inquiries about copyright and reproduction should be addressed to:  
Technical Cooperation Section,  
Technology Management Division,  
Japan Nuclear Cycle Development Institute  
4-49 Muramatsu, Tokai-mura, Naka-gun, Ibaraki, 319-1184  
Japan

© 核燃料サイクル開発機構 (Japan Nuclear Cycle Development Institute)



NOT FOR PUBLICATION  
TSJ 201 82-03  
FEBRUARY 1982

Supplement to Radiation Shielding Analyses of JOYO - (A)\*

Masayoshi KAWAI\*\*  
Yoshihisa HAYASHIDA\*\*  
Michinori YAMAUCHI\*\*  
Mikio UEMATSU\*\*  
Yoshiaki SATOH\*\*\*  
Jiro NIIDOME\*\*\*  
Masaru NAKAI\*\*

Abstract

Analyses of JOYO shielding experimental data have been performed for the purpose of studying the shielding design technique of fast breeder reactor, confirming the shielding calculation procedure of proto-type fast breeder reactor MONJU, and acquiring the data for the evaluation of the uncertainty shielding design.

This paper describes the analyses for the effect of neutron streaming through the detector guide tube in the pedestal heavy concrete upon the experimental data, for the neutron streaming through the primary coolant and the argon cover gas pipe penetrations in the biological shield concrete and for the neutron

---

\*) Works performed under the contract between Power Reactor and Nuclear Fuel Development Corporation and Toshiba Corporation.

\*\*) NAIG Nuclear Research Laboratory, Nippon Atomic Industry Group Co., Ltd.

\*\*\*) Advanced Reactor Engineering Department, Nuclear Energy Group, Toshiba Corporation.

behaviour in the primary pump room and in the intermediate heat exchanger room. The calculation was carried out by using the albedo Monte Carlo code MORSE-ALB with 21 neutron groups and  $P_5$  anisotropic scattering cross section. The calculated results were compared with the shielding performance test data of JOYO.

It was found that the present albedo Monte Carlo method predicted the thermal and intermediate-energy neutron streaming within a factor of 2, taking off the source intensity uncertainty which leads to the underestimation of absolute reaction rates by an order of magnitude at maximum. As for fast neutron reaction rates which were likely influenced by uncertainties of the calculational model and the neutron source distributions, the calculated results agreed within a factor of 6 with the experimental ones. The authors also discuss the source of the discrepancy between the calculated value and the experimental data.

CONTENTS

		PAGE
1.	INTRODUCTION.....	1-1
2.	OUTLINE OF STREAMING EXPERIMENT OF JOYO.....	2-1
	2.1 DETECTOR CHANNEL A .....	2-1
	2.2 PRIMARY COOLANT OUTLET PIPE PENETRATION.....	2-2
	2.3 PRIMARY PUMP ROOM .....	2-3
	2.4 IHX ROOM .....	2-4
3.	STREAMING ANALYSES BY ALBEDO MONTE CARLO METHOD .....	3-1
	3.1 PREPARATION OF GROUP CONSTANTS AND ALBEDO DATA.....	3-3
	3.2 ANALYSIS OF THE NEUTRON STREAMING IN THE CHANNEL A .....	3-14
	3.3 NEUTRON STREAMING ANALYSIS FOR THE PRIMARY COOLANT OUTLET PIPE PENETRATION.....	3-26
	3.4 ANALYSIS OF NEUTRON BEHAVIOUR IN THE PRIMARY PUMP ROOM.....	3-59
	3.5 NEUTRON STREAMING ANALYSIS FOR THE IHX ROOM .....	3-90
	3.6 DISCUSSION.....	3-117
	3.7 SUMMARY OF STREAMING ANALYSES BY ALBEDO MONTE CARLO METHOD.....	3-120
4.	CONCLUSION .....	4-1
	ACKNOWLEDGEMENT.....	4-5
	REFERENCE.....	4-6

## 1. INTRODUCTION

The purposes of this work are the study of the shielding design technique through the analyses of shielding experimental data in the fast breeder reactor, the confirmation of the shield design method for the proto-type FBR "MONJU" and acquisition of the data for evaluating the shielding design uncertainty.

As a part of activities of the Specialists' Committee on Shielding Calculation of PNC, the shielding analyses 1,2) of in-vessel and enclosure shield system of "JOYO" were conducted with one- and two-dimensional Sn transport theory using the evaluated nuclear data file ENDF/B-IV and the photon production data file POPOP-4 library 3) during the period from April 1977 to March 1979. The calculated results were compared with the reactor performance test data 2,4,5) of JOYO. In the report, the authors conclude that the two-dimensional Sn transport calculation can predict the neutron fluxes and the gamma-ray dose rates in and around the reactor vessel and in the head access area within an order of magnitude. However, the compromise of the RZ calculational model brought about the disagreement between the calculated results and some experimental data which were influenced by neutron streaming through the detector guide tube located off the reactor center axis. In the reactor performance test, the neutron streaming data were also measured along the primary coolant pipe chase-way of JOYO. 2,4 ~ 6)

In this work, the authors investigated the following items concerning neutron streaming by using the albedo Monte Carlo code, MORSE-ALB<sup>7 ~ 11</sup>) with 21 group-P<sub>5</sub> approximation:

- (i) the effect of neutron streaming through the detector guide tube in the pedestal heavy concrete upon the experimental data,
- (ii) analyses of the experimental data measured in the primary coolant outlet pipe penetration, primary pump room and intermediate heat exchanger room (hereafter called as IHX room).

In the albedo Monte Carlo calculation, Sn results obtained in the activities of the PNC Specialists' Committee were used as a neutron source. The calculated results were compared with the measured data, and the applicability of the present albedo Monte Carlo technique to the neutron streaming analysis in the LMFBR was studied.

In Chapter 2, the "JOYO" streaming experiments are summarized. In Chapter 3, the calculational method used for the present analysis by means of albedo Monte Carlo technique is briefly explained and the calculated results are compared with experimental results. Concluding remarks are given in the last chapter.

## 2. OUTLINE OF STREAMING EXPERIMENT OF JOYO

Neutron streaming through the Detector Channel A, the primary coolant outlet pipe penetration (A loop of heat transfer systems) in biological shield concrete, primary pump room (called R206) and the IHX room (R302) of JOYO were analyzed by the albedo Monte Carlo method<sup>7, 11)</sup>. In this chapter, outline of measurements<sup>2, 5, 6)</sup> in these areas is explained. Detectors used for this experiment are shown in Table 2-0-1.

### 2.1 Detector Channel A

The measurement for this channel was made at the low power test of about 1 kW, 100 kW and 500 kW<sup>2, 5)</sup>. This channel was located 290 cm apart from the center axis of the reactor and penetrated both of the pedestal and the graphite shield. Measured values were obtained from 100 cm under the core mid-plane up to over the pedestal and had been already analyzed by using the two dimensional Sn transport code DOT-3,5<sup>12)</sup> as an activity of the PNC Specialists' Committee. However, the agreement between the calculation and the experiments was poor, since the calculation neglected neutron streaming effect in the detector guide tube upon the experimental data.

The detectors used here are B-10 proportional counter, TLD, fissile or activation foils of reactions such as  $^{235}\text{U}$ ,  $^{238}\text{U}$ ,  $^{63}\text{Cu}$  and  $^{197}\text{Au}$ , and ionization chamber. Vertical and horizontal view of JOYO are shown with the Detector Channel A



on the cross section in Fig. 2-1-1 and Fig. 2-1-2. Measured data were obtained at locations for foil arrangement shown in Fig. 2-1-3. Those obtained in the pedestal (at the height between 496.5 cm and 646 cm) are relevant to the present study and shown in Tables 2-1-1 through 2-1-5.

## 2.2 Primary Coolant Outlet Pipe Penetration

Neutron flux distributions were measured<sup>5)</sup> in and around the primary coolant outlet pipe penetration (A loop of JOYO heat transfer systems) which penetrates biological concrete shield at the height of 366 cm from core mid-plane. The radius of the duct is about 70 cm and that of the coolant pipe is about 28 cm. At the exit of the duct, B<sub>4</sub>C shields are surrounding the coolant pipe to reduce streaming neutrons. TLD-600 and TLD-700 detectors were irradiated at the power of 1.1 kW and Au foils at 114 kW. In the power-up test, a foil holder of SS316 (type 316 stainless steel) pipe with 18.5 mm diameter and 1.5 mm thickness was irradiated and reaction rate distributions of <sup>50</sup>Cr(n,γ) <sup>51</sup>Cr, <sup>58</sup>Fe(n,γ) <sup>59</sup>Fe, <sup>59</sup>Co(n,γ) <sup>60</sup>Co and <sup>123</sup>Sb(n,γ) <sup>124</sup>Sb were obtained. The measurement in the coolant pipe duct is illustrated in Fig. 2-2-1. In addition, reaction rates were obtained on and around the outer surface of the B<sub>4</sub>C shield by the foils such as Ag, Ta and Ir and by the fission track detectors.

The measured <sup>197</sup>Au(n,γ) reaction rates and the estimated values taking account of TLD data for thermal neutron flux are shown in Table 2-2-1 for seven points in the coolant pipe duct.

After the irradiation during the power-up test of 50 MWT, the SS316 holder was cut into pieces of 2 cm length every 10 cm and the induced activities of each piece were measured. The absolute values of reaction rate for SS316 constituent isotope were obtained 120 cm reactor-wards from the outer surface of the B<sub>4</sub>C shield as follows:

<sup>50</sup> Cr(n,γ) <sup>51</sup> Cr	7.18 × 10 <sup>-20</sup>	reactions/sec/atom/kW
<sup>58</sup> Fe(N,γ) <sup>59</sup> Fe	5.49 × 10 <sup>-21</sup>	reactions/sec/atom/kW
<sup>59</sup> Co(n,γ) <sup>60</sup> Co	1.65 × 10 <sup>-19</sup>	reactions/sec/atom/kW

Relative distribution of the above three reactions and <sup>123</sup>Sb(n,γ)<sup>124</sup>Sb reaction along the duct are shown in Table 2-2-2. Figure 2-2-2 shows a distribution of <sup>50</sup>Cr(n,γ)<sup>51</sup>Cr reaction rate compared with the thermal neutron flux. Shapes of the two distributions are similar to each other. The results from the foils such as Ag, Ta, Ir and from fission track detectors located behind the B<sub>4</sub>C shield are mentioned in the next section for the primary pump room.

### 2.3 Primary Pump Room (R206, A-loop)

A cross section view of reactor vessel including the primary pump room and the IHX room is shown in Fig. 2-3-1. Main passes of neutron streaming to pump room are primary coolant inlet and outlet pipe penetrations. Neutron streaming through these ducts enhances background level of FFD/DN-method (fuel fracture detector which counts delayed neutrons) in the primary pump room. The measurements<sup>4,6)</sup> of reaction

rate distribution in the primary pump room were performed at several points such as coolant pipe duct exit, surface of the sodium pump and surface of the FFD/DN-method. Figure 2-3-2 shows the detector locations by marks of cross. Table 2-3-1 shows the measured data at each detector position for  $^{235}\text{U}(n,f)$ ,  $^{238}\text{U}(n,f)$ ,  $^{232}\text{Th}(n,f)$ ,  $^{32}\text{S}(n,p)$ ,  $^{32}\text{P}$ ,  $^{109}\text{Ag}(n,\gamma)$ ,  $^{110\text{m}}\text{Ag}$ ,  $^{181}\text{Ta}(n,\gamma)$ ,  $^{182}\text{Ta}$  and  $^{191}\text{Ir}(n,\gamma)$ ,  $^{192}\text{Ir}$  reactions.

#### 2.4 IHX Room (R302, A-loop)

The location of the IHX room in the containment vessel is shown in Fig. 2-3-1. Radiation streaming passes to IHX room from reactor vessel are argon cover-gas pipe duct and over-flow pipe duct penetrating the biological concrete shield. Neutrons were measured<sup>4,6)</sup> on the surface of the  $\text{B}_4\text{C}$  shield panel surrounding each pipe, on the front and back sides of the IHX surface and at the intermediate point between the duct exit and the IHX as shown in Table 2-4-1 and Fig. 2-4-1.

Detectors were irradiated during the power-up test of 50 MWt. Integrated power is  $2.389 \times 10^3$  MWD and average power is 19.745 MWt. Reaction rates of  $^{235}\text{U}(n,f)$ ,  $^{238}\text{U}(n,f)$ ,  $^{232}\text{Th}(n,f)$ ,  $^{32}\text{S}(n,p)$ ,  $^{32}\text{P}$ ,  $^{109}\text{Ag}(n,\gamma)$ ,  $^{110\text{m}}\text{Ag}$ ,  $^{181}\text{Ta}(n,\gamma)$ ,  $^{182}\text{Ta}$  and  $^{191}\text{Ir}(n,\gamma)$ ,  $^{192}\text{Ir}$  reactions are also shown in Table 2-4-1.

Table 2-0-1 Detectors used for measurement

Detector	Comment
TLD	HARSHAW TLD600 (for n, $\gamma$ ), TLD700 (for $\gamma$ )
B-10 Counter	Tube type 232 made by LND,INC (bare and Cd-covered) sensitivity: 1.0 cps/nv <sub>th</sub>
<sup>235</sup> U(n,f)	Measured $\gamma$ -ray: > 600 keV and 1.596 MeV $\gamma$ from La-140
<sup>238</sup> U(n,f)	Used in the pump room (R206) and the IHX room (R302)
<sup>238</sup> U(n, $\gamma$ )	Measured $\gamma$ -ray: $\sim$ 100 keV from <sup>239</sup> Np
<sup>232</sup> Th(n,f)	Measured $\gamma$ -ray: $\sim$ 300 keV from <sup>233</sup> Pa
<sup>197</sup> Au(n, $\gamma$ )	Bare and Cd-covered
<sup>109</sup> Ag(n, $\gamma$ ) <sup>110m</sup> Ag	t <sub>1/2</sub> = 255 days, resonance detector
<sup>181</sup> Ta(n, $\gamma$ ) <sup>182</sup> Ta	t <sub>1/2</sub> = 115.1 days, resonance detector
<sup>191</sup> Ir(n, $\gamma$ ) <sup>192</sup> Ir	t <sub>1/2</sub> = 74.2 days, resonance detector
<sup>32</sup> S(n,p) <sup>32</sup> P	Used for fast neutron
<sup>50</sup> Cr(n, $\gamma$ ) <sup>51</sup> Cr	$\gamma$ -ray energy: 0.320 MeV
<sup>58</sup> Fe(n, $\gamma$ ) <sup>59</sup> Fe	$\gamma$ -ray energy: 1.095, 1.292 MeV
<sup>59</sup> Co(n, $\gamma$ ) <sup>60</sup> Co	$\gamma$ -ray energy: 1.173, 1.332 MeV
<sup>123</sup> Sb(n, $\gamma$ ) <sup>124</sup> Sb	$\gamma$ -ray energy: 0.603, 1.692 MeV

Table 2-1-1 Measured U235(n,f) reaction rate relative distribution in the Ch.A by EU foils.

Distance from core center	Relative Values	Probable errors by countings	Comment
( cm )		( % )	• 580KW
- 7 5	0.4 8 5	0.6 8	• Deviations of Foil Setting : ~5cm (* including Neutron Streaming due to Guide Tube)
- 2 5	0.9 6 3	0.5 9	
0	1.0 0	Normalized	
7 5	0.7 5 9	0.3 8	
1 5 0	0.3 2 8	0.5 5	
2 5 0	0.1 3 7	0.9 9	
3 5 0	0.0 3 4 4	1.8	
4 5 0	0.0 1 7	2.5	
5 5 0	0.0 0 2 0 6(*)	7.0	

Table 2-1-2 Measured U238(n, $\gamma$ ) reaction rate relative distribution in the Ch.A.

Distance from core center	Relative Values	Comments
( cm )		• 580KW
- 7 5	0.5 3	} $\pm 5\%$ (Normalization Point) (Estimated Errors) } $\pm 5\%$ } $\pm 10\%$ } $\pm 5\%$ } $\pm 10\%$ Deviations of Foil Position $\pm 5cm$
- 2 5	1.0 3	
0	1.0 0	
7 5	0.7 7	
1 5 0	0.3 9	
2 5 0	0.2 3	
3 5 0	0.1 6	
4 5 0	0.4 6	
5 5 0	0.2 1	

Table 2-1-3 Au197(n, $\gamma$ ) reaction rate distribution in the Channel A.

Distance from core center	Au Bare		Au Cd-covered		Comment		
	$\langle \sigma_c \phi \rangle / \text{watt}$	Errors	$\langle \sigma_c \phi \rangle / \text{watt}$	Errors			
(cm)	$\times 10^{-24}$ 1/sec/atom/watt	(%)	$\times 10^{-24}$ 1/sec/atom/watt	(%)	Probable errors by countings only		
- 75	$8.75 \times 10^3$	} $\pm 3$	$2.19 \times 10^2$	} $\pm 3$			
- 25	$1.73 \times 10^4$		$5.16 \times 10^2$				
0	$1.83 \times 10^4$		$5.61 \times 10^2$				
75	$1.38 \times 10^4$		$3.31 \times 10^2$				
150	$6.17 \times 10^3$						
200			$1.18 \times 10^2$				
250	$2.52 \times 10^3$						
300			$2.86 \times 10$			$\pm 3.1$	
350	$6.55 \times 10^2$					$3.82 \times 10^2$	$\pm 3.3$
450	$1.04 \times 10^3$					$8.42 \times 10^2$	} $\pm 3$
500			$2.19 \times 10^2$				
550	$7.70 \times 10^2$						
Comment	(Reactor Power 580KW)						

Table 2-1-4 Count rate distribution by B-10 counter in the Channel A.

Distance from core center (cm)	B 10 counter count rate(cps/watt)	
	Bare cps/watt	Cd/covered cps/watt
0	214.9	1.20
50	180.3	0.953
100	120.0	0.613
150	68.37	0.268
200	45.42	0.203
250	30.15	0.134
300	16.78	$7.2 \times 10^{-2}$
350	7.960	$5.4 \times 10^{-2}$
400	3.807	0.355
450	3.698	0.950
500	1.889	0.584
550 (*)	$6.1_e \times 10^{-2}$	$1.2_e \times 10^{-2}$
600 (*)	$7.9_e \times 10^{-3}$	$1.2_e \times 10^{-3}$
650 (*)	$1.0_e \times 10^{-3}$	$1.8_e \times 10^{-4}$
Comments	Reactor Power: 0.5kw ( $\pm 15\%$ ) (*) Including Neutron Streaming due to Guide Tube	

Table 2-1-5 Thermal neutron flux distribution in the Channel A.

Channel A						
< Au Foil >			< TLD-600-700 >		< B10 counter - >	
Distance from core center(cm)	$n/cm^2 \cdot sec/watt$ $\phi$ th/watt	Cd-ratio	Distance from core center(cm)	$\phi$ th/watt	Distance from core center(cm)	$\phi$ th/watt
-75	$1.03 \times 10^2$	39.94	-100	$1.54 \times 10^2$	0	$2.14 \times 10^2$
-25	$2.01 \times 10^2$	33.44	-50	$2.12 \times 10^2$	50	$1.79 \times 10^2$
0	$2.13 \times 10^2$	32.61	0	$2.12 \times 10^2$	100	$1.20 \times 10^2$
75	$1.62 \times 10^2$	41.74	25	$2.24 \times 10^2$	150	$6.81 \times 10^1$
150	$7.17 \times 10^1$	31.84	50	$2.03 \times 10^2$	200	$4.52 \times 10^1$
200	$4.41 \times 10^1$	32.2	100	$1.14 \times 10^2$	250	$3.00 \times 10^1$
250	$2.96 \times 10^1$	53.1	150	$8.88 \times 10^1$	300	$1.67 \times 10^1$
300	$1.62 \times 10^1$	48.0	200	$5.35 \times 10^1$	350	7.91
350	7.13	10.9	300	$1.38 \times 10^1$	400	3.45
400	5.54	2.21	400	3.93	450	2.75
450	2.36	1.23	500	1.68	500	1.31
500	8.71	4.37	600	—	550	$4.99 \times 10^{-2}$
550	—	—			600	$6.70 \times 10^{-3}$
					650	$9.3 \times 10^{-4}$

Table 2-2-1 Reaction rate of  $^{197}\text{Au}(n, \gamma)^{198}\text{Au}$  reaction and thermal neutron flux in the primary coolant pipe duct

a) Measured value

Distance from outside of the $\text{B}_4\text{C}$	Au (Bare)		AU (Cd-covered)		Comments
	$\langle \sigma_c \phi \rangle / \text{kW}$ ( $\times 10^{24} \text{n/sec/atom/kW}$ )	** Errors	$\langle \sigma_c \phi \rangle / \text{kW}$ ( $\times 10^{24} \text{n/sec/atom/kW}$ )	** Errors	
(cm)					Reactor power 114kW *) Counts are not sufficient **) By countings only
0	* $3.38 \times 10^3$	$\pm 15 \%$	* $4.72 \times 10^3$	$\pm 13 \%$	
20	$9.7_4 \times 10^3$	$\pm 9.1\%$	$6.87 \times 10^3$	$\pm 10.8\%$	
40	$2.27 \times 10^4$	$\pm 5.9\%$	$1.61 \times 10^4$	$\pm 7.1\%$	
60	$4.82 \times 10^4$	$\pm 4.1\%$	$2.89 \times 10^4$	$\pm 5.3\%$	
80	$7.7_3 \times 10^4$	$\pm 3.3\%$	$4.9_4 \times 10^4$	$\pm 4.1\%$	
100	$1.19 \times 10^5$	$\pm 2.6\%$	$8.15 \times 10^4$	$\pm 3.2\%$	
120	$2.25 \times 10^5$	$\pm 1.9\%$	$1.64 \times 10^5$	$\pm 2.2\%$	

b) Evaluated value (corrected for reactor power normalization)

Distance from outside of $\text{B}_4\text{C}$	Au-foil		Cd-ratio		Thermal neutron flux	
	n/sec·atom/kW	Errors	Cd-ratio	Errors	$\phi_{\text{th}}$	Errors
(cm)					(n/cm <sup>2</sup> ·sec)/kW	
0						
20	$1.1 \times 10^{-20}$	$\pm 11 \%$	1.42	$\pm 14.3\%$	$3.7 \times 10$	$\pm 26\%$
40	$2.6 \times 10^{-20}$	$\pm 8.1\%$	1.42	$\pm 10 \%$	$8.7 \times 10$	$\pm 24\%$
60	$5.5 \times 10^{-20}$	$\pm 7 \%$	1.67	$\pm 7 \%$	$2.5 \times 10^2$	$\pm 23\%$
80	$8.8 \times 10^{-20}$	$\pm 6 \%$	1.56	$\pm 6 \%$	$3.6 \times 10^2$	$\pm 20\%$
100	$1.4 \times 10^{-19}$	$\pm 6 \%$	1.46	$\pm 5 \%$	$4.9 \times 10^2$	$\pm 20\%$
120	$2.6 \times 10^{-19}$	$\pm 6 \%$	1.37	$\pm 4 \%$	$8.0 \times 10^2$	$\pm 20\%$
Comments	<ul style="list-style-type: none"> <li>• Errors of reaction rate (excluding error by countings)               <ol style="list-style-type: none"> <li>1. Detection efficiency of NaI ; <math>\pm 2\%</math></li> <li>2. Operation pattern ; <math>\pm 5\%</math> (presumed)</li> <li>3. Weight of gold foil ; <math>\pm 1\%</math></li> </ol> </li> <li>• Error of <math>\pm 15\%</math> was added to the thermal neutron flux considering the difference between Au-foil and TLD.</li> <li>• Deviations of foil setting ; <math>\sim \pm 3</math> cm.</li> <li>• The above values do not include absolute error by reactor power.</li> </ul>					



Table 2-2-2 Relative reaction rate distribution in the primary coolant pipe duct.

$\gamma$ -ray position (cm)	$\text{Cr}^{50}(\text{n}, \gamma) \text{Cr}^{51}$	$\text{Fe}^{58}(\text{n}, \gamma) \text{Fe}^{59}$	$\text{Co}^{59}(\text{n}, \gamma) \text{Co}^{60}$	$\text{Sb}^{123}(\text{n}, \gamma) \text{Sb}^{124}$	
	0.320 MeV	1.095 MeV	1.173 MeV	0.603 MeV	1.692 MeV
reactor-ward ①-120	1.00 <sup>1)</sup>	1.00 <sup>2)</sup>	1.00 <sup>3)</sup>	1.00 <sub>0</sub>	1.00 <sub>0</sub>
②-110	0.555 ± 0.2 %	0.540 ± 1.1%	0.560 ± 0.6%	0.496 ± 2 %	0.592 ± 6.2%
③-100	0.463 ± 0.2 %	0.460 ± 1.2%	0.454 ± 0.6%	0.418 ± 2.2%	0.496 ± 6.8%
④-90	0.357 ± 0.2 %	0.357 ± 1.3%	0.352 ± 0.6%	0.346 ± 2.2%	0.339 ± 7.3%
⑤-80	0.280 ± 0.2 %	0.280 ± 1.4%	0.273 ± 0.7%	0.256 ± 2.4%	0.274 ± 7.7%
⑥-70	0.269 ± 0.3 %	0.259 ± 1.5%	0.252 ± 0.8%	0.227 ± 2.9%	0.222 ± 9.4%
⑦-60	0.192 ± 0.3 %	0.194 ± 1.5%	0.178 ± 0.8%	0.176 ± 2.8%	0.118 ± 11 %
⑧-50	0.145 ± 0.3 %	0.152 ± 1.7%	0.144 ± 0.9%	0.132 ± 3.1%	0.190 ± 8.9%
⑨-40	0.0935 ± 0.4 %	0.0928 ± 2.1%	0.0947 ± 1.1%	0.0987 ± 3.6%	0.0695 ± 14%
⑩-30	0.0493 ± 0.5 %	0.0486 ± 2.5%	0.0510 ± 1.4%	0.0737 ± 4.0%	0.0797 ± 13%
⑪-20	0.0302 ± 0.7 %	0.0332 ± 3.3%	0.0353 ± 1.6%	0.0538 ± 4.5%	0.0385 ± 18%
⑫-10	0.0224 ± 0.7 %	0.0229 ± 3.9%	0.0253 ± 1.9%	0.0374 ± 5.7%	0.0424 ± 17%
outside of B4C ⑬ <sub>0</sub>	0.0245 ± 1.0 %	0.0285 ± 5.0%	0.0311 ± 2.4%	0.0825 ± 5.4 %	—
⑭ 1	0.0147 ± 0.9 %	0.0166 ± 4.5%	0.0171 ± 2.2%	0.0456 ± 5.0%	—
⑮ 3	$5.88 \times 10^{-3} \pm 1.4\%$	$7.32 \times 10^{-3} \pm 6.9\%$	$8.85 \times 10^{-3} \pm 3.2\%$	0.0293 ± 6.6%	—
⑯ 5	$4.06 \times 10^{-3} \pm 1.7\%$	$5.51 \times 10^{-3} \pm 7.8\%$	$6.17 \times 10^{-3} \pm 3.9\%$	0.0341 ± 5.6%	—
⑰ 10	$2.47 \times 10^{-3} \pm 2.3\%$	$4.83 \times 10^{-3} \pm 8.6\%$	$5.18 \times 10^{-3} \pm 4.3\%$	0.0347 ± 5.8%	—
⑱ 15	$2.02 \times 10^{-3} \pm 2.1\%$	$3.27 \times 10^{-3} \pm 10.3\%$	$4.33 \times 10^{-3} \pm 4.6\%$	0.0249 ± 6.7%	—
Comments	⑮ : Corresponding to the number in Fig. 2.2.2. 1) Absolute value is $7.18 \times 10^{-20}$ reactions/s/atom/kw 2) " " $5.49 \times 10^{-21}$ " " 3) " " $1.65 \times 10^{-19}$ " "				

Table 2-3-1 Reaction rate distribution in primary pump room R206

No.	Position	Reaction rate						
		$^{235}\text{U}(n,f)$	$^{238}\text{U}(n,f)$	$^{232}\text{Th}(n,f)$	$^{32}\text{S}(n,P)$ $^{32}\text{P}$	$^{109}\text{Ag}(n,\gamma)$ $^{110m}\text{Ag}$	$^{181}\text{Ta}(n,\gamma)$ $^{182}\text{Ta}$	$^{191}\text{Ir}(n,\gamma)$ $^{192}\text{Ir}$
		(fissions/g·MW·h)			(Reactions/ g·MW·h)	$(\times 10^{-24})$ reactions/atom·sec·50·MWt)		
1	Outer surface of B <sub>4</sub> C shield of outlet primary coolant pipe (over the pipe)	1.30+7 <sup>1)</sup>	3.59+2	1.1+2	5.45+1	1.161+6 1.225+6	1.924+7 2.392+7	4.268+7 4.006+7
2	ditto (under the pipe)	9.84+6	2.90+2	9.2+1	4.40+1	1.393+6 1.035+6	2.343+7 2.412+7	4.940+7 4.556+7
3	Outer surface of B <sub>4</sub> C shield of inlet primary coolant pipe (over the pipe)	1.50+7	3.12+2	9.9+1	4.74+1	1.488+6 1.443+6	2.495+7 2.592+7	6.420+7 6.157+7
4	ditto (under the pipe)	1.22+7	2.80+2	8.8+1	4.25+1	1.387+6 1.618+6	2.570+7 1.856+7	3.768+7 4.382+7
5	Surface of primary pump (looking at the outlet pipe duct)	3.22+6	2.9 +1	9+0	-	3.498+5 3.542+5	4.301+6 4.000+6	1.398+7 1.405+7
6	Surface of primary pump (looking at the inlet pipe duct)	3.13+6	1.5+1	5+0	-	3.845+5 3.753+5	4.322+6 4.377+6	1.591+7 1.723+7
7	Over the polyethylene shield of FFD/DN	2.72+6	2.8+0	9-1	-	1.804+5 1.857+5	1.634+6 -	9.289+6 9.408+6
8	Side of sodium pipe beside the FFD/DN	9.66+5	1.2+0	4-1	-	-	-	-
9	70 cm from the B <sub>4</sub> C shield of outlet sodium duct (side of duct)	-	-	-	-	8.651+5 9.042+5	1.231+7 1.030+7	3.062+7 3.402+7
10	Same as No.5	-	-	-	-	3.815+5 3.265+5	3.618+6 3.630+6	1.452+7 1.173+7

N. B. 1) Read as  $1.30 \times 10^7$  fissions/g·MW·h.

Table 2-4-1 Reaction rate distribution in IHX room R302

1) No.	Position							
		$^{235}\text{U}(n,f)$	$^{238}\text{U}(n,f)$	$^{232}\text{Th}(n,f)$	$^{32}\text{S}(n,P)$ $^{32}\text{P}$	$^{109}\text{Ag}(n,\gamma)$ $^{110m}\text{Ag}$	$^{181}\text{Ta}(n,\gamma)$ $^{182}\text{Ta}$	$^{191}\text{Ir}(n,\gamma)$ $^{192}\text{Ir}$
		$(\times 10^{-24} \text{ fissions/atom}\cdot\text{sec}\cdot 50\text{MWt})$			$(\times 10^{-24} \text{ reactions/atom}\cdot\text{sec}\cdot 50\text{MWt})$			
1	110 cm from the $\text{B}_4\text{C}$ shield of Ar gas pipe duct (on streaming pass)	-	-	-	-	5.499+5 5.578+5	7.058+6 6.955+6	2.338+7 2.483+7
2	Outer surface of $\text{B}_4\text{C}$ shield of Ar gas pipe	4.42+7 <sup>2)</sup>	7.91+2	2.5+2	1.70+1	6.021+5 4.819+5	8.257+6 7.562+6	2.177+7 2.181+7
3	Surface of IHX (reverse side of No.4)	1.38+6	1.8	5-1	-	1.414+4 1.488+4	1.547+5 1.658+5	8.656+5 8.512+5
4	Surface of IHX (on the stretched line from Ar gas pipe duct)	1.34+7	6.64+2	2.0+2	1.42+1	2.823+5 2.470+5	2.246+6 2.625+6	8.263+6 9.237+6
5	Outer surface of $\text{B}_4\text{C}$ shield of Ar gas pipe	-	-	-	-	6.600+5 8.211+5	1.560+7 1.532+7	3.602+7 3.186+7
6	Outer surface of $\text{B}_4\text{C}$ shield of Na overflow pipe	3.50+7	7.52+2	2.3+2	1.61+1	1.077+6 9.642+5	1.907+7 1.864+7	4.282+7 4.152+7

1) Corresponding to the location number in Fig. 2-4-1.

2) Read as  $4.42 \times 10^7$  fissions/ $10^{24}$  atom/sec/50mWt.

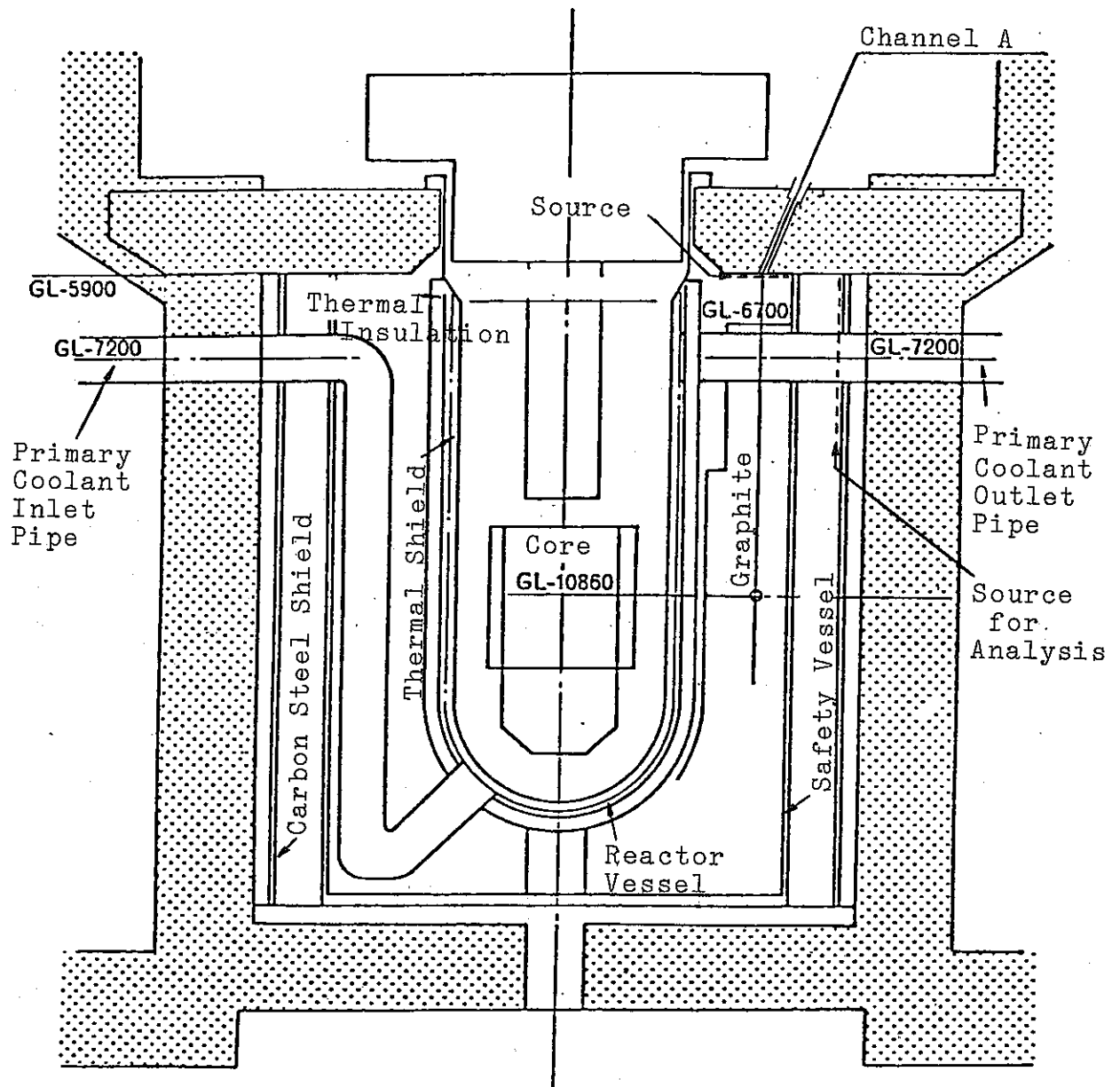


Fig. 2-1-1 Vertical cross sectional view of JOYO

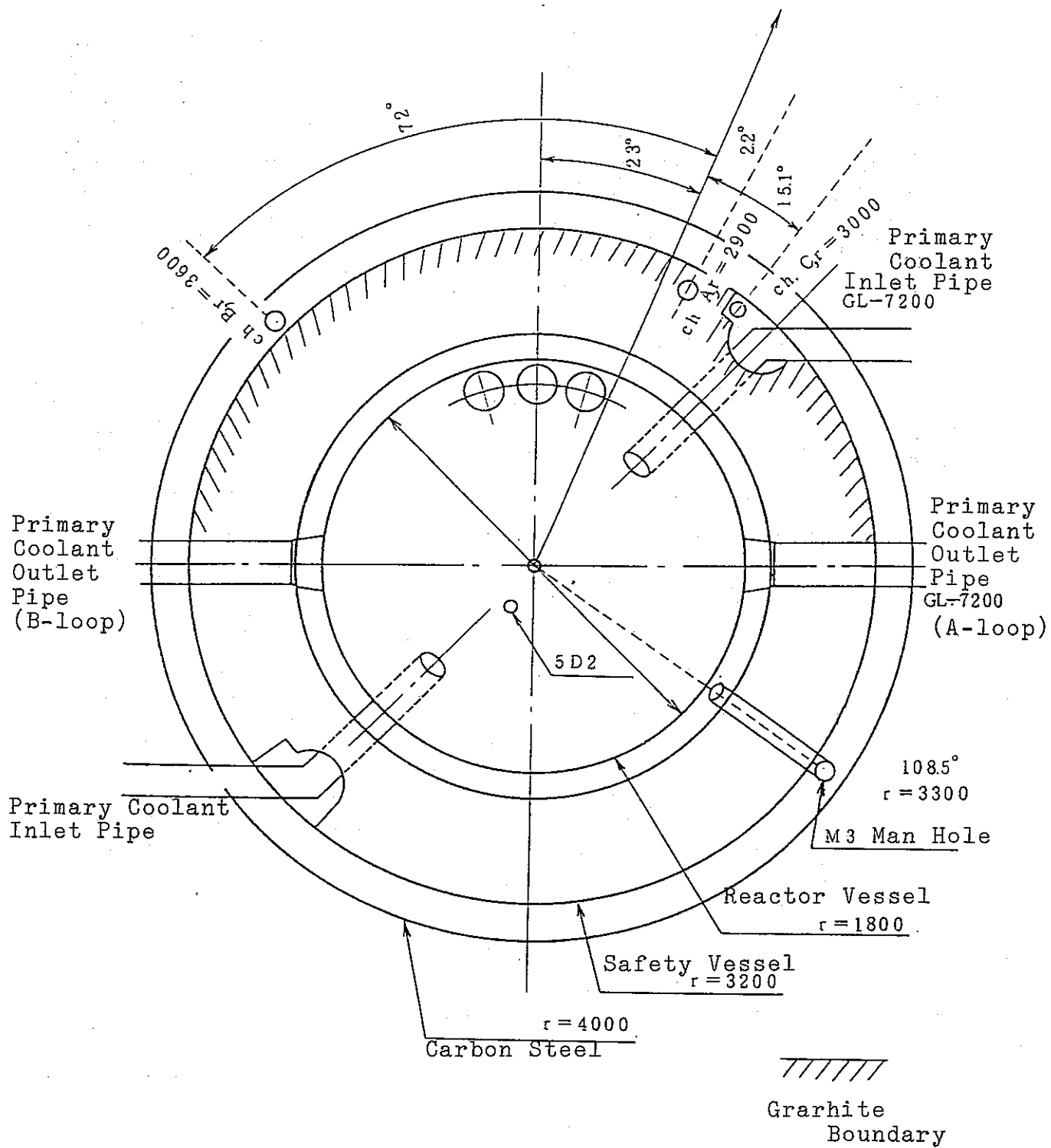


Fig. 2-1-2 Horizontal cross sectional view of JOYO

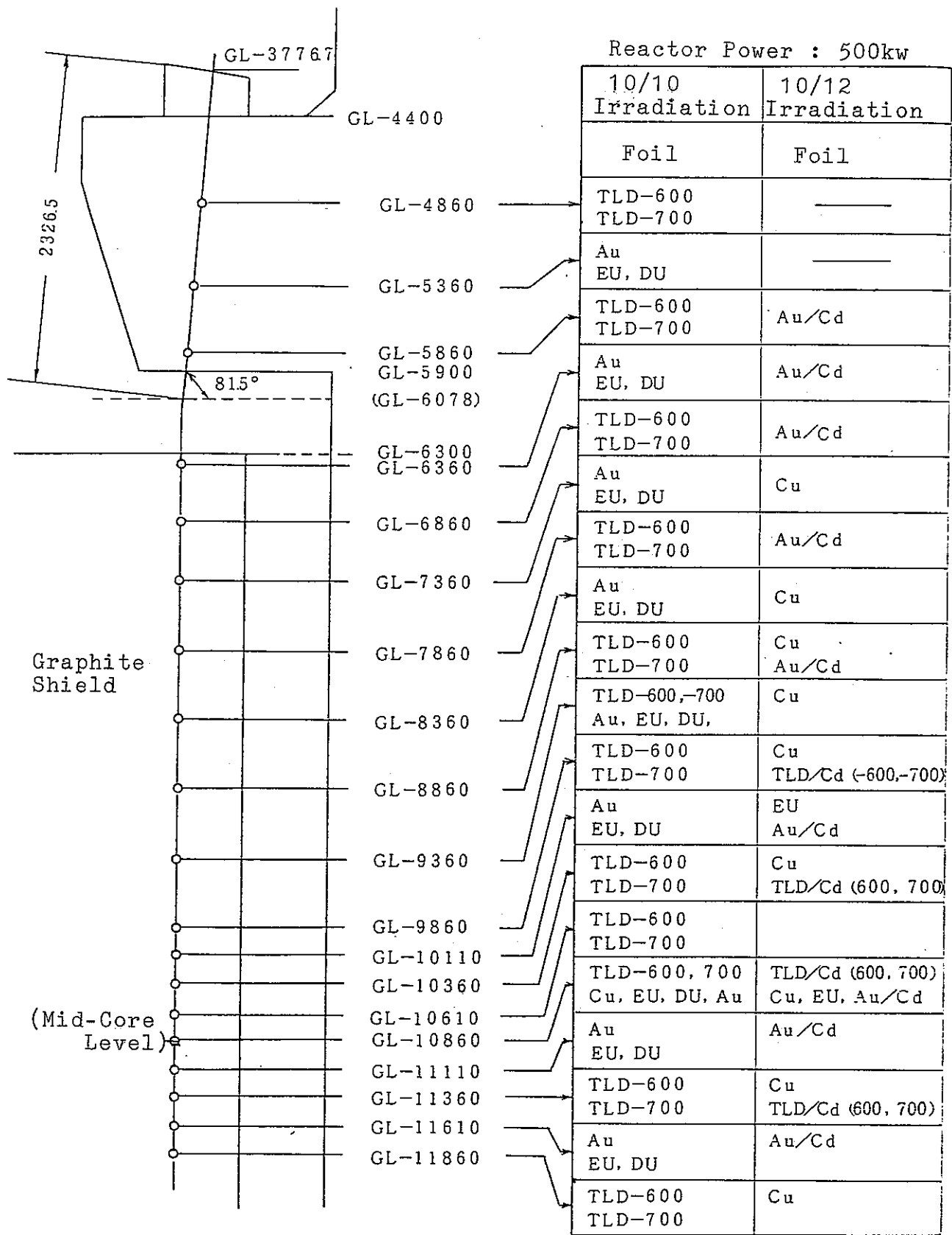


Fig. 2-1-3 Foil arrangement in the Channel A  
2-15

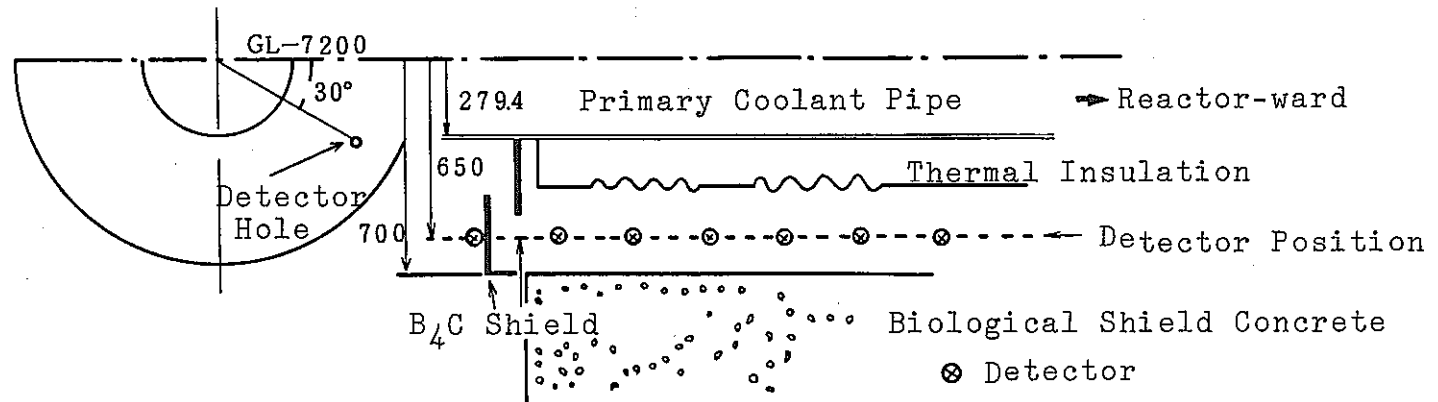


Fig. 2-2-1 Detector arrangement in primary coolant outlet pipe penetration

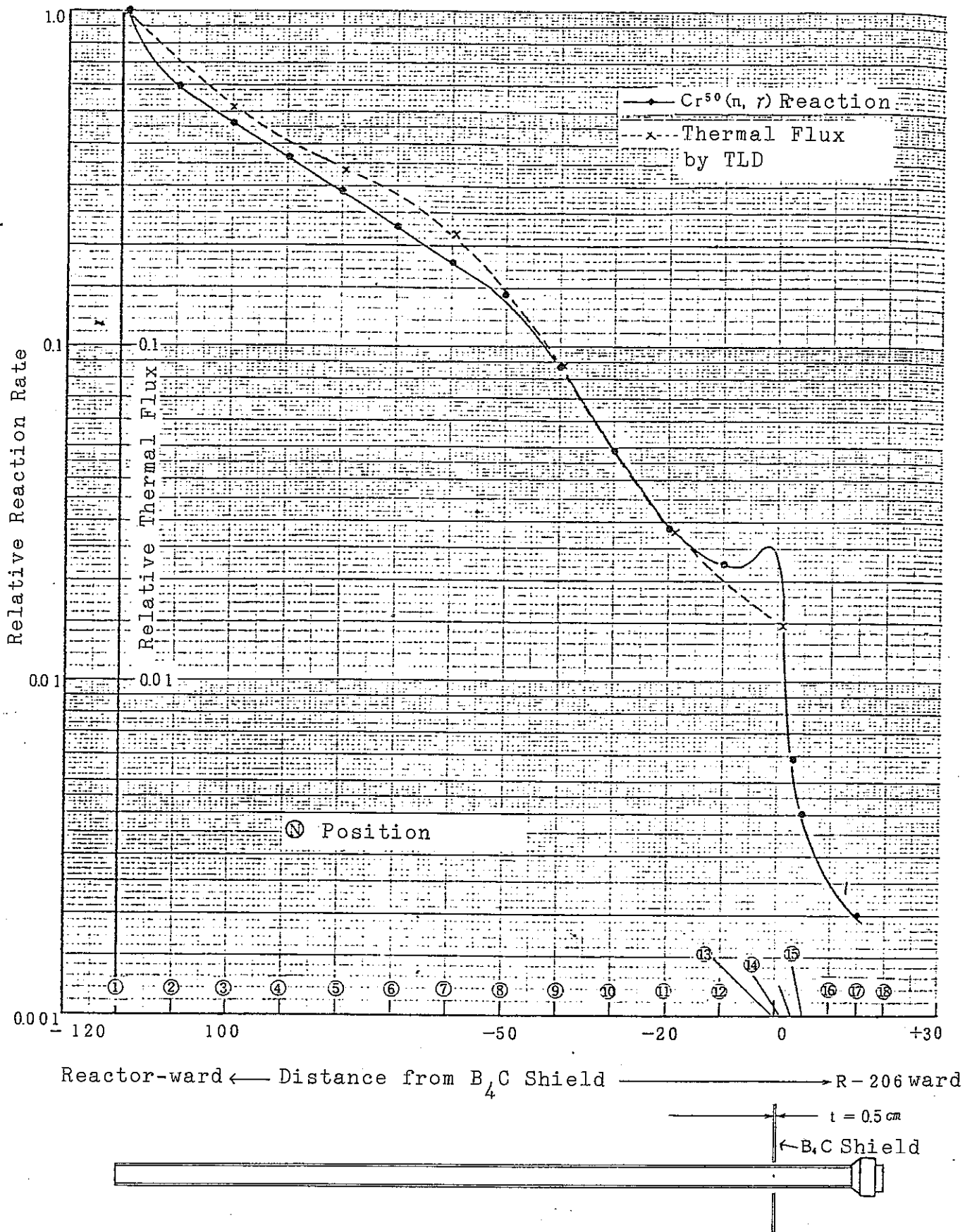
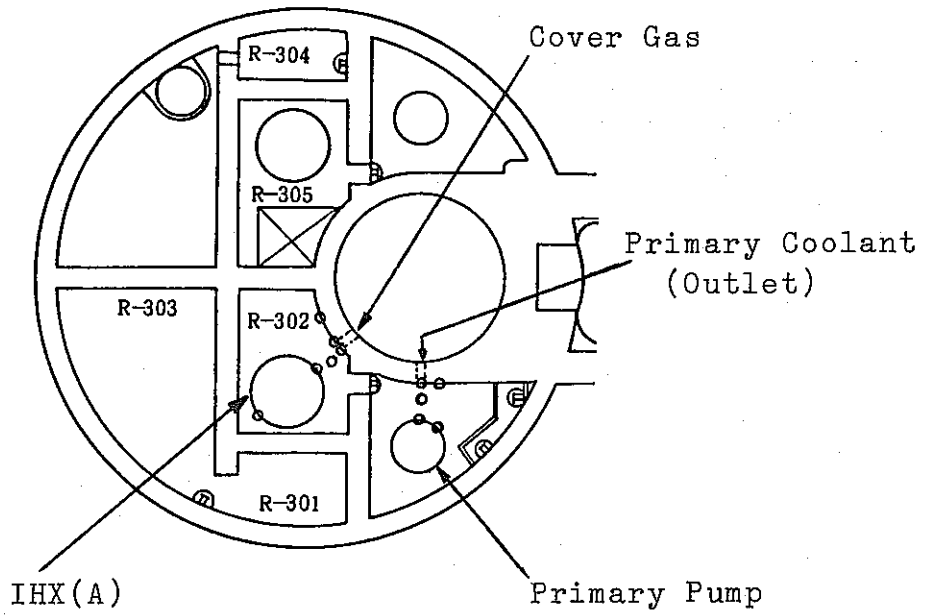


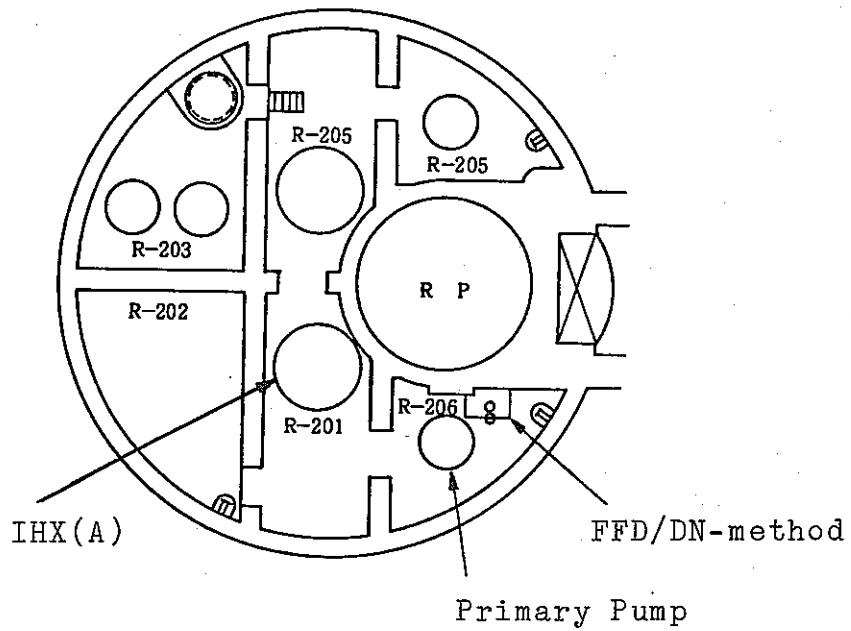
Fig. 2-2-2  $^{50}\text{Cr}(n, \gamma)^{50}\text{Cr}$  reaction and thermal neutron flux distribution in the primary coolant pipe duct.



B I F



B M 2 F



◦ Measuring Position

Fig. 2-3-1 Detector arrangement in the primary pump room and the IHX room.

①~⑨ : Detector Number

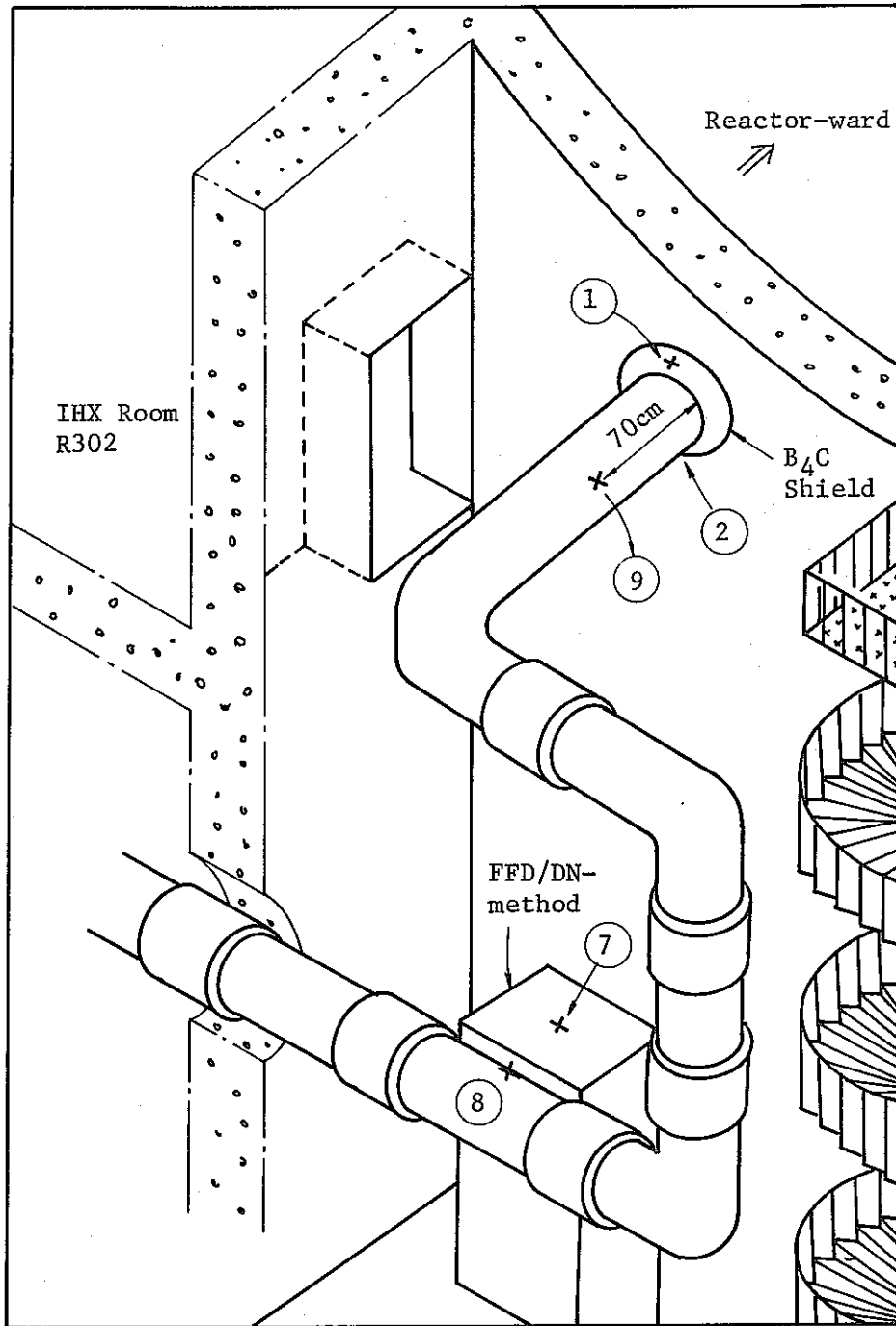


Fig. 2-3-2 Conceptual view of the primary pump room

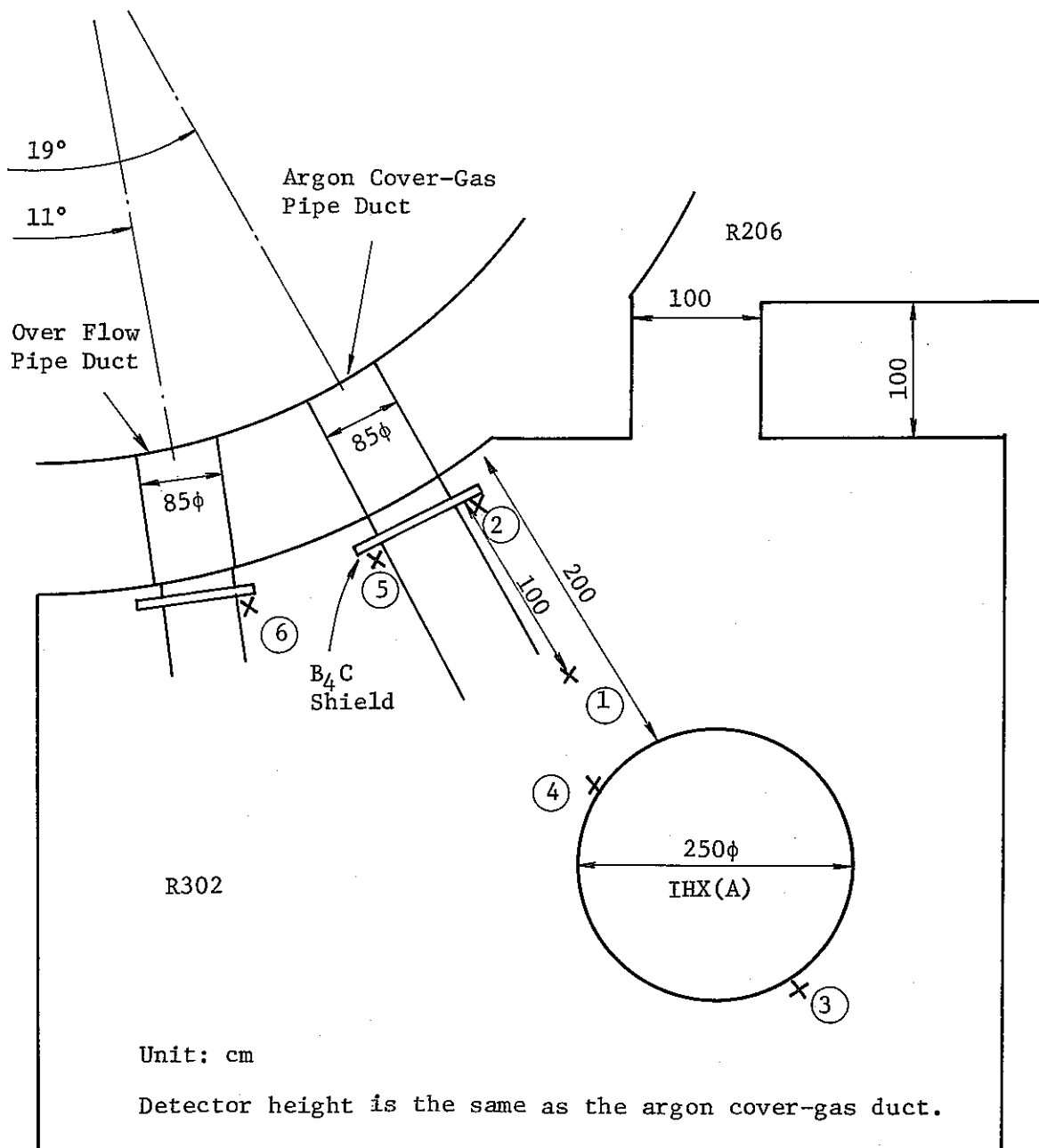


Fig. 2-4-1 Measuring locations in the IHX room

### 3. STREAMING ANALYSES BY ALBEDO MONTE CARLO METHOD

The shielding performance test data concerning neutron streaming through the cavities of JOYO were analyzed by using the albedo Monte Carlo code system, MORSE-ALB<sup>7-11)</sup> to examine the applicability of the albedo Monte Carlo method to the neutron streaming analysis in the LMFBR.

The analyzed items are as follows:

- (1) Effect of neutron streaming through the detector guide tube (Channel A) in the pedestal heavy concrete.
- (2) Neutron streaming through the primary coolant pipe penetration in the biological concrete shield into the primary pump room.
- (3) Neutron behaviour in the primary pump room.
- (4) Neutron streaming through the argon cover gas penetration in the biological concrete shield into the IHX room and neutron behaviour in the IHX room.
- (5) Comparison of the calculated values and the experimental data<sup>2,4 ~ 5)</sup> which are described in Chapter 2.

The analyses concerning items of (2) through (4) were made for the loop A of JOYO heat transfer system. The IHX room has two different openings which supplies the room with neutron source. One is a rectangular gateway to the primary pump room with the size of 100 cm × 150 cm. Another is the argon cover

gas pipe and overflow sodium pipe penetrations leading to the reactor room. In this analysis, the latter contributions were found to be more significant as will be discussed in Section 3.5.

Calculational procedures are shown in Fig. 3-0-1 as a flow diagram for processing group constants and differential albedo data and for neutron transport calculations. In these calculations, the Sn - Monte Carlo and the Monte Carlo - Monte Carlo coupling techniques were employed by generating the neutron source for Monte Carlo calculation with the DOMINO-N code<sup>10)</sup>. The code is a NAIG revised version of DOMINO code<sup>13)</sup> and can treat more general source geometry and Monte Carlo - Monte Carlo interface. The neutron sources for analysis on neutron streaming through the Detector Channel A, the primary coolant outlet pipe penetration and the argon cover gas pipe penetration were generated from the Sn results<sup>1,2)</sup> (which has been performed to analyze the in-vessel and enclosure shield system of JOYO by using the DOT-3.5 code<sup>12)</sup>) as shown in Fig. 3-0-2. The source for Channel A was assumed to be uniform and isotropic, and has the intensity equal to the scalar flux at the position C because the neutron flux distributions were nearly flat under the pedestal. The neutron sources for analyses on neutron streaming through the penetrations in the biological concrete shield were also assumed to be isotropic and dependent on the spatial position along the core-center axis direction. The source data were generated from the neutron fluxes (by the Sn calculation, with a P<sub>1</sub>-S30 approximation) at the position of  $r = 386.5$  cm

which is in front of the carbon steel liner, and corrected by using the P<sub>3</sub>-S124 results<sup>1,2)</sup>, which was limited to the regions of the radius between 130.8 cm and 321.9 cm, in order to taking into account the neutron streaming through the nitrogen gas region around the graphite shield. This procedure may correspond to that employed to the Analysis-(B)<sup>14)</sup> by Sn method, and ignores the neutron streaming through a pipe penetration at the upper part of the graphite shield.

In the albedo Monte Carlo calculation, such importance sampling techniques as source energy biasing, exponential transformation and Russian roulette kill were used. The neutron scoring were made by point detectors, next event surface crossing estimators<sup>11)</sup> and boundary crossing estimators.

In the following sections, the calculational method and results are described for each item of streaming analyses.

### 3.1 Preparation of Group Constants and Albedo Data

Atomic Number densities used for the present analysis are given in Table 3-1-1. Number densities for sodium correspond to the outlet temperature at 435°C and the inlet temperature at 370°C in the initial start-up test reactor of JOYO MARK-I core. The composition of thermal insulation covering sodium pipe is that of silicalite of which thickness is the largest. As for the IHX, two different homogenized densities were calculated. Sodium density in the IHX was assumed to be that at the average temperature of 400°C due to the fact that the primary sodium

temperature decreased from 435°C to 370°C and the secondary sodium temperature increased from 355°C to 420°C. The bellows in the argon cover gas penetration were considered as a diluted stainless steel with a volume ratio of 6.05%.

Effective macroscopic group cross sections were generated by the RADHEAT-V3.5 code system<sup>15)</sup> from the 100-group cross section library JSD-100<sup>16)</sup> with P5 anisotropy based on the evaluated nuclear data library ENDF/B-IV. The 100-group constants were collapsed to 21-group cross sections with a weighting spectrum shown in Table 3-1-2. Table 3-1-3 shows the 21-neutron-energy-group structure. Detector cross sections are mainly based on ENDF/B-IV and given in Table 3-1-4.

Energy and angle dependent doubly differential albedos were produced for a single slab layer of SS-304, carbon steel, ordinary concrete, polyethylene, IHX lower part medium and heavy concrete by using the one-dimensional transport code SLDN<sup>8,9)</sup> with the invariant imbedding method. The albedo data for a multilayer of ordinary concrete covered with a carbon steel liner were calculated by one-dimensional Sn transport code, ANISN-N.<sup>7)</sup> The model for Sn calculation is shown in Fig. 3-1-1. The mesh sizes near the source boundary which is an albedo boundary are taken fine enough to keep an accuracy of albedo data for slant incident and reflected angle. The double Gaussian quadrature set with the 8th order was taken to be same as angular mesh points in both of SLDN and ANISN calculations. Table 3-1-5 shows the angular quadrature set for ANISN calculation.

Table 3-1-1 Atomic number densities for analyzing JOYO shield data

(Unit:  $10^{24}$  atoms/cm<sup>3</sup>)

	Sodium 435 C	Sodium 370°C	SS304 <sup>1)</sup>	Carbon steel	Ordinary concrete	B <sub>4</sub> C(60% density)	Thermal insula- tion	Poly- ethylene	IHX (upper region)	IHX (lower region)	N <sub>2</sub> gas	Heavy concrete
H	-	-	-	-	6.513-3	-	1.769-3	7.918-2	-	-	-	4.788-3
B-10	-	-	-	-	-	1.216-2	-	-	-	-	-	-
B-11	-	-	-	-	-	5.377-2	-	-	-	-	-	-
C	-	3.124-4	3.124-4	9.459-4	3.039-4	1.648-2	-	3.959-2	4.861-5	4.861-5	-	2.352-4
N	-	-	-	-	-	-	-	-	-	-	2.69-5	-
O	-	-	-	-	4.216-2	-	3.840-3	-	-	-	-	3.263-2
Na	2.223-2 <sup>2)</sup>	2.264-2	-	-	6.549-4	-	-	-	3.404-3	1.895-2	-	5.069-4
Mg	-	-	-	-	-	-	3.765-5	-	-	-	-	-
Al	-	-	-	-	-	-	1.191-4	-	-	-	-	-
Si	-	-	1.775-3	4.497-4	1.721-2	-	9.683-4	-	2.762-4	2.762-4	-	1.332-2
K	-	-	-	-	2.787-4	-	-	-	-	-	-	2.157-4
Ca	-	-	-	-	2.810-3	-	7.352-4	-	-	-	-	2.175-3
Cr	-	-	1.714-2	-	-	-	-	-	2.667-3	2.667-3	-	-
Mn	-	-	1.708-3	6.894-4	-	-	-	-	2.658-4	2.658-4	-	-
Fe	-	-	5.679-2	8.365-2	6.233-4	-	4.435-5	-	8.837-3	8.837-3	-	1.963-2
Co*	-	-	1.990-4	-	-	-	-	-	3.096-5	3.096-5	-	-
Ni	-	-	7.991-3	-	-	-	-	-	1.243-3	1.243-3	-	-
*Smeared into Mn	0.8486 g/cm <sup>3</sup> MARK-I (outlet)	0.8641 g/cm <sup>3</sup> MARK-I (inlet)	7.788 g/cm <sup>2</sup> Bellows: 6.95V/O	6.95 V/O SS304	2.227 g/cm <sup>3</sup>	1.512 g/cm <sup>3</sup>	0.21 g/cm <sup>3</sup>	CH <sub>2</sub> : 0.722 g/cm <sup>3</sup> ~65%T.D.	SS: 15.56V/O Na: 15.17V/O (400°C)	SS: 15.56V/O Na: 84.44V/O (400°C)		

N. B. 1) Type 304 stainless steel.

2) Read as  $2.223 \times 10^{-2} \times 10^{24}$  atoms/cm<sup>3</sup>.



Table 3-1-2 Weighting spectrum<sup>1)</sup>

Group	Weight	Group	Weight
1	1.883	14	610.7
2	4.45	15	693.1
3	9.53	16	766.3
4	18.77	17	827.0
5	34.2	18	873.7
6	57.9	19	905.5
7	92.1	20	921.6
8	138.1	21	925.4
9	196.6	22-49	925.0
10	266.8	50-99	2313
11	346.7	100	1.0 <sup>2)</sup>
12	433.3		
13	522.7	-	-

N. B. 1) Fission spectrum ( $E \geq 2\text{Mev}$ )  
+  $1/E$  spectrum ( $E < 2\text{Mev}$ )

2) Maxwellian ( $300^\circ\text{K}$ )

Table 3-1-3 Energy group structure.

	No.	No.	Energy (ev)		Lethagy Width
Neutron	1	1 - 10	1.4918+7	5.4881+6	1.0
	2	11 - 15	5.4881+6		0.5
	3	16 - 20	3.3287+6		0.5
	4	21 - 25	2.0190+6		0.5
	5	26 - 30	1.2246+6		0.5
	6	31 - 35	7.4274+5		0.5
	7	36 - 40	4.5049+5		0.5
	8	41 - 45	2.7324+5		0.5
	9	46 - 51	1.6573+5		0.9
	10	52 - 55	6.7379+4		1.0
	11	56 - 59	2.4788+4		1.0
	12	60 - 63	9.1188+3		1.0
	13	64 - 67	3.3546+3		1.0
	14	68 - 71	1.2341+3		1.0
	15	72 - 75	4.5400+2		1.0
	16	76 - 80	1.6702+2		1.25
	17	87 - 85	4.7851+1		1.25
	18	86 - 90	1.3710+1		1.25
	19	91 - 95	3.9279+0		1.25
	20	96 - 99	1.1254+0		1.0
	21	100	4.1399-1	1.0-3	

Table 3-1-4 21 Group detector cross sections

(Unit: barns)

g	$^{197}\text{Au}(n,\gamma)$	$^{10}\text{B}(n,\alpha)$	$^{235}\text{U}(n,f)$	$^{232}\text{Th}(n,f)$	$^{238}\text{U}(n,f)$	$^{32}\text{S}(n,p)$
1	0.014	0.124	1.361	0.227	0.784	0.314
2	0.018	0.226	1.142	0.142	0.560	0.249
3	0.039	0.319	1.258	0.120	0.548	0.0917
4	0.070	0.345	1.259	0.070	0.315	2.71-3
5	0.087	0.232	1.197	5.1-5 <sup>1)</sup>	0.0160	2.04-5
6	0.124	0.595	1.156	0.0	8.1-4	0.0
7	0.185	0.948	1.238		1.0-4	
8	0.249	1.327	1.344		5.7-5	
9	0.316	1.920	1.580		4.3-5	
10	0.504	2.98	1.942		5.6-5	
11	0.926	4.85	2.530		8.5-5	
12	1.946	8.03	3.86		1.2-6	
13	4.14	13.35	6.17		8.2-9	
14	11.44	22.2	11.12		1.5-4	
15	13.28	36.8	17.45		3.5-9	
16	35.8	65.2	29.7		3.1-9	
17	0.551	122.1	48.1		4.8-9	
18	1128.1	229	40.9		8.5-9	
19	45.7	427	23.7		1.8-8	
20	25.4	746	72.9		1.6-8	
21	78.9	3041	448	0.0	1.8-9	0.0
MAT	1283	1273	1261	1296	1262	—

N. B. 1) Read as  $5.1 \times 10^{-5}$  barns

Table 3-1-4 (continued)

(Unit: barns)

g	$^{109}\text{Ag}(n,\gamma)^{109}\text{Ag}$ <sup>1)</sup>	$^{181}\text{Ta}(n,\gamma)$	$^{58}\text{Fe}(n,\gamma)$	$^{59}\text{Co}(n,\gamma)$	$^{123}\text{Sb}(n,\gamma)$	$^{50}\text{Cr}(n,\gamma)$	Dose conv. factors <sup>2)</sup>
1	2.16-3 <sup>3)</sup>	9.46-3	1.09-3	1.95-3	3.46-3	1.76-3	0.148
2	0.0230	0.0158	1.22-3	2.51-3	0.0145	3.34-3	0.146
3	0.0653	0.0378	1.22-3	3.35-3	0.0351	4.08-3	0.143
4	0.0914	0.0843	1.24-3	5.79-3	0.0579	4.35-3	0.135
5	0.0971	0.134	1.72-3	8.19-3	0.0810	5.96-3	0.115
6	0.128	0.183	2.57-3	8.50-3	0.0788	9.74-3	0.0827
7	0.229	0.240	2.68-3	0.0116	0.0851	0.0105	0.0569
8	0.356	0.278	2.97-3	0.0150	0.104	0.0129	0.0388
9	0.552	0.313	4.23-3	0.0175	0.155	0.0173	0.0236
10	0.936	0.600	4.96-3	0.0208	0.280	0.0349	0.0118
11	1.364	1.424	0.0178	0.0499	0.510	0.0327	5.49-3
12	2.007	2.916	0.0216	0.164	0.857	0.370	3.61-3
13	3.513	5.798	5.52-4	0.0425	1.377	0.110	3.67-3
14	5.734	12.41	9.70-4	0.0259	1.828	0.111	3.78-3
15	10.41	26.57	1.044	0.743	3.306	0.164	3.98-3
16	27.16	31.36	0.0107	47.613	7.949	0.278	4.18-3
17	26.53	87.12	0.0302	1.716	85.906	0.512	4.28-3
18	1044.3	416.3	0.0659	2.431	0.556	0.952	4.38-3
19	36.86	14.09	0.129	4.265	0.562	1.77	4.49-3
20	23.43	5.132	0.228	7.325	0.882	3.10	4.49-3
21	80.60	18.60	1.019	33.00	3.790	14.1	3.85-3
MAT	1373	1285	6432	1199	514	1241	

N. B. 1) Branching of  $^{109}\text{Ag}(n,\gamma)^{110\text{m}}\text{Ag}$  is 0.045

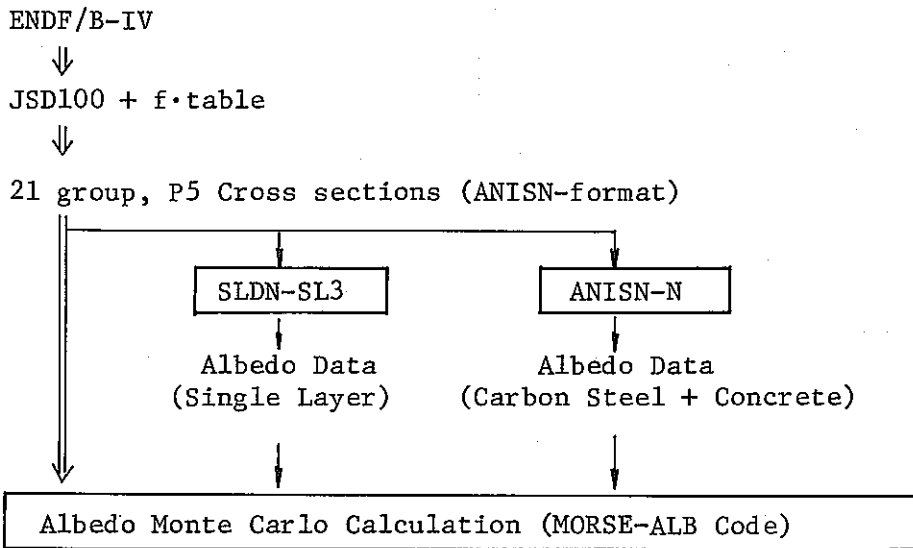
2) Unit: (mrem/hour)/(n/sec/cm<sup>2</sup>)

3) Read as  $2.16 \times 10^{-3}$  barns.

Table 3-1-5  $S_{16}$  Discrete Ordinates

n	$\mu_n$	$W_n$
1	-1.0	0.0
2	-0.98014493	0.02530713
3	-0.89833324	0.05559526
4	-0.76276621	0.07842666
5	-0.59171732	0.09067095
6	-0.40828268	0.09067095
7	-0.23723380	0.07842666
8	-0.10166676	0.05559526
9	-0.01985507	0.02530713
10	0.01985507	0.02530713
11	0.10166676	0.05559526
12	0.23723380	0.07842666
13	0.40828268	0.09067095
14	0.59171732	0.09067095
15	0.76276621	0.07842666
16	0.89833324	0.05559526
17	0.98014493	0.02530713

Group Constants



Streaming Analyses

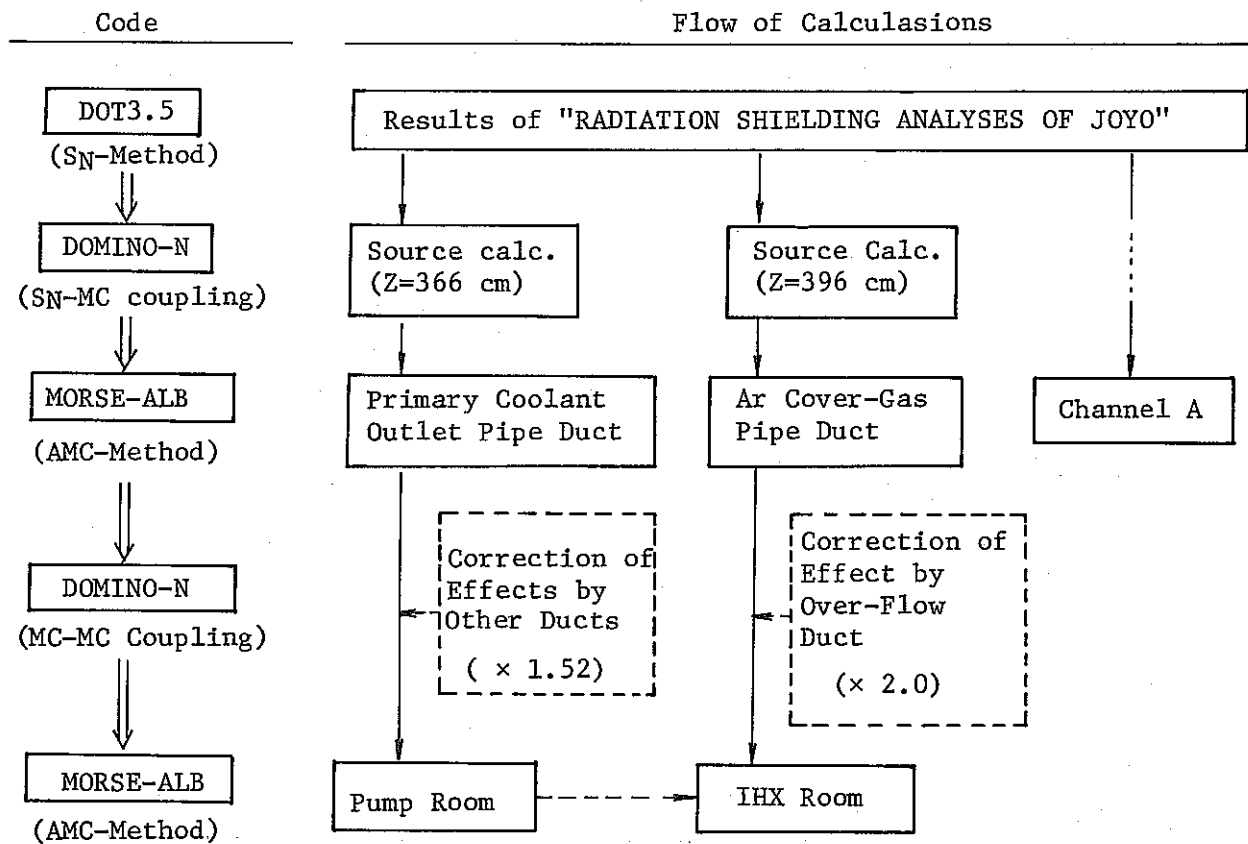


Fig. 3-0-1 Flow chart of neutron streaming analyses

C : (r=290cm, z=495cm)  
 D : (r=319cm, z=456cm)

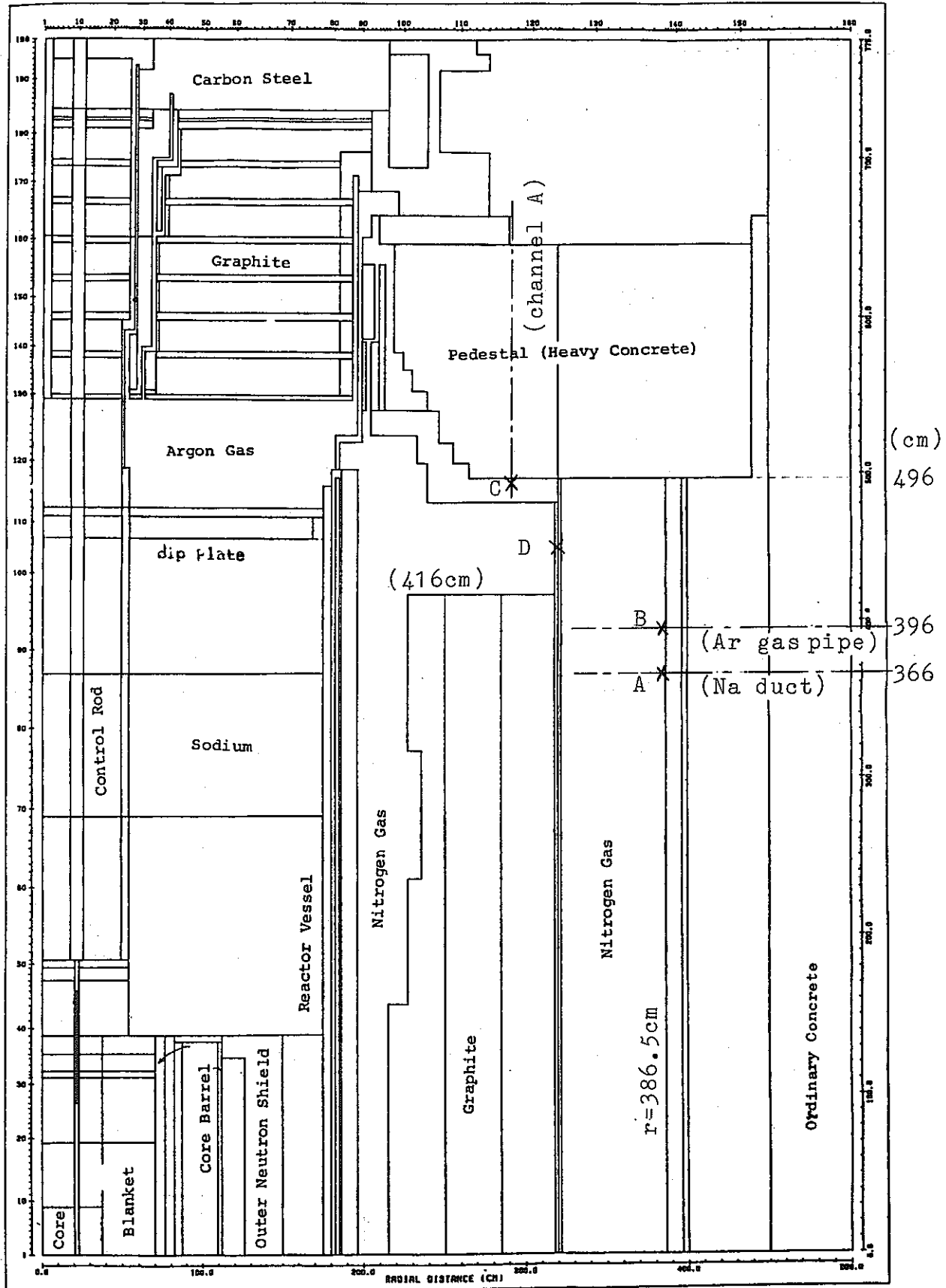
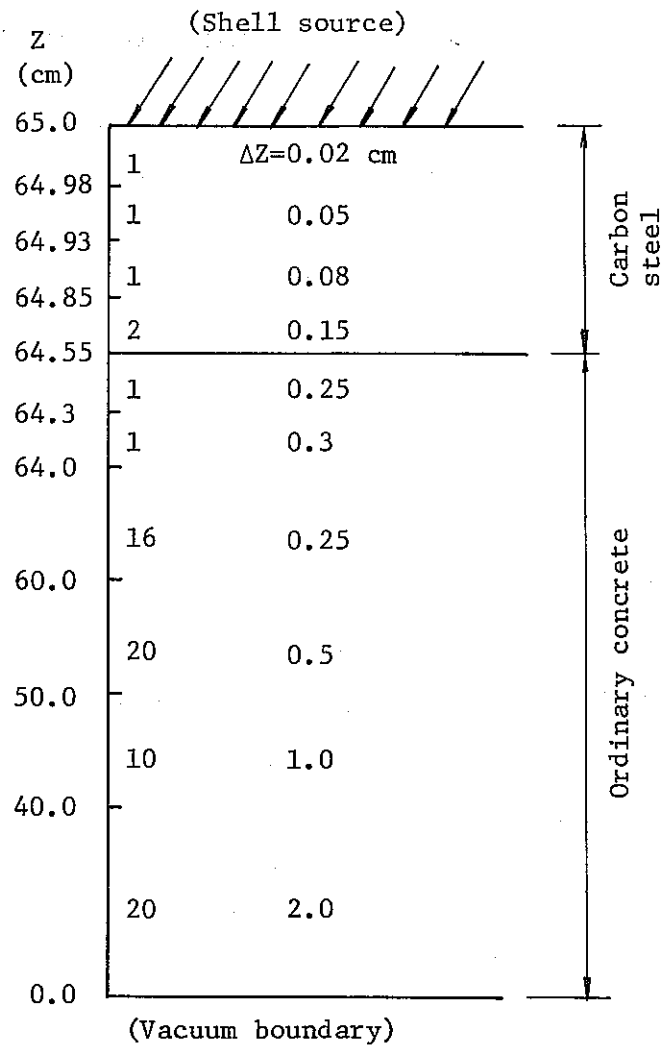


Fig. 3-0-2 Monte Carlo source locations in the two-dimensional configurations of JOYO.



Source : right boundary shell source  
 (21 groups \* 8 angle cases)

Approximation : P5-S16 (double Gauss quadrature)

Point flux convergence criteria : maximum error  $\leq 5 \times 10^{-4}$

Inner iteration limit : 30 times

Difference scheme : linear step mode

Computer code : ANISN-N (Improved version of ANISN code)

Computer : CYBER-176

Fig. 3-1-1 One dimensional model for albedo calculation.  
 (concrete slab with carbon steel liner of 0.45cm)



### 3.2 Analysis of the Neutron Streaming in the Channel A

As shown in Fig. 2-1-1, the Channel A is located 290 cm apart from the center axis of the reactor and penetrates pedestal and graphite shield. Measured values are obtained at the positions from 100 cm under the core mid-plane up to the top of the pedestal<sup>2,5)</sup>. In the previous analysis<sup>1,2)</sup>, the underestimation in the pedestal heavy concrete, (C/E) thermal flux =  $5.6 \times 10^{-3}$ , was found. It was because the streaming effect of the guide tube in the Channel A were not considered in the previous analysis. In this report, the neutron streaming in Channel A was calculated by using the albedo Monte Carlo code MORSE-ALB<sup>7 (11)</sup> and the calculated values were compared with the measured values.

#### 3.2.1 Model and Conditions of the Calculation

As shown in Fig. 3-2-1, the guide tube of the Channel A has a diameter of 16.52 cm and is made of 0.71 cm thick stainless steel. The calculational R-Z model is shown in Fig. 3-2-2. The source for the channel A is uniform and isotropic, and has the intensity equal to the scalar flux at the position C in Fig. 3-0-2, because the neutron flux distributions are nearly flat under the pedestal. The source spectrum for the Channel A is shown in Table 3-2-1. The albedo boundary of the heavy concrete was set on the outer surface of the guide tube. The number of histories in Monte Carlo calculation is 5,000 for this analysis.

### 3.2.2 Results

Albedo Monte Carlo calculation was carried out with the computer CYBER-176. The computing time was about 13 minutes in C.P.U. time.

Table 3-2-2 gives the calculated values of the thermal neutron flux, total neutron flux and neutron reaction rates. Standard deviations of the point detectors could be reduced to less than 9%, but standard deviation of the next event flux estimators<sup>11)</sup> got 54% at  $Z = 650$  cm. Nevertheless, results of the point detector and those of the next event flux estimator are in good agreement.

In the following discussion, results of the next event flux estimator at  $Z = 500$  cm and those of the point detector at  $Z = 550, 600, 650$  cm are compared with results of measurements<sup>5)</sup>.

### 3.2.3 Comparison with Measured and Calculated Value

The measured values of the thermal neutron flux and the reaction rates in the channel A are compared with the calculated values.

#### A. Thermal neutron flux

Thermal neutron flux in the Channel A was measured by using B-10 counter, TLD and Au foil. The measured values (E) are shown with the calculated values (C) and the C/E value in Table 3-2-3. The symbol  $\overline{C/E}$  means the normalized value by the value at  $Z = 500$  cm. The symbol  $(C/E)_{S_n}$  means the value which

was obtained in the previous analyses<sup>1,2)</sup> by using two-dimensional Sn transport code DOT-3.5<sup>12)</sup> in which the neutron streaming effect of the detector guide tube was not considered.

As shown in Table 3-2-3, the C/E values in the pedestal concrete (Z = 550 cm ~ 650 cm) distribute between 3.69 ~ 9.62, while the C/E values by the Sn calculation<sup>1,2)</sup> distribute between 0.15 ~  $5.6 \times 10^{-3}$ . The  $\overline{C/E}$  values show that the albedo Monte Carlo predicts the thermal neutron streaming within a factor of 2, taking off the uncertainty of source intensity. Fig. 3-2-3 shows the distribution of measured and calculated thermal neutron flux in the Channel A.

B. Reaction rates of  $^{10}\text{B}(n,\alpha)$

The reaction rates of  $^{10}\text{B}(n,\alpha)$  with and without the cadmium cover in the Channel A are measured. These measured values (E), the calculated values (C) and the C/E values are shown in Table 3-2-4. The calculated reaction rates of  $^{10}\text{B}(n,\alpha)$  without the Cd cover agree with the measured values within a factor of 3, while the calculated reaction rates of  $^{10}\text{B}(n,\alpha)$  with the Cd cover agree with the measured values within a factor of 5.

C. Reaction rates of  $\text{Au}(n,\gamma)$  and  $^{235}\text{U}(n,f)$

The reaction rates of  $\text{Au}(n,\gamma)$  and  $^{235}\text{U}(n,f)$  were also measured in the Channel A. These measured values (E), the calculated values and the C/E values are shown in Table 3-2-5. It is seen in the table that the previous  $S_n$  analyses

underestimated the reaction rates by about three orders of magnitude. However, the present albedo Monte Carlo calculation gave much better results within the error of an order of magnitude even if source uncertainty was included.

#### 3.2.4 Conclusion

In this study, it was clarified that the neutron streaming effect of detector guide tube was so large as to increase flux level in the channel by a few orders of magnitude, and that the effect could be estimated well. In conclusion, the present albedo Monte Carlo method evaluates the neutron streaming through the Channel A within a factor of  $2 \sim 3$ .

Table 3-2-1 Source for Channel A

Group	Upper energy of group (eV)	Source (n/cm <sup>2</sup> ·sec)
1	1.4918 + 7 <sup>1)</sup>	6.20 + 1
2	5.4881 + 6	1.99 + 2
3	3.3287 + 6	9.30 + 2
4	2.0190 + 6	6.46 + 3
5	1.2246 + 6	2.96 + 4
6	7.4274 + 5	7.89 + 4
7	4.5049 + 5	2.75 + 5
8	2.7324 + 5	7.19 + 5
9	1.6573 + 5	3.49 + 6
10	6.7379 + 4	8.60 + 6
11	2.4788 + 4	1.40 + 7
12	9.1188 + 3	2.09 + 7
13	3.3546 + 3	2.32 + 7
14	1.2341 + 3	3.26 + 7
15	4.5400 + 2	3.92 + 7
16	1.6702 + 2	6.16 + 7
17	4.7851 + 1	8.78 + 7
18	1.3710 + 1	1.13 + 8
19	3.9279 + 0	1.28 + 8
20	1.1254 + 0	1.01 + 8
21	4.1399 - 1	6.82 + 8
Total		1.32 + 9

N. B. 1) Read as  $1.4918 \times 10^7$  ev.

Table 3-2-2 Results of calculation by MORSE-ALB

Detector number	Detector	Position Z (cm)	Total flux (n/cm <sup>2</sup> ·s)	Thermal flux (n/cm <sup>2</sup> ·s)	Reaction rates of Au(n,γ)	Reaction rates (of <sup>10</sup> B(n,α))
1	Next Event	500	1.28+9 <sup>1)</sup> (1.3% <sup>2)</sup>	6.24+8(1.6%)	1.96+11(4.0%)	1.95+12(1.4%)
2	Point	550	4.08+7(3.2%)	1.84+7(2.8%)	6.67+9(5.4%)	5.82+10(2.6%)
3	Next Event		4.30+7(8.1%)	2.14+7(12.0%)	6.11+9(13.6%)	6.68+10(11.1%)
4	Point	600	6.42+6(5.9%)	3.04+6(6.4%)	1.04+9(8.9%)	9.57+9(6.0%)
5	Next Event		5.44+6(15.7%)	2.40+6(28.4%)	1.05+9(32.4%)	7.66+9(25.0%)
6	Point	650	1.87+6(3.2%)	8.95+5(1.9%)	2.81+8(2.9%)	2.81+9(2.0%)
7	Next Event		1.58+6(26.7%)	4.32+5(48.9%)	3.94+8(53.5%)	1.46+9(41.3%)

N. B. 1) Read as  $1.28 \times 10^9$  n/cm<sup>2</sup>/sec.

2) Standard Deviation.

Table 3-2-3 Comparison of thermal neutron flux with measured and calculated value in Channel A.

		500 cm	550 cm	600 cm	650 cm
Calculated value (n/cm <sup>2</sup> ·s)		6.24+8 <sup>3)</sup>	1.84 + 7	3.04 + 6	8.95 + 5
B-10 counter	Measured value (n/cm <sup>2</sup> ·s)	1.31 + 8	4.99 + 6	6.70 + 5	9.30 +44
	C/E	4.76	3.69	4.54	9.62
	$\overline{C/E}^{1)}$	1.0	0.78	0.95	2.02
	$(C/E)_{S_n}^{2)}$	3.14	0.15	0.029	5.6-3
TLD	Measured value (n/cm <sup>2</sup> ·s)	1.68 + 8	-	5.60 + 5	-
	C/E	3.71	-	5.43	-
	$\overline{C/E}^{1)}$	1.0	-	1.46	-
	$(C/E)_{S_n}^{2)}$	2.45	-	0.035	-
Au foil	Measured value (n/cm <sup>2</sup> ·s)	8.71 + 8			
	C/E	0.73	-	-	-
	$\overline{C/E}^{1)}$	-	-	-	-
	$(C/E)_{S_n}^{2)}$	0.47	-	-	-

N.B. 1) Normalized by the value at Z = 500 cm .

2) Obtained from "Radiation Shielding Analyses of Joyo"

(Ref. 1, 2) .

3) Read as  $6.24 \times 10^8$  n/cm<sup>2</sup>/sec.

Table 3-2-4 Comparison of B-10 reaction rates with measured and calculated value in Channel A

Position Z	B-10 Bare			B-10/Cd-Covered		
	Measured value (relative)	Calculated value	$C/E^1$	Measured value (relative)	Calculated value	$C/E^1$
500 cm	1.89 + 0 <sup>2)</sup>	2.08 + 12	1.0	5.84 - 1	1.84 + 11	1.0
550 cm	6.18 - 2	6.21 + 10	0.91	1.20 - 2	6.15 + 9	1.63
600 cm	7.90 - 3	1.02 + 10	1.17	1.20 - 3	9.67 + 8	2.56
650 cm	1.03 - 3	3.00 + 9	2.65	1.86 - 4	2.76 + 8	4.71

N. B. 1) Normalized by the value at Z = 500 cm.

2) Read as  $1.89 \times 10^0$ .



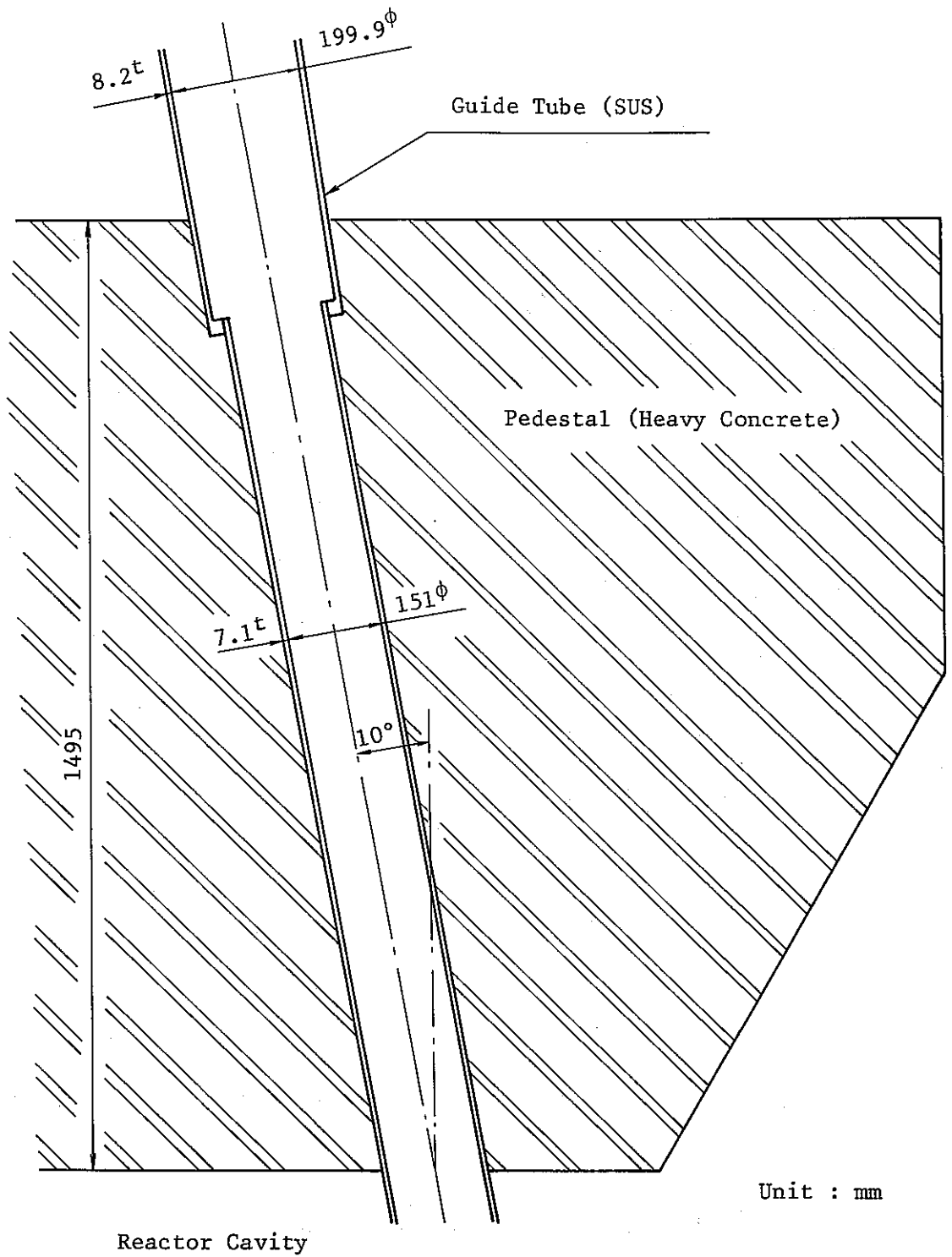
Table 3-2-5 Comparison of reaction rates with measured and calculated value in Channel A

Reaction & position	Measured value	Calculated value	C/E	$(C/E)_{S_n}^{1)}$
$^{197}\text{Au}(n,\gamma)$ at Z = 550 cm	$7.70 + 10^{2)}$	$6.67 + 9$	0.09	1.1 - 3
$^{197}\text{Au}(n,\gamma)/\text{Cd covered}$ at Z = 500 cm	$2.19 + 10$	$1.47 + 11$	6.70	3.69
$^{235}\text{U}(n,f)$ at Z = 550 cm	$2.06 - 3^{3)}$	$6.95 - 4^{3)}$	0.34	1.54 - 3

N. B. 1) Obtained from "Radiation Shielding Analysis of JOYO" (Ref. 1,2).

2) Read as  $7.70 \times 10^{10}$  reactions/ $10^{24}$  atom sec/100Mwt.

3) Normalized by the value on the core mid-plane (Z = 0 cm).



Unit : mm

Fig. 3-2-1 Configuration of Channel A

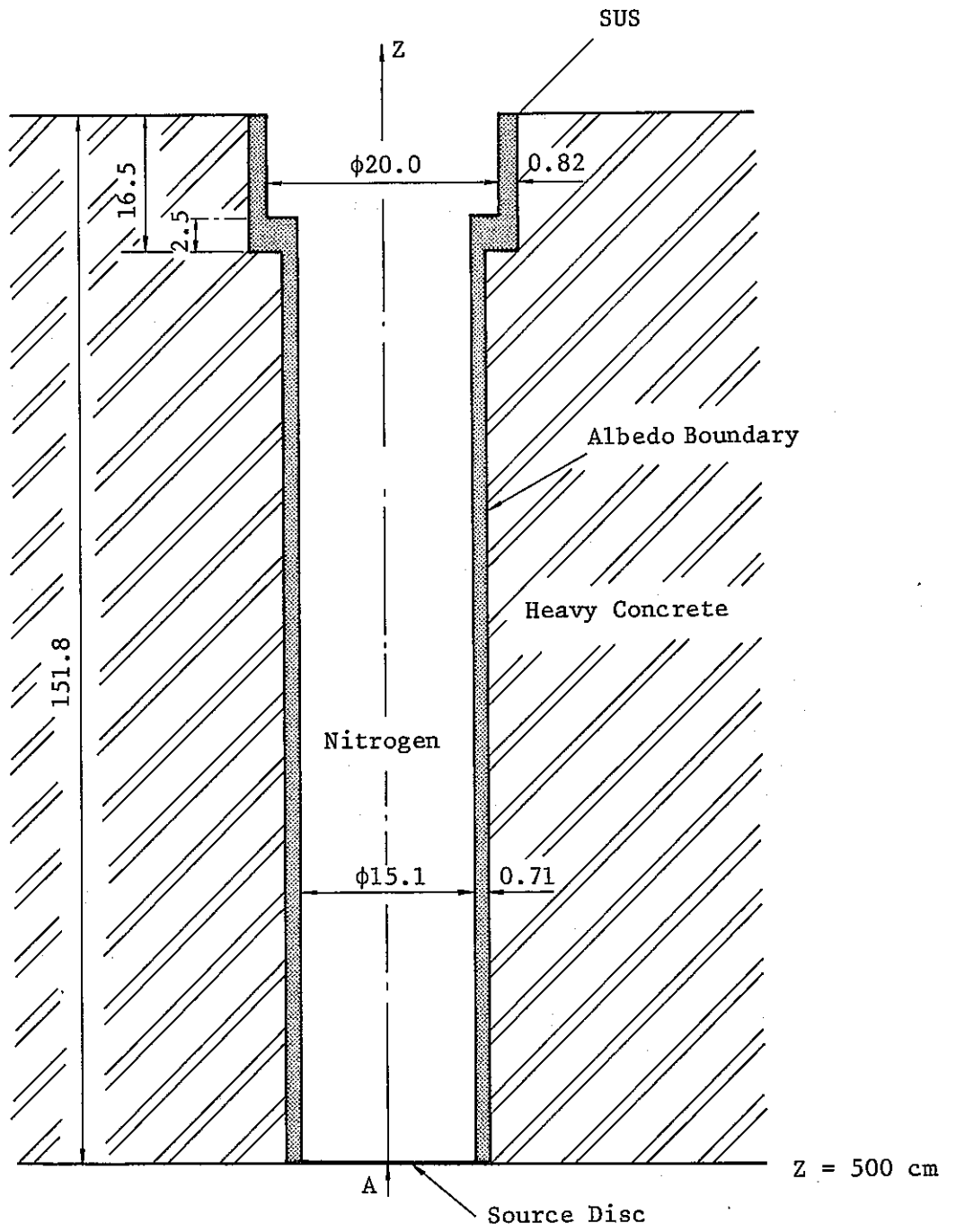


Fig. 3-2-2 MORSE R-Z geometry for the calculation of streaming in Channel A

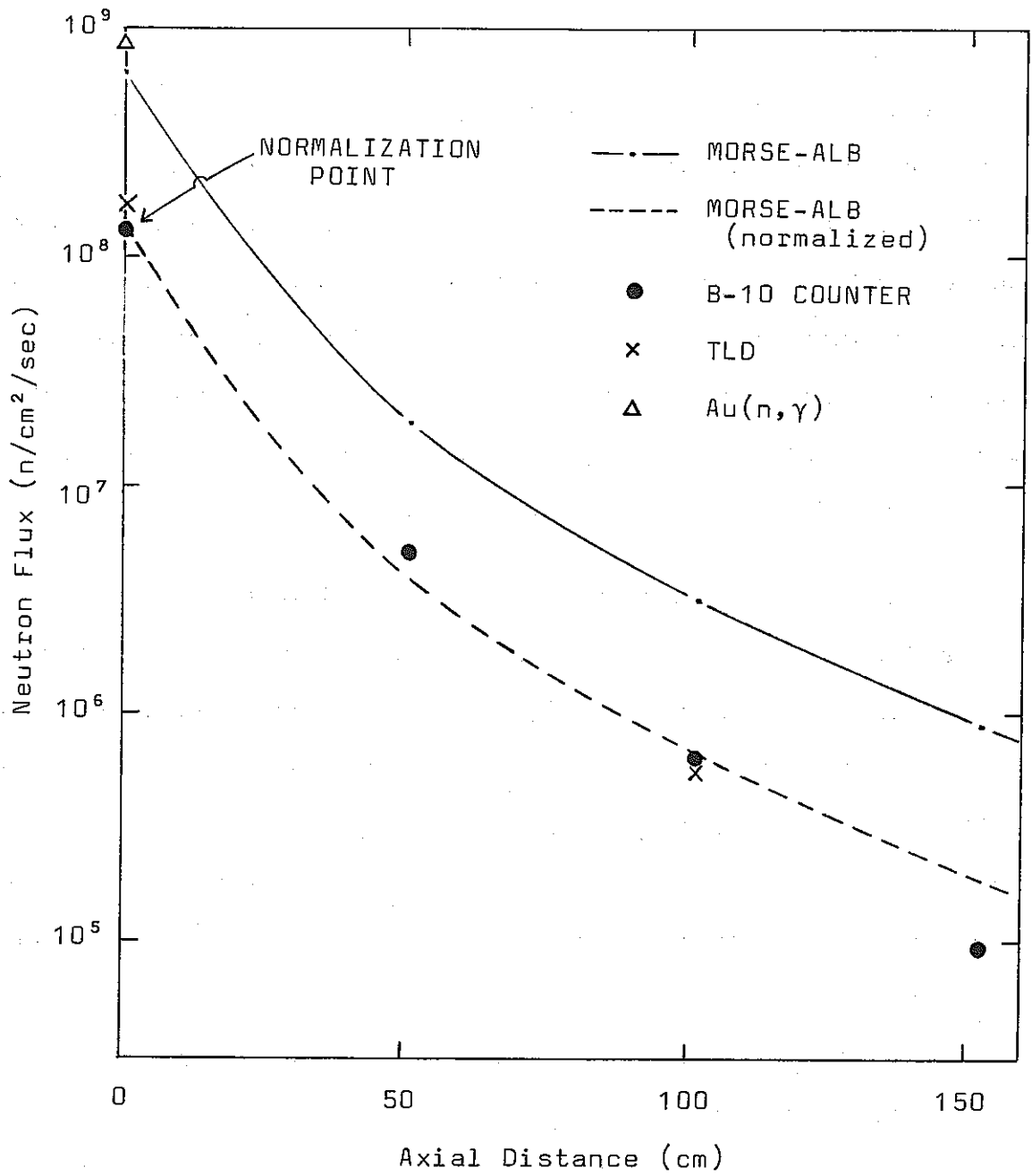


Fig. 3-2-3 Comparison of calculated and measured thermal neutron fluxes.

### 3.3 Neutron Streaming Analysis for the Primary Coolant Outlet Pipe Penetration

#### 3.3.1 Calculational Model

There are four penetrations through the biological concrete shield between the reactor vessel and the primary pump room. The penetrations are duct spaces for the primary coolant outlet and inlet pipes, argon cover gas pipe and the conduit for instrumentation cables. The shielding performance data concerning neutron streaming in JOYO were measured in the primary coolant outlet pipe penetration<sup>5)</sup> and were analyzed by the albedo Monte Carlo method<sup>7 ~ 11)</sup>.

Figure 3-3-2 shows the calculational model composed of 40 regions which are defined by the combination of 33 bodies with combinatory geometry<sup>17)</sup>, that is, 31 cylinders (RCC body) and 2 coniform bodies (TRC body) having a center axis coincident with the main axis of primary coolant pipe. The origin of the coordinate was set at the intersection of the pipe center axis and the reactor side surface of the concrete liner. The center axis of coolant pipe was taken as X-axis, and Z-axis was parallel to the core center axis. The area analyzed by Monte Carlo method extends from -20 cm to 140 cm in the X-direction and is inside a radius of 115 cm around the main axis of primary coolant pipe.

In the figure, neutron source position is also shown. A disc source with a radius of 80 cm was located 1.5 cm apart from the concrete liner towards the reactor. It was generated

by the DOMINO-N code<sup>10)</sup> from the scalar flux at R=382.9 cm of two-dimensional Sn transport calculation<sup>1,2)</sup> which was performed as an activity of PNC Specialists' Committee on FBR shielding calculation. Therefore, the source has a Z-dependence corresponding to the axial distribution of scalar flux in the two-dimensional RZ geometry and its overall intensity was  $8.42 \times 10^{11}$  n/sec. In Fig. 3-3-2, the hatched region of biological concrete shield was treated as an albedo medium. B<sub>4</sub>C shield was modeled with keeping a heterogeneous structure so as to evaluate the strong absorption.

### 3.3.2 Computational Condition

The albedo Monte Carlo calculations were carried out under the condition given in Table 3-3-1. Number of media is 8 including albedo medium in Table 3-3-2.

Neutron scoring was made by 13 point detectors which were located at the positions where the experimental data were measured and by 28 next event flux estimators<sup>11)</sup>, some of which gave the angle, space and energy dependent source data for the analysis of the primary pump room. The boundary crossing estimators were also arranged. The detector arrangement is shown in Table 3-3-3 and Fig. 3-3-3. The importance sampling techniques such as source energy biasing, exponential transformation and Russian roulette kill and survivals were employed for reducing a variance of Monte Carlo calculation. In Fig. 3-3-2, the biasing directions of path length stretching by exponential transformation are shown by an arrow (parameter PATH=0.5).

Table 3-3-4 lists the values of parameters for source energy biasing, Russian roulette kill and survival. Two Monte Carlo calculations were carried out in order to obtain the neutron spectrum in the overall energy range. One of them was executed for the whole neutron energy range with the 1st - 21st group neutron source, and another was for the fast neutrons with the 1st - 8th group neutron source by cutting off a history of which particle had slowed down to the lower energy than the 8th group. The source energy biasing factors were given as they are larger according as the neutron energy increase in order to make more neutrons generated in higher energy range. The common values were used in the 1st - 8th energy group for both runs. The number of histories were 7,500 for whole energy run (Case A) and 20,000 for fast neutron run (Case B).

### 3.3.3 Results

Albedo Monte Carlo calculations were made with the computer FACOM M200. The computing times were 73 minutes in C.P.U. time for Case A and 48 minutes for Case B. The first 8-groups results of Case A were replaced by the results of Case B. The calculated results were normalized to the condition of 100 MWth power.

#### A. Neutron flux and dose rate distributions

In this paragraph, the neutron flux and dose rate distributions are described to show the streaming effect upon the

neutron spatial and energetic distributions, and the effect of the neutron source distributed in the vertical direction.

Table 3-3-5 gives the calculated values for fast, thermal and total neutron flux and neutron dose rates. Figures 3-3-4 and 3-3-5 show their spatial distributions in the cavity between the thermal insulation and the biological shield concrete along the primary coolant pipe. The data plotted in the figures were obtained by the next event flux estimators (detector number 14-35). The data by point detectors are also plotted for thermal neutron flux so as to supplement the next event flux estimator results with a large variance behind B<sub>4</sub>C shield. The open symbol denotes the value in the upper half zone of cavity, while dotted symbol does the value in the lower-half zone.

In the figure, systematic differences are observed between the open and the dotted symbols according to the source spatial distribution in the vertical direction. For fast neutron, the value in the upper zone is larger than the value in the lower zone, because the fast neutrons outside the graphite shield are highly influenced by the downward streaming around the graphite shield. This tendency is clearer for total neutron flux and neutron dose rates of which the statistical error is much smaller. On the other hand, thermal neutron is much affected by the component of neutrons having slowed down in the graphite where thermal neutron flux



decreases as the height increases, so the value in the lower zone of the penetration is larger than the value in the higher zone.

The flux decreases to 1/23 for fast neutrons, 1/33 for thermal neutrons, 1/30 for total neutrons and 1/28 for neutron dose rates from the point 120 cm apart from the inner surface of B<sub>4</sub>C shield (reactor side) to the point 20 cm apart from that (pump room side) through the pipe penetration. This result suggests the weak spectrum hardening in the penetrations.

In Fig. 3-3-6, calculated neutron spectra at the typical positions in the penetration are compared with the source spectrum measured by the 42nd detector. It is observed that the spectra at the positions from the rear of the seal plate up to the front of B<sub>4</sub>C shield resembles to the source neutron spectrum. The dip of neutron spectrum behind the seal plate in the energy range between 167 eV and 454 eV seems to have been caused by the resonance of Mn in stainless steel. The neutron spectrum in the lower energy below 1 keV changes much due to the transmission through the B<sub>4</sub>C shield because of its strong shield effect upon slow neutron. Especially, so many particles representing thermal neutrons could not transmit the B<sub>4</sub>C shield. Therefore, the statistical errors of the calculated results by boundary crossing estimator became large. The results by point detector are of the accuracy nearly acceptable. The experimental data <sup>5)</sup> will be compared with the point detector results as described in the following paragraph.

B. Comparison of the calculation and the experiments

In the primary coolant outlet pipe penetration, the experimental data<sup>5)</sup> were obtained for thermal neutron flux, gold foil activation, reaction rate of  $^{50}\text{Cr}(n,\gamma)$ ,  $^{58}\text{Fe}(n,\gamma)$ ,  $^{59}\text{Co}(n,\gamma)$ , and  $^{123}\text{Sb}(n,\gamma)$ . Tables 3-3-6 through 3-3-9 show the C/E values for these measurements.

Quantities	Penetration at the reactor side of B <sub>4</sub> C shield	Behind B <sub>4</sub> C
Thermal neutron flux	0.63 ~ 0.80	-
$^{197}\text{Au}(n,\gamma)^{198}\text{Au}$	0.91 ~ 1.61	0.16
$^{197}\text{Au}(n,\gamma)^{198}\text{Au}/\text{Cd cover}$	0.92 ~ 2.35	0.15
Cd ratio of $^{197}\text{Au}(n,\gamma)$	0.89 ~ 1.18	0
$^{50}\text{Cr}(n,\gamma)^{51}\text{Cr}$	0.54 ~ 1.24	1/202 - 0.14
$^{58}\text{Fe}(n,\gamma)^{59}\text{Fe}$	0.53 ~ 1.23	1/54 - 0.20
$^{59}\text{Co}(n,\gamma)^{60}\text{Co}$	0.54 ~ 1.23	0.036 - 0.34
$^{123}\text{Sb}(n,\gamma)^{124}\text{Sb}$	0.57 ~ 1.64	0.083 - 0.25

The values mentioned above are relative ones normalized to the data at X = -100 cm in order to take off an ambiguity in the source spectrum and intensity for the Monte Carlo calculation. The calculated value agrees with the experimental value within the gap of 50% in the penetration at the reactor side of the B<sub>4</sub>C shield. In Figs. 3-3-7 through 3-3-13, the spatial distributions of the calculated reaction rates are compared with the experimental data. A good agreement between the calculated and the measured values is observed, although

slight fluctuations are seen in the calculated values of thermal neutron flux and gold foil activation.

Behind the  $B_4C$  shield, the present calculation underestimated the reaction rates. The reasons of this underestimation are as follows:

(1) There was a hole for inserting a foil holder in the  $B_4C$  shield, and neutrons streamed through this hole. Such a streaming effect is observed in the experimental data that the value behind the  $B_4C$  shield is higher than the value in the penetration at the reactor side of the shield and decreases sharply as the detector position leaves the shield. The calculation ignoring the hole underestimated the reaction rate along the hole.

(2) A wall scattering in the primary pump room behind the  $B_4C$  shield must have increased the experimental value. This effect increased thermal neutron flux by a factor of 3 as will be described in the following section.

The first reason should be main factor of discrepancy between the calculation and the experiment.

Comparing the measured data with the nominal values obtained by the albedo Monte Carlo calculation, the C/E values are 1/5 - 1/10 for thermal neutron flux and gold foil activation rate and 1/20 - 1/50 for capture rates such as  $^{50}Cr(n,\gamma)$ ,  $^{51}Cr$ ,  $^{58}Fe(n,\gamma)$ ,  $^{59}Fe$  and  $^{59}Co(n,\gamma)$ ,  $^{60}Co$ . These results suggests the trend that the neutron flux is underestimated more as the

neutron energy gets higher. The discrepancies between the calculational and the experimental results do not mean the defect of the albedo Monte Carlo method, but is fairly sure to have been caused by the underestimation of the source intensity and the too soft spectrum as is explained below. The primary coolant pipe penetrates through the hollow in the upper part of graphite from the reactor vessel to the biological shield concrete. The neutron streaming through this hollow increases neutron fluxes significantly near the duct mouth of primary coolant pipe in the biological concrete shield, and was not considered in the present calculation.

It can be concluded that the albedo Monte Carlo method predicts quite well neutron streaming through a penetration by using a well-described neutron source.

Table 3-3-1 Description of Input Parameters of Monte Carlo Calculation for Primary Coolant Outlet Pipe Penetration

Geometry .....	33 bodies with combinatory geometry <sup>17)</sup> 40 regions (see Fig. 3-3-2) 8 media include 1 albedo medium.
Corss section .....	P <sub>5</sub> , 21 groups (see Table 3-3-2)
Neutron source .....	Circular disc source with 80 cm radius. Energy-space-angular dependent. Generated by DOMINO-N code <sup>10)</sup> from the results of JOYO main shield analysis <sup>1,2)</sup>
Flux estimator .....	13 point, 29 next event surface crossing <sup>11)</sup> and 12 boundary crossing estimators (see Table 3-3-3 & Fig. 3-3-3)
Importance sampling ...	Russian roulette kill and survival (see Table 3-3-4) Source energy biasing (see Table 3-3-4) Exponential transformation (see Fig.3-3-2)
Calculation case .....	Case A: whole group calculation Case B: fast neutron calculation (1st - 8th group)
Histories .....	Case A: 7,500 histories Case B: 20,000 histories

Table 3-3-2 Cross section and albedo data for the streaming analysis of primary coolant outlet pipe penetration

Cross section

Medium No.	Input No.	Medium	(binary ID)
1	1	Sodium	100
2	2	SS304	200
3	3	Carbon steel	300
4	4	Concrete	400
5	5	B <sub>4</sub> C shield	500
6	6	Thermal insulation	600
7	7	Nitrogen gas	1000
8	-4	Concrete (albedo)	400

Albedo

No.	Medium No.	Medium
1	8	Concrete

Table 3-3-3 Detectors of Neutron Streaming Calculation for Primary Coolant Outlet Pipe Penetration

No.	Type	X	Y	Z	R <sub>1</sub>	R <sub>2</sub>	Comment
1	Point	3.6	56.3	-32.5	-	-	Attenuation in the sodium duct  Behind the B <sub>4</sub> C shield
2	↑	23.6	↑	↑	-	-	
3		43.6			-	-	
4		63.6			-	-	
5		83.6			-	-	
6		103.6			-	-	
7		113.6			-	-	
8		123.6			-	-	
9		126.6			-	-	
10		128.6	↓	↓	-	-	
11		138.6	56.3	-32.5	-	-	
12	↓	123.6	0.0	65.0	-	-	
13	Point	123.6	0.0	-65.0	-	-	
14	Ring	3.6	0.0	0.0	61.73	68.68	U <sup>1)</sup>
15	↑	3.6	↑	↑	↑	↑	L
16		23.6					U
17		23.6					L
18		43.6					U
19		43.6					L
20		63.6					U
21		63.6					L
22		83.6					U
23		83.6					L
24		103.6					U
25		103.6					L
26	↓	113.6	↓	↓	↓	↓	U
27	Ring	113.6	0.0	0.0	61.73	68.68	L

N.B. 1) U: upper half,  
L: lower half

Table 3-3-3 (cont'd)

No.	Type	X	Y	Z	R <sub>1</sub>	R <sub>2</sub>	Comment
28	Ring	123.6	0.0	0.0	61.73	68.68	} Behind the B <sub>4</sub> C shield
29	↓	123.6					
30		126.6					
31		126.6					
32		128.6					
33		128.6					
34	↓	138.6					
35	Ring	138.6	0.0	0.0	61.73	68.68	
36	Ring	123.6	0.0	0.0	0.0	24.45	} Source for R-206 room
37	↑				24.45	29.35	
38					29.35	49.5	
39					49.5	68.68	
40					68.68	76.5	
41	↓	123.6	0.0	0.0	76.5	110.0	
42	Ring	-1.4	0.0	0.0	0.0	90.0	On the source plane
43	Cylinder	92.58	0.0	0.0	R= 110.0	H= 31.02	Source for R-206 room
44	Boundary cross.	<u>Region</u>	<u>Region</u>	-	-	-	} Pump room side
		12	26				
45	↑	12	24	-	-	-	
46		13	24	-	-	-	
47		30	19	-	-	-	
48		19	31	-	-	-	
49		36	37	-	-	-	
50		15	17	-	-	-	
51		33	17	-	-	-	
52		23	16	-	-	-	
53		23	6	-	-	-	} Reactor side
54		38	5	-	-	-	
55	Bound. Cros.	39	1	-	-	-	



Table 3-3-4 Importance sampling parameters for Monte Carlo calculation of primary coolant pipe penetration.

Source energy biasing factor

g	Case A	Case B	g	Case A	Case B	
1	30,000	30,000	12	7.62	0.0	
2	16,000	16,000	13	7.06		
3	5,000	5,000	14	6.26		
4	1,200	1,200	15	5.82		
5	245.1	245.1	16	4.55		
6	125.9	125.9	17	3.94		
7	63.56	63.56	18	3.58		
8	39.82	39.82	19	3.50		
9	16.75	0.0	20	4.13		
10	10.48		21	1.35		0.0
11	9.34	0.0				

Russian roulette kill condition

Region	g = 1-4	5-8	5-15	16-20	21
1-14	$10^{-7}$	$10^{-6}$	$10^{-5}$	$10^{-4}$	$10^{-3}$
15-16	$10^{-6}$	$10^{-4}$	$10^{-3}$	$10^{-2}$	$5 \times 10^{-2}$
17-31	$10^{-7}$	$10^{-6}$	$10^{-5}$	$10^{-4}$	$10^{-3}$
32-33	$10^{-5}$	$10^{-4}$	$10^{-3}$	$10^{-2}$	$5 \times 10^{-2}$
34-40	$10^{-7}$	$10^{-6}$	$10^{-4}$	$10^{-3}$	$10^{-2}$

Table 3-3-5 Neutron flux and dose rate distribution in the primary sodium duct

FAST NEUTRON FLUENCE ABOVE 0.1 MEV

THERMAL FLUXES

DETECTOR	FLUX	FSD	MIN	MAX	DETECTOR	FLUX	FSD	MIN	MAX
1	7.4833E+04	.223	5.8179E+04	9.1487E+04	1	9.8941E+06	.118	8.7245E+06	1.1064E+07
2	5.5051E+04	.227	4.2529E+04	6.7572E+04	2	8.4229E+06	.103	7.5592E+06	9.2865E+06
3	2.6031E+04	.165	2.1747E+04	3.0314E+04	3	6.4678E+06	.209	5.1147E+06	7.8210E+06
4	1.4812E+04	.123	1.2987E+04	1.6636E+04	4	3.1513E+06	.285	2.2532E+06	4.0495E+06
5	9.7792E+03	.106	8.7423E+03	1.0816E+04	5	9.4661E+05	.103	8.4924E+05	1.0440E+06
6	5.5293E+03	.129	4.8181E+03	6.2405E+03	6	5.0758E+05	.218	3.9672E+05	6.1844E+05
7	4.4031E+03	.130	3.8315E+03	4.9747E+03	7	3.8618E+05	.133	3.3477E+05	4.3760E+05
8	2.8063E+03	.137	2.4210E+03	3.1916E+03	8	4.1363E+02	.499	2.0713E+02	6.2013E+02
9	2.7471E+03	.134	2.3793E+03	3.1149E+03	9	1.5753E+03	.545	7.1669E+02	2.4338E+03
10	2.6339E+03	.132	2.2866E+03	2.9811E+03	10	3.0957E+03	.444	1.7201E+03	4.4713E+03
11	2.3612E+03	.138	2.0347E+03	2.6876E+03	11	3.4183E+03	.488	1.7487E+03	5.0879E+03
12	6.7362E+03	.120	5.9284E+03	7.5440E+03	12	7.5195E+02	.455	4.0986E+02	1.0940E+03
13	2.7490E+03	.213	2.1639E+03	3.3340E+03	13	1.8538E+03	.491	9.4285E+02	2.7648E+03
14	1.5935E+05	.205	1.2662E+05	1.9207E+05	14	1.2640E+07	.124	1.1074E+07	1.4206E+07
15	9.0831E+04	.283	6.5128E+04	1.1653E+05	15	1.4632E+07	.095	1.3239E+07	1.6024E+07
16	1.9081E+05	.712	5.5021E+04	3.2660E+05	16	6.7675E+06	.078	6.2413E+06	7.2937E+06
17	5.3195E+04	.265	3.9085E+04	6.7306E+04	17	1.0826E+07	.114	9.5934E+06	1.2059E+07
18	3.9188E+04	.262	2.8911E+04	4.9464E+04	18	4.1395E+06	.107	3.6982E+06	4.5809E+06
19	3.3880E+04	.407	2.0081E+04	4.7679E+04	19	6.2679E+06	.145	5.3601E+06	7.1757E+06
20	1.6751E+04	.239	1.2743E+04	2.0758E+04	20	4.1055E+06	.190	3.3256E+06	4.8854E+06
21	2.1836E+04	.482	1.1318E+04	3.2355E+04	21	3.9628E+06	.158	3.3358E+06	4.5898E+06
22	2.8596E+04	.329	1.9180E+04	3.8012E+04	22	1.1974E+06	.180	9.8235E+05	1.4125E+06
23	9.9112E+03	.288	7.0536E+03	1.2769E+04	23	1.7302E+06	.144	1.4818E+06	1.9786E+06
24	1.1761E+04	.395	7.1146E+03	1.6408E+04	24	4.7330E+05	.333	3.1562E+05	6.3099E+05
25	7.1501E+03	.436	4.0319E+03	1.0268E+04	25	7.5655E+05	.279	5.4559E+05	9.6751E+05
26	6.8876E+03	.341	4.5415E+03	9.2337E+03	26	4.4816E+05	.284	3.2075E+05	5.7557E+05
27	3.7502E+03	.339	2.4789E+03	5.0215E+03	27	3.6842E+05	.219	2.8780E+05	4.4904E+05
28	2.7516E+03	.106	2.4605E+03	3.0426E+03	28	2.5120E+04	.998	5.0294E+01	5.0190E+04
29	2.7038E+03	.293	1.9116E+03	3.4960E+03	29	1.1283E+02	1.000	6.8405E-05	2.2567E+02
30	2.4243E+03	.087	2.2134E+03	2.6353E+03	30	1.1955E+01	1.000	5.6482E-05	2.3911E+01
31	2.7052E+03	.293	1.9118E+03	3.4985E+03	31	1.8815E-03	.966	6.4897E-05	3.6981E-03
32	2.5546E+03	.118	2.2529E+03	2.8563E+03	32	2.0714E+03	.548	9.3626E+02	3.2065E+03
33	1.8884E+03	.235	1.4453E+03	2.3314E+03	33	1.5788E+04	.999	1.7848E+01	3.1558E+04
34	2.1873E+03	.237	1.6695E+03	2.7052E+03	34	2.2488E+02	.922	1.7582E+01	4.3219E+02
35	9.3312E+02	.153	7.9063E+02	1.0756E+03	35	4.5087E+02	.974	1.1774E+01	8.8996E+02
36	1.5498E+03	.352	1.0038E+03	2.0957E+03	36	1.5500E+05	.239	1.1798E+05	1.9202E+05
37	8.2993E+02	.296	5.8392E+02	1.0759E+03	37	1.6704E+05	.366	1.0593E+05	2.2815E+05
38	2.4982E+03	.342	1.6429E+03	3.3536E+03	38	2.0969E+04	.248	1.5761E+04	2.6178E+04
39	2.5555E+03	.120	2.2501E+03	2.8609E+03	39	5.1484E+03	.974	1.3628E+02	1.0161E+04
40	2.2688E+03	.366	1.4386E+03	3.0990E+03	40	3.8284E-01	.644	1.3631E-01	6.2937E-01
41	1.1079E+03	.228	8.5495E+02	1.3608E+03	41	6.1484E+03	.655	2.1215E+03	1.0175E+04
42	3.0927E+05	.165	2.5820E+05	3.6035E+05	42	6.4458E+07	.032	6.2404E+07	6.6512E+07
43	1.5590E+02	.295	1.0988E+02	2.0192E+02	43	5.2392E+02	.616	2.0124E+02	8.4660E+02
44	1.5028E+08	.216	1.1787E+08	1.8269E+08	44	1.1978E+10	.194	9.6586E+09	1.4298E+10
45	3.9212E+07	.318	2.6740E+07	5.1685E+07	45	1.7435E+09	.223	1.3548E+09	2.1322E+09
46	5.1199E+07	.360	3.2758E+07	6.9641E+07	46	2.1537E+07	.589	8.8473E+06	3.4227E+07
47	1.5106E+07	.713	4.3349E+06	2.5877E+07	47	7.9929E+08	.303	5.5708E+08	1.0415E+09
48	1.3736E+07	.782	2.9907E+06	2.4481E+07	48	1.0831E+07	.848	1.6426E+06	2.0020E+07
49	1.2733E+06	.275	9.2333E+05	1.6233E+06	49	6.2663E+08	.267	4.5910E+08	7.9416E+08
50	5.7058E+06	.377	3.5535E+06	7.8581E+06	50	7.8619E+08	.290	5.5794E+08	1.0144E+09
51	6.2898E+06	.546	2.8578E+06	9.7218E+06	51	1.0094E+09	.458	5.4757E+08	1.4712E+09
52	3.9704E+09	.106	3.5499E+09	4.3909E+09	52	1.0084E+12	.042	9.6593E+11	1.0508E+12
53	2.2743E+08	.242	1.7249E+08	2.8237E+08	53	7.7597E+10	.147	6.6163E+10	8.9031E+10
54	5.2839E+08	.128	4.6053E+08	5.9625E+08	54	2.5513E+11	.071	2.3693E+11	7.7332E+11
55	2.6476E+08	.219	2.0680E+08	3.2272E+08	55	1.0998E+11	.079	1.0126E+11	1.1870E+11

Table 3-3-5 (cont'd)

## TOTAL FLUXES

## UNIT RESPONSE FOR ALL GROUPS

## NEUTRON DOSE CONVERSION 21G MREM/HR

DETECTOR	FLUX	FSD	MIN	MAX	DETECTOR	DOSE RATE	FSD	MIN	MAX
1	1.6690E+07	.081	1.5333E+07	1.8046E+07	1	7.6235E+04	.077	7.0328E+04	8.2141E+04
2	1.5044E+07	.091	1.3681E+07	1.6407E+07	2	6.9207E+04	.089	6.3034E+04	7.5381E+04
3	1.0333E+07	.136	8.9287E+06	1.1737E+07	3	4.4876E+04	.122	3.9399E+04	5.0354E+04
4	5.8898E+06	.163	4.9278E+06	6.8518E+06	4	2.5543E+04	.148	2.1771E+04	2.9316E+04
5	2.5173E+06	.115	2.2266E+06	2.8080E+06	5	1.1469E+04	.112	1.0190E+04	1.2748E+04
6	1.0680E+06	.128	9.3080E+05	1.2051E+06	6	4.9332E+03	.113	4.3748E+03	5.4916E+03
7	8.8339E+05	.097	7.9757E+05	9.6920E+05	7	4.0559E+03	.090	3.6926E+03	4.4192E+03
8	7.8888E+04	.092	7.1666E+04	8.6110E+04	8	5.9088E+02	.071	5.4873E+02	6.3303E+02
9	8.3717E+04	.093	7.5935E+04	9.1499E+04	9	6.2109E+02	.072	5.7638E+02	6.6579E+02
10	8.6800E+04	.092	7.8821E+04	9.4779E+04	10	6.2902E+02	.073	5.8302E+02	6.7502E+02
11	8.0004E+04	.092	7.2649E+04	8.7360E+04	11	5.8239E+02	.078	5.3704E+02	6.2774E+02
12	2.3235E+05	.093	2.1071E+05	2.5399E+05	12	1.7273E+03	.074	1.5987E+03	1.8559E+03
13	7.3903E+04	.081	6.7953E+04	7.9852E+04	13	6.0198E+02	.107	5.3758E+02	6.638E+02
14	4.0668E+07	.079	3.7437E+07	4.3898E+07	14	2.1917E+05	.093	1.9879E+05	2.3956E+05
15	2.9662E+07	.136	2.5621E+07	3.3702E+07	15	1.4011E+05	.126	1.2248E+05	1.5775E+05
16	2.0024E+07	.053	1.8965E+07	2.1083E+07	16	1.0522E+05	.078	9.7036E+04	1.1340E+05
17	1.6227E+07	.084	1.4866E+07	1.7588E+07	17	6.9782E+04	.079	6.4301E+04	7.5264E+04
18	1.0118E+07	.067	9.4351E+06	1.0801E+07	18	4.7301E+04	.067	4.4137E+04	5.0466E+04
19	1.0125E+07	.106	9.0543E+06	1.1196E+07	19	4.4457E+04	.098	4.0101E+04	4.8813E+04
20	8.8367E+06	.119	7.7891E+06	9.8843E+06	20	4.4254E+04	.122	3.8833E+04	4.9675E+04
21	7.1870E+06	.112	6.3829E+06	7.9912E+06	21	3.1223E+04	.107	2.7871E+04	3.4574E+04
22	2.8535E+06	.096	2.5803E+06	3.1266E+06	22	1.6047E+04	.101	1.4427E+04	1.7667E+04
23	3.3492E+06	.128	2.9204E+06	3.7780E+06	23	1.5052E+04	.128	1.3129E+04	1.6974E+04
24	1.4153E+06	.147	1.2067E+06	1.6239E+06	24	7.6900E+03	.140	6.6129E+03	8.7671E+03
25	1.2582E+06	.182	1.0289E+06	1.4874E+06	25	5.8516E+03	.167	4.8770E+03	6.8262E+03
26	1.4542E+06	.136	1.2563E+06	1.6522E+06	26	7.7267E+03	.135	6.6808E+03	8.7726E+03
27	1.0274E+06	.156	8.6671E+05	1.1881E+06	27	4.8679E+03	.157	4.1013E+03	5.6345E+03
28	3.7753E+05	.288	2.6880E+05	4.8625E+05	28	3.1595E+03	.281	2.2729E+03	4.0460E+03
29	8.5883E+04	.215	6.7398E+04	1.0437E+05	29	5.2519E+02	.185	4.2786E+02	6.2252E+02
30	2.4410E+05	.228	1.8851E+05	2.9970E+05	30	1.9678E+03	.230	1.5156E+03	2.4200E+03
31	1.5780E+05	.523	7.5242E+04	2.4035E+05	31	8.4007E+02	.417	4.8952E+02	1.1906E+03
32	2.4201E+05	.229	1.8648E+05	2.9755E+05	32	1.9607E+03	.231	1.5085E+03	2.4130E+03
33	9.5151E+04	.262	7.0233E+04	1.2007E+05	33	5.3979E+02	.214	4.2411E+02	6.5548E+02
34	1.8764E+05	.187	1.5255E+05	2.2274E+05	34	1.5294E+03	.255	1.1401E+03	1.9187E+03
35	6.0464E+04	.272	4.4015E+04	7.6913E+04	35	3.4693E+02	.242	2.6304E+02	4.3083E+02
36	4.0814E+05	.144	3.4948E+05	4.6681E+05	36	1.7725E+03	.139	1.5266E+03	2.0184E+03
37	2.7074E+05	.242	2.0510E+05	3.3637E+05	37	1.5481E+03	.247	1.1658E+03	1.9305E+03
38	1.9712E+05	.254	1.4697E+05	2.4727E+05	38	1.0781E+03	.200	8.6231E+02	1.2939E+03
39	2.0107E+05	.139	1.7310E+05	2.2904E+05	39	1.6930E+03	.168	1.4083E+03	1.9778E+03
40	5.0165E+04	.189	4.0668E+04	5.9662E+04	40	4.4023E+02	.186	3.5844E+02	5.2202E+02
41	4.0126E+04	.154	3.3944E+04	4.6309E+04	41	2.4030E+02	.120	2.1148E+02	2.6912E+02
42	1.0702E+08	.021	1.0474E+08	1.0929E+08	42	4.9649E+05	.021	4.8612E+05	5.0687E+05
43	1.6916E+04	.256	1.2587E+04	2.1244E+04	43	8.9124E+01	.221	6.9439E+01	1.0881E+02
44	2.6741E+10	.114	2.3680E+10	2.9802E+10	44	1.2598E+08	.103	1.1296E+08	1.3899E+08
45	6.6857E+09	.113	5.9269E+09	7.4444E+09	45	3.4897E+07	.112	3.0972E+07	3.8823E+07
46	1.9057E+09	.232	1.4633E+09	2.3482E+09	46	1.1207E+07	.185	9.1343E+06	1.3279E+07
47	2.1900E+09	.156	1.8479E+09	2.5320E+09	47	1.0632E+07	.153	9.0001E+06	1.2264E+07
48	4.2489E+08	.223	3.3013E+08	5.1966E+08	48	3.2254E+06	.261	2.3823E+06	4.0685E+06
49	1.0976E+09	.179	9.0109E+08	1.2941E+09	49	4.5481E+06	.173	3.7601E+06	5.3362E+06
50	1.0977E+09	.220	8.5581E+08	1.3395E+09	50	4.7912E+06	.202	3.8253E+06	5.7571E+06
51	1.4137E+09	.339	9.3498E+08	1.8924E+09	51	7.8399E+06	.338	5.1881E+06	1.0492E+07
52	1.6922E+12	.027	1.6458E+12	1.7386E+12	52	7.8784E+09	.026	7.6750E+09	8.0818E+09
53	1.1751E+11	.105	1.0522E+11	1.2979E+11	53	5.3529E+08	.096	4.8394E+08	5.8665E+08
54	3.9407E+11	.049	3.7483E+11	4.1330E+11	54	1.7339E+09	.045	1.6552E+09	1.8125E+09
55	2.1100E+11	.075	1.9525E+11	2.2674E+11	55	9.3520E+08	.067	8.7208E+08	9.9831E+08

Table 3-3-6 Thermal neutron flux in the primary coolant pipe penetration

(Unit: n/cm<sup>2</sup>/sec/100MW<sub>t</sub>)

Position <sup>1)</sup> (cm)	Exp.	Point detector		Next event (upper half)		Next event (lower half)	
		Calc. (fsd %)	Relative (Absolute) C/E <sup>2)</sup> (C/E)	Calc. %	Relative (Absolute) C/E <sup>2)</sup> (C/E)	Calc. (fsd %)	Relative (Absolute) C/E <sup>2)</sup> (C/E)
Core-ward							
-120	8.0+7 <sup>3)</sup> ±20%	9.89+6 (12)	0.71 (0.12)	1.27+7 (12)	1.15 (0.16)	1.46+7 (9.5)	0.87 (0.18)
-100	4.9+7 ±20%	8.42+6 (10)	1.00 (0.17)	6.76+6 (7.8)	1.00 (0.14)	1.08+7 (11)	1.00 (0.22)
-80	3.6+7 ±20%	6.47+6 (21)	1.05 (0.18)	4.14+6 (11)	0.83 (0.12)	6.27+6 (15)	0.79 (0.17)
-60	2.5+7 ±23%	3.15+6 (29)	0.73 (0.13)	4.11+6 (19)	1.19 (0.16)	3.97+6 (16)	0.72 (0.16)
-40	8.7+6 ±24%	9.47+6 (10)	0.63 (0.11)	1.20+6 (18)	1.00 (0.14)	1.73+6 (14)	0.90 (0.20)
-20	3.7+6 ±26%	5.08+5 (22)	0.80 (0.14)	4.73+5 (33)	0.93 (0.13)	7.57+5 (28)	0.93 (0.20)
-10	-	3.86+5 (13)	- -	4.48+5 (28)	- -	3.69+5 (22)	- -
0	-	4.14+2 (50)	- -	2.51+4 (100)	- -	1.13+2 (100)	- -
3	-	1.58+3 (55)	- -	1.20+1 (100)	- -	1.88-3 (97)	- -
5	-	3.10+3 (44)	- -	2.07+3 (55)	- -	1.58+4 (100)	- -
15	-	3.42+3 (49)	- -	2.25+2 (92)	- -	4.51+2 (97)	- -

3-41

- N.B. 1) Distance from outer surface of B<sub>4</sub>C shield.  
 2) Normalized at the position of -100 cm near the source  
 3) Read as 8.0 × 10<sup>7</sup> n/cm<sup>2</sup>/sec.

Table 3-3-7  $^{197}\text{Au}(n, \gamma) ^{198}\text{Au}$  reaction rate in the primary coolant pipe penetration

Position <sup>1)</sup> (cm)	$^{197}\text{Au}(n, \gamma) ^{198}\text{Au}$ (bare foil)			$^{197}\text{Au}(n, \gamma) ^{198}\text{Au}$ (with Cd cover)		
	Exp.	Calc. (fsd %)	Relative (Absolute) C/E <sup>2)</sup> C/E	Exp.	Calc. (fsd %)	Relative (Absolute) CE <sup>2)</sup> C/E
Core-ward						
-120	2.25+10 <sup>3)</sup>	2.08+9 (19)	0.81 (0.092)	1.64+10	1.29+9 (30)	0.92 (0.079)
-100	1.19+10	1.36+9 (9)	1.00 (0.11)	8.15+9	6.98+8 (15)	1.00 (0.086)
-80	7.70+9	1.42+9 (19)	1.61 (0.18)	4.90+9	9.12+8 (28)	2.17 (0.19)
-60	4.82+9	7.67+8 (24)	1.39 (0.16)	2.89+9	5.18+8 (32)	2.09 (0.18)
-40	2.27+9	2.36+8 (10)	0.91 (0.10)	1.61+9	1.61+8 (14)	1.17 (0.10)
-20	9.70+8	1.78+8 (45)	1.61 (0.18)	6.87+8	1.38+8 (57)	2.35 (0.20)
-10	-	8.79+7 (13)	-	-	5.74+7 (19)	-
0 <sup>4)</sup>	3.38+8	5.99+6 (20)	0.16 (1/56)	4.72+8	5.96+6 (20)	0.15 (1/79)
3 <sup>4)</sup>	-	5.65+6 (13)	-	-	5.53+6 (13)	-
5 <sup>4)</sup>	-	5.70+6 (12)	-	-	5.45+6 (13)	-
15 <sup>4)</sup>	-	5.30+6 (13)	-	-	5.03+6 (13)	-

N.B. 1) Distance from outer surface of B<sub>4</sub>C shield.

2) Normalized at the position of -100 cm near the source.

3) Read as  $2.25 \times 10^{10}$  reactions/(sec·10<sup>24</sup>atoms·100MW<sub>t</sub>)

4) The experimental value is uncertain because of low power level and is influenced by neutron streaming through a detector hole in the B<sub>4</sub>C shield. Calculated value does not contain a contribution of wall scattering in the primary pump room.

Table 3-3-8 Cd Ratio for  $^{197}\text{Au}(n,\gamma)^{198}\text{Au}$  reaction in the primary coolant pipe penetration

Position <sup>1)</sup> (cm)	Exp.	Calc. (f.s.d.) %	Relative C/E <sup>2)</sup>	(Absolute) C/E
Core-ward				
-120	1.37 ±2.9%	1.61 (36)	1.04	(1.18)
-100	1.46 ±4.1%	1.67 (17)	1.00	(1.14)
-80	1.56 ±5.3%	1.55 (34)	0.87	(0.99)
-60	1.67 ±6.7%	1.48 (40)	0.78	(0.89)
-40	1.42 ±9.3%	1.47 (17)	0.91	(1.04)
-20	1.42 ±14.1%	1.29 (73)	0.80	(0.91)
-10	-	1.53 (23)	-	-
0	-	1.01 (28)	-	-
3	-	1.02 (18)	-	-
5	-	1.05 (18)	-	-
15	-	1.05 (18)	-	-

N.B. 1) Distance from outer surface of B<sub>4</sub>C shield.

2) Normalized at the position of -100cm near the source.

Table 3-3-9 Reaction rates in the primary coolant pipe penetration

(Unit: Reactions/sec/ $10^{24}$  atoms/100MW<sub>e</sub>)

Position <sup>1)</sup> (cm)	$^{50}\text{Cr}(n,\gamma)^{51}\text{C}$				$^{58}\text{Fe}(n,\gamma)^{59}\text{Fe}$			
	Exp.	Calc. (fsd %)	Relative C/E <sup>2)</sup>	(Absolute) C/E	Exp.	Calc. (fsd %)	Relative C/E <sup>2)</sup>	(Absolute) C/E
Core-ward								
-120	7.18+9 <sup>3)</sup>	1.48+8 (11)	0.54	(1/49)	5.49+8	1.08+7 (11)	0.53	(1/51)
-100	3.32+9	1.27+8 (9.7)	1.00	(1/26)	2.53+8	9.46+6 (9.5)	1.22	(1/27)
-80	2.01+9	9.57+7 (20)	1.24	(1/21)	1.54+8	7.08+6 (20)	1.23	(1/22)
-60	1.38+9	4.77+7 (27)	0.90	(1/29)	1.07+8	3.60+6 (26)	0.90	(1/30)
-40	6.71+8	1.54+7 (9.9)	0.60	(1/44)	5.09+7	1.20+6 (9.4)	0.63	(1/42)
-20	2.17+8	7.82+6 (20)	0.94	(1/28)	1.82+7	5.97+5 (19)	0.88	(1/30)
-10	1.61+8	6.05+6 (12)	0.98	(1/27)	1.26+7	4.63+5 (12)	0.98	(1/27)
0 <sup>4)</sup>	1.76+8	3.32+4 (14)	1/202	(1/5300)	1.56+7	1.08+4 (27)	1/54	(1/1400)
3 <sup>4)</sup>	4.22+7	4.91+4 (25)	1/33	(1/860)	4.02+6	1.29+4 (25)	0.086	(1/310)
5 <sup>4)</sup>	2.92+7	7.39+4 (27)	1/15	(1/400)	3.02+6	1.34+4 (23)	0.12	(1/230)
15 <sup>4)</sup>	1.45+7	7.55+4 (32)	0.14	(1/190)	1.80+6	1.34+4 (23)	0.20	(1/130)

N.B. 1) Distance from outer surface of B<sub>4</sub>C shield.

2) Normalized at the position of -100 cm near the source.

3) Read as  $7.18 \times 10^9$  reactions/(sec $\cdot 10^{24}$  atoms $\cdot 100\text{MW}_e$ ).4) The experimental value is influenced by neutron streaming through a detector hole in the B<sub>4</sub>C shield. Calculated value does not contain a contribution of wall scattering in the primary pump room.

Table 3-3-9 (cont'd)

(Unit: Reactions/sec/10<sup>24</sup>atoms/100MW<sub>t</sub>)

Position <sup>1)</sup> (cm)	<sup>59</sup> Co(n,γ) <sup>60</sup> Co				<sup>123</sup> Sb(n,γ) <sup>124</sup> Sb				
	Exp.	Calc. (fsd) %	Relative C/E <sup>2)</sup>	(Absolute) C/E	Exp. <sup>3)</sup>		Calc. (fsd) %	Relative C/E <sup>2)</sup>	
Core-ward									
-120	1.65+10 <sup>4</sup> )	3.85+8 (10)	0.54	(1/43)	1.0	1.0	1.26+8 (16)	0.57	0.67
-100	7.49+9	3.27+8 (9.0)	1.00	(1/23)	0.418	0.496	9.27+7 (10)	1.00	1.00
-80	4.50+9	2.42+8 (19)	1.23	(1/19)	0.256	0.274	8.68+7 (23)	1.53	1.70
-60	2.94+9	1.34+8 (23)	1.04	(1/22)	0.176	0.118	4.81+7 (18)	1.23	2.18
-40	1.56+9	4.98+7 (15)	0.73	(1/31)	9.87-2	6.95-2	1.97+7 (13)	0.90	1.52
-20	5.82+8	2.10+7 (18)	0.83	(1/28)	5.38-2	3.85-2	9.94+6 (17)	0.83	1.38
-10	4.17+8	1.65+7 (11)	0.91	(1/25)	3.74-2	4.24-2	1.36+7 (28)	1.64	1.72
0 <sup>5)</sup>	5.13+8	7.95+5 (23)	0.036	(1/650)	8.25-2	-	1.51+6 (26)	0.083	-
3 <sup>5)</sup>	1.46+8	9.19+5 (23)	0.14	(1/160)	2.93-2	-	1.59+6 (26)	0.25	-
5 <sup>5)</sup>	1.02+8	9.98+5 (24)	0.22	(1/100)	3.41-2	-	1.57+6 (23)	0.21	-
15 <sup>5)</sup>	7.14+7	1.05+6 (25)	0.34	(1/68)	2.49-2	-	1.36+6 (19)	0.25	-

- N.B. 1) Distance from outer surface of B<sub>4</sub>C shield.  
 2) Normalized at the position of -100 cm near the source.  
 3) Relative value. The data in the left column were obtained by 0.603 MeV γ-ray detection, the others were by 1.692 MeV γ-ray detection.  
 4) Read as 1.65 × 10<sup>10</sup> reactions/(sec·10<sup>24</sup>atoms·100MW<sub>t</sub>)  
 5) The experimental value is influenced by neutron streaming through a detector hole in the B<sub>4</sub>C shield. Calculated value does not contain a contribution of wall scattering in the primary pump room.



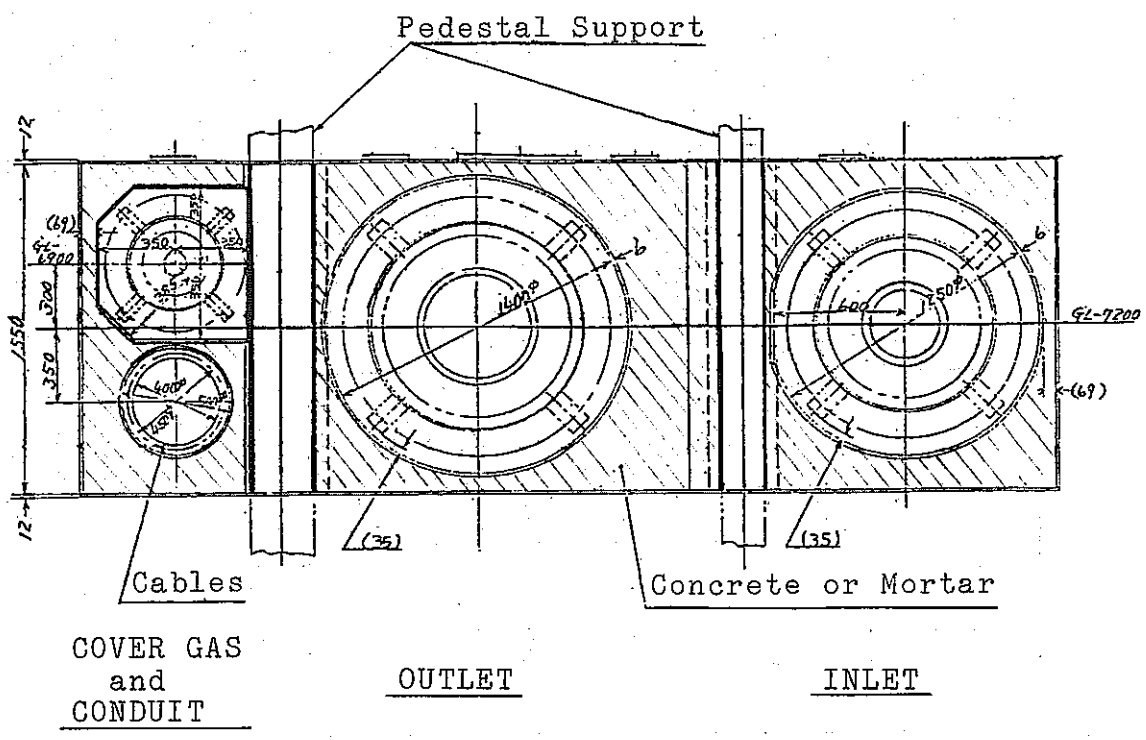
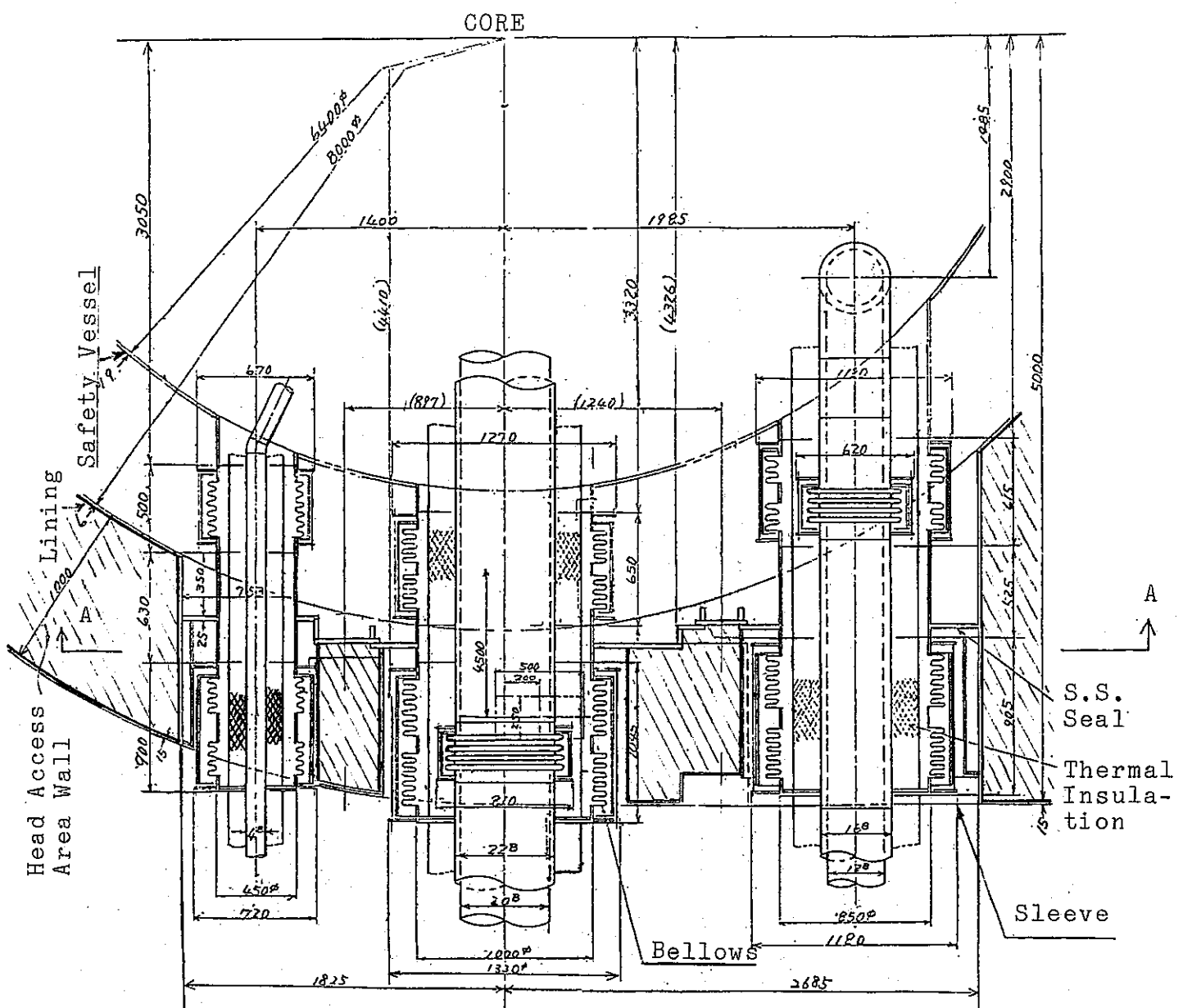


Fig. 3-3-1 Horizontal and vertical cross sections of primary coolant pipe penetration in the biological shield concrete (loop A).

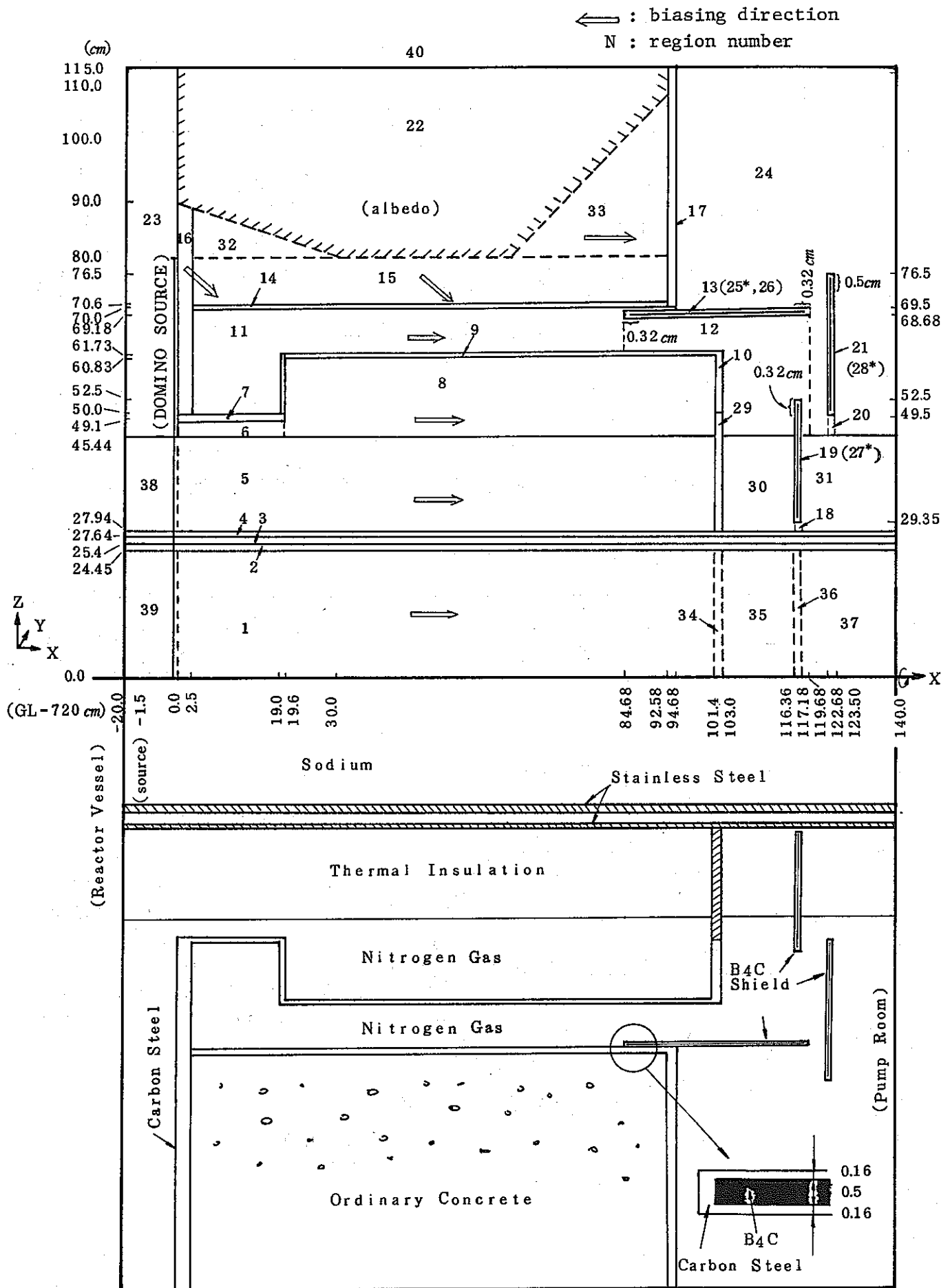


Fig. 3-3-2 Region configuration in the calculational model of primary coolant outlet pipe penetration.

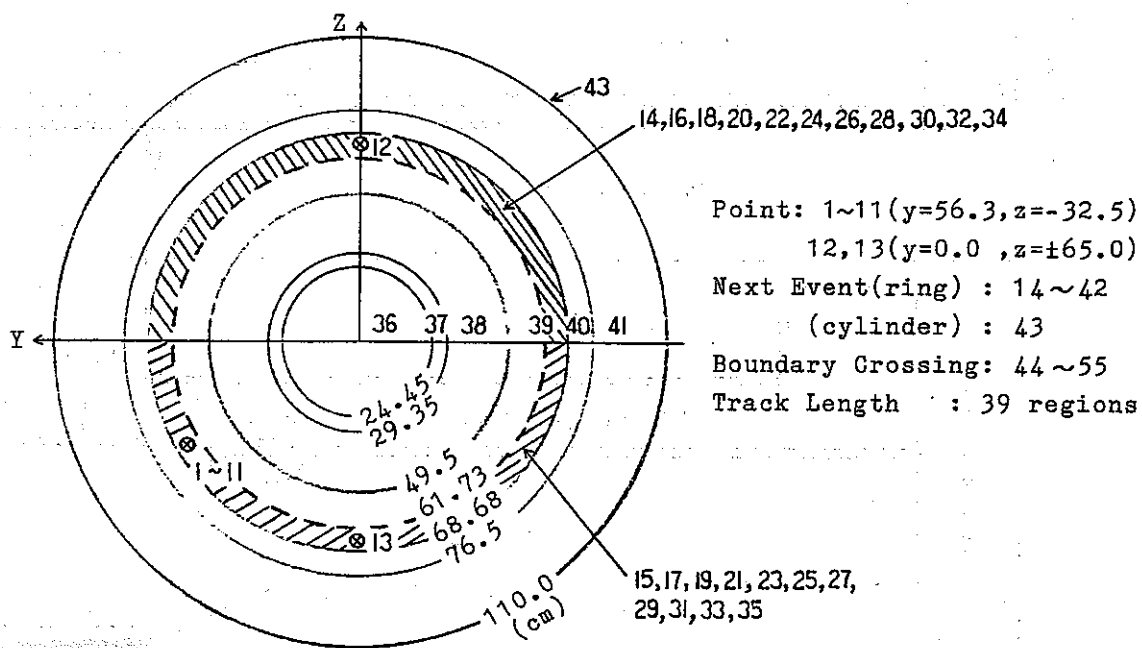
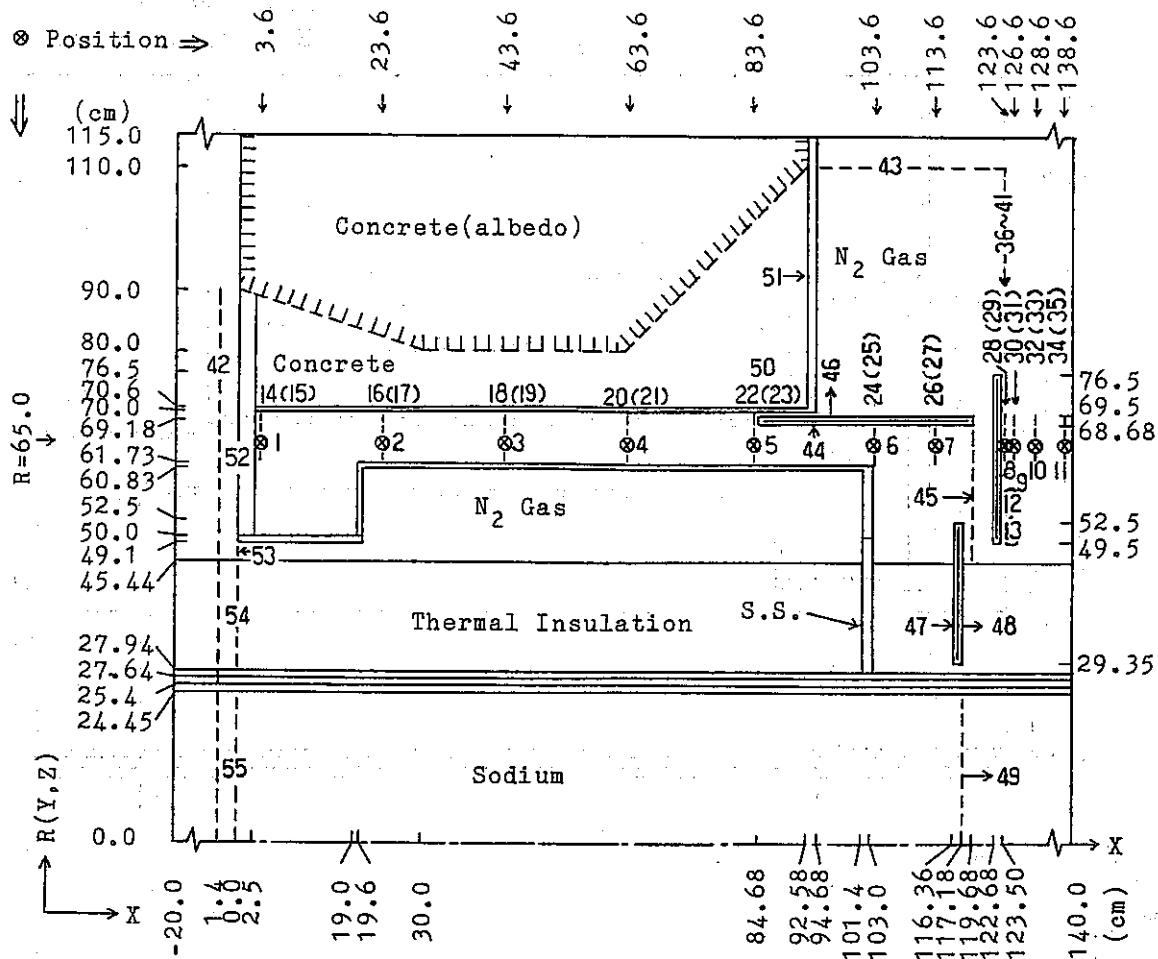


Fig. 3-3-3 Detector locations for neutron streaming analysis in the primary coolant pipe penetration.

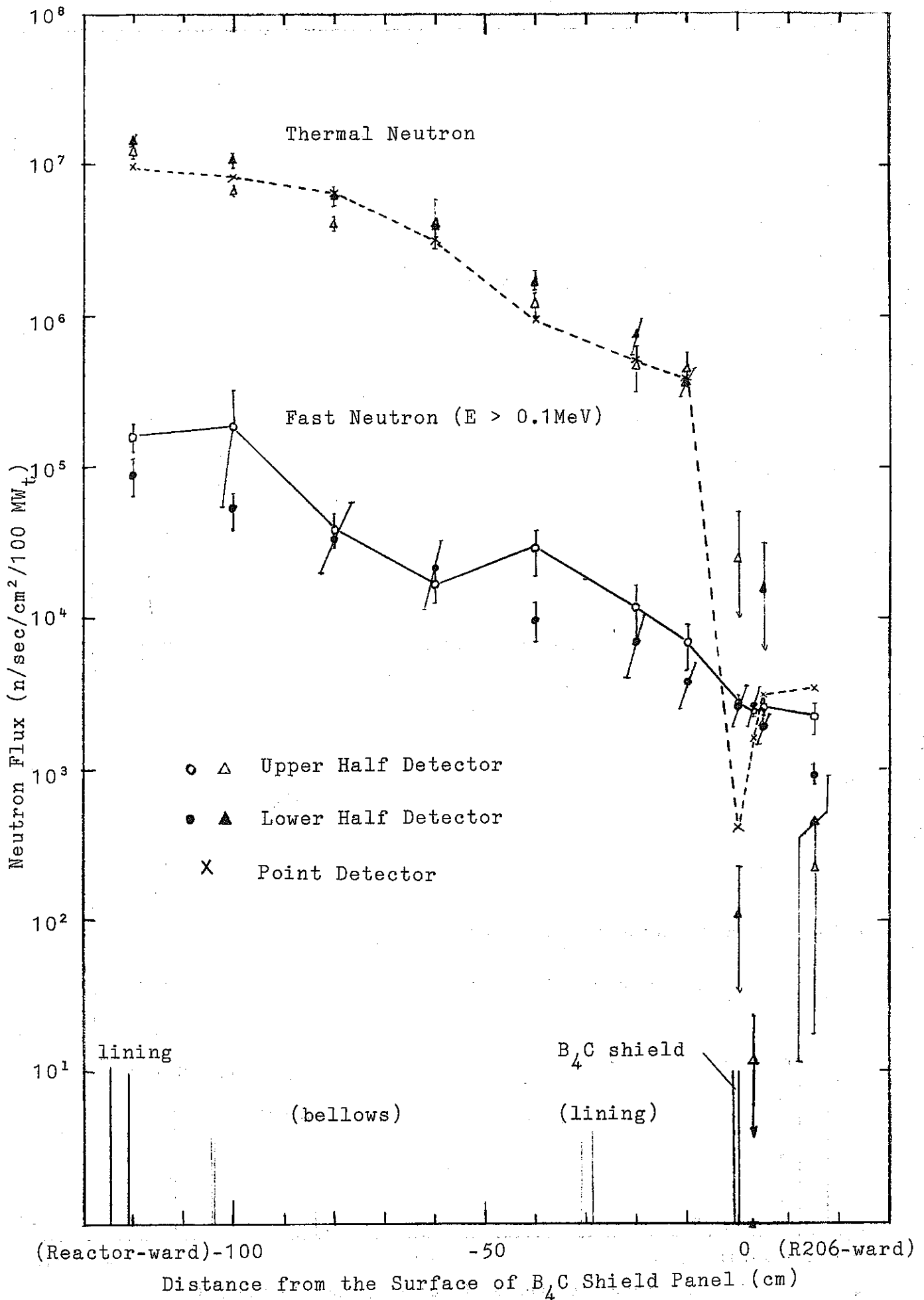


Fig. 3-3-4 Fast and thermal neutron flux distributions along the primary coolant outlet pipe penetration in the biological shield concrete.

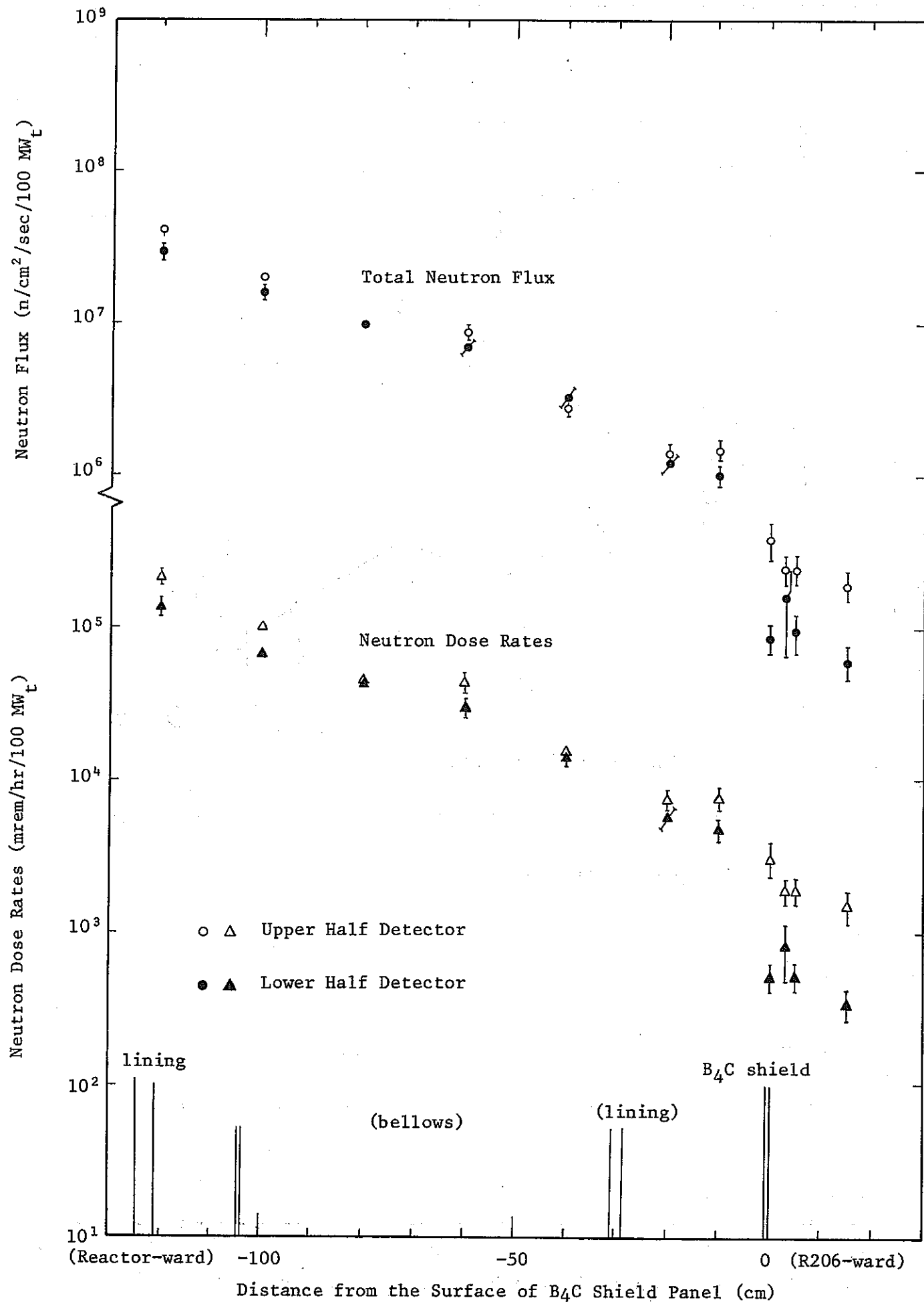


Fig. 3-3-5 Total neutron flux and neutron dose rate distributions along the primary coolant outlet pipe penetration in the biological shield concrete.

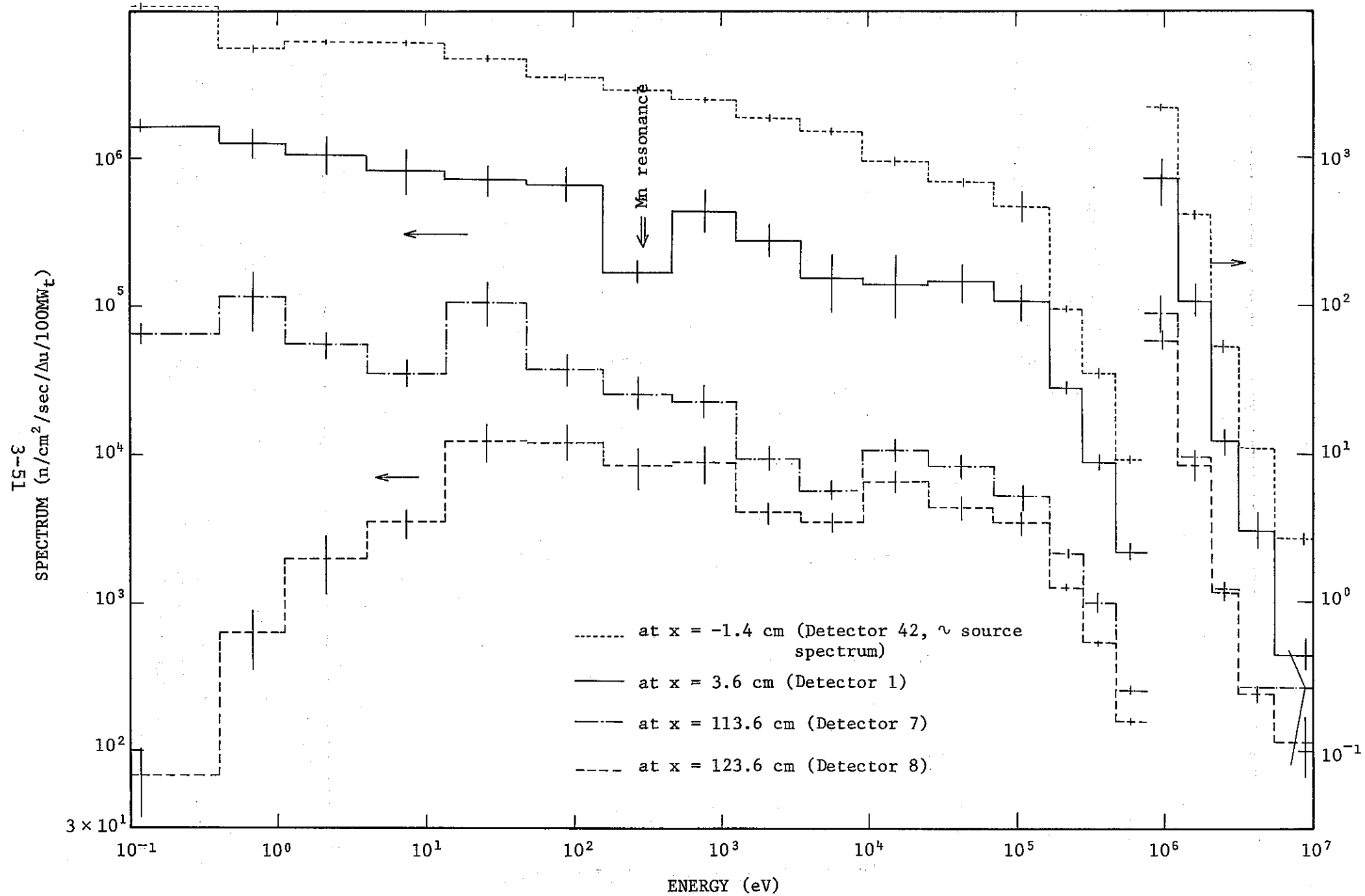


Fig. 3-3-6 Neutron spectrum in the primary coolant outlet pipe penetration

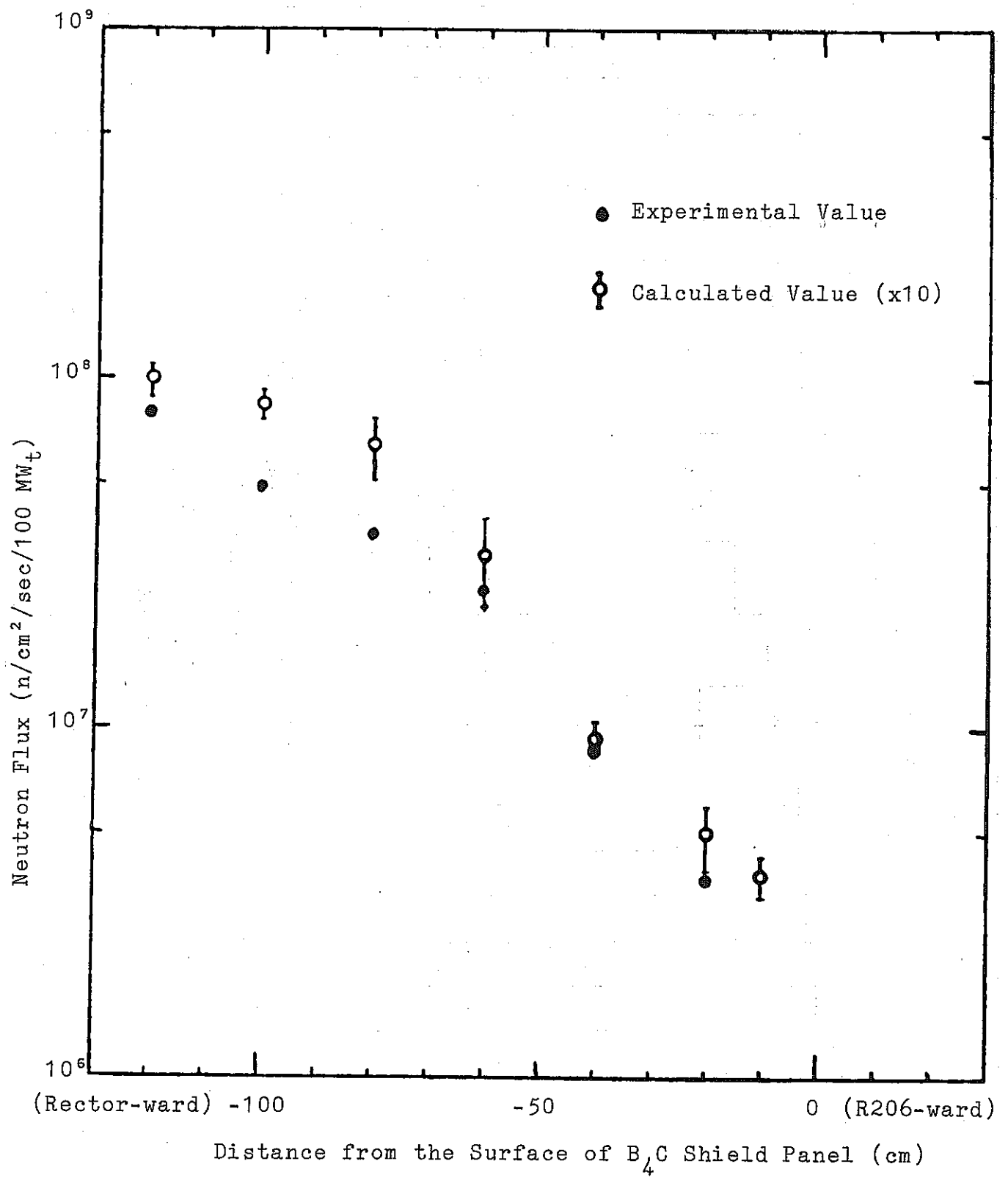


Fig. 3-3-7 Thermal neutron flux distributions along the primary coolant outlet pipe penetration in the biological shield concrete.

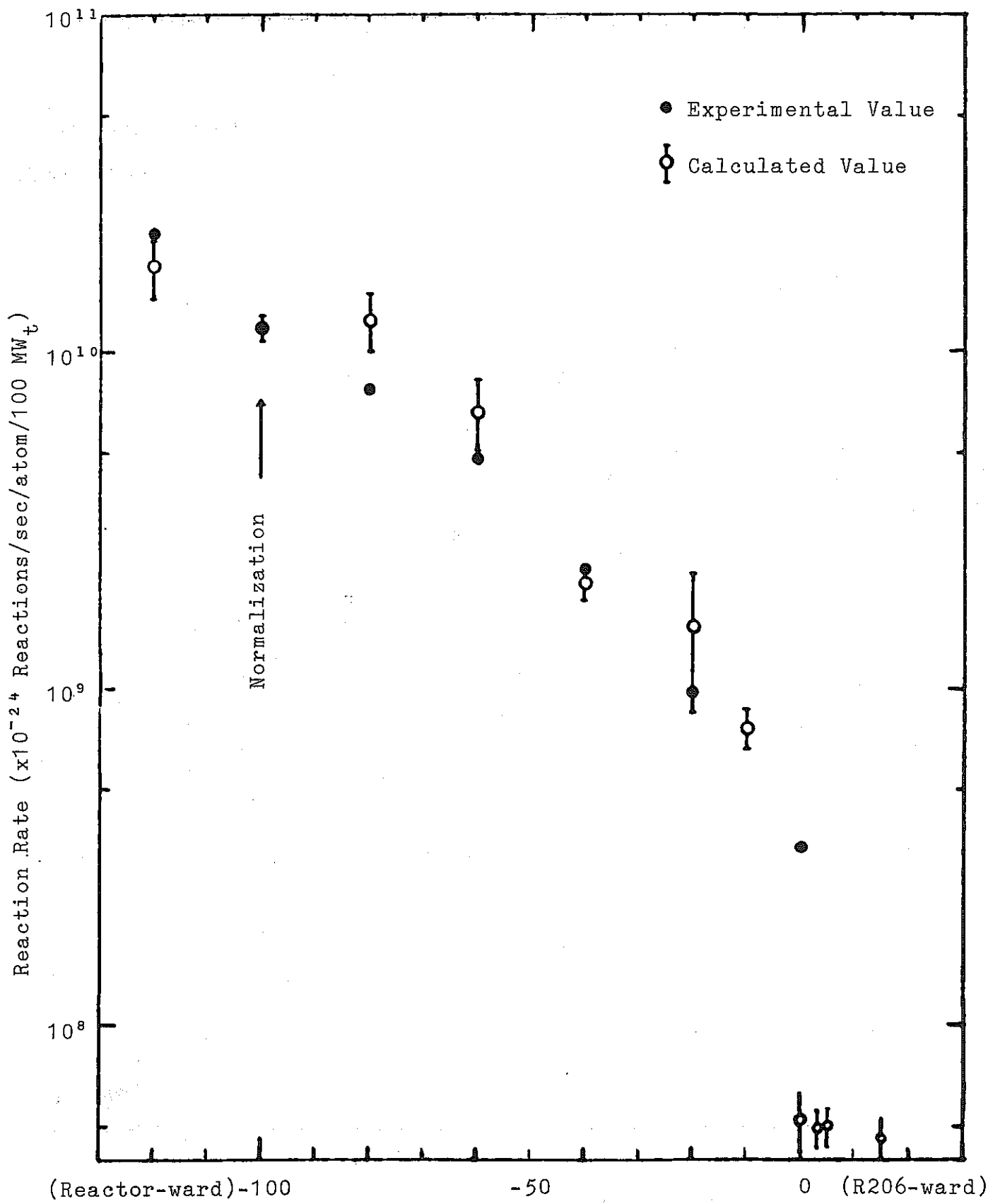


Fig. 3-3-8  $^{197}\text{Au}(n,\gamma)^{198}\text{Au}$  reaction rate distributions along the primary coolant outlet pipe penetration in the biological shield concrete.



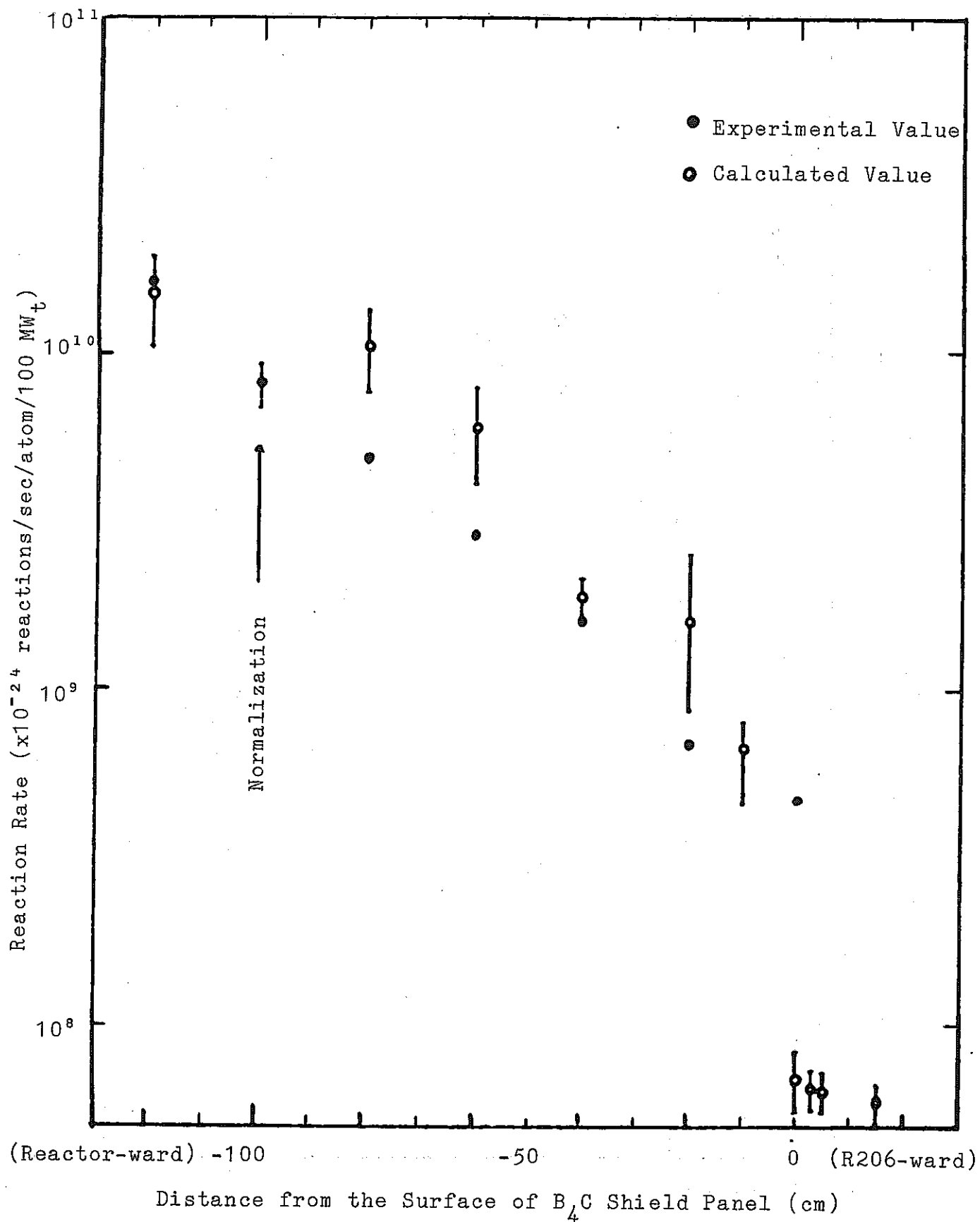


Fig. 3-3-9 Reaction rate distributions of Cd-covered gold foil along the primary coolant outlet pipe penetration in the biological shield concrete.

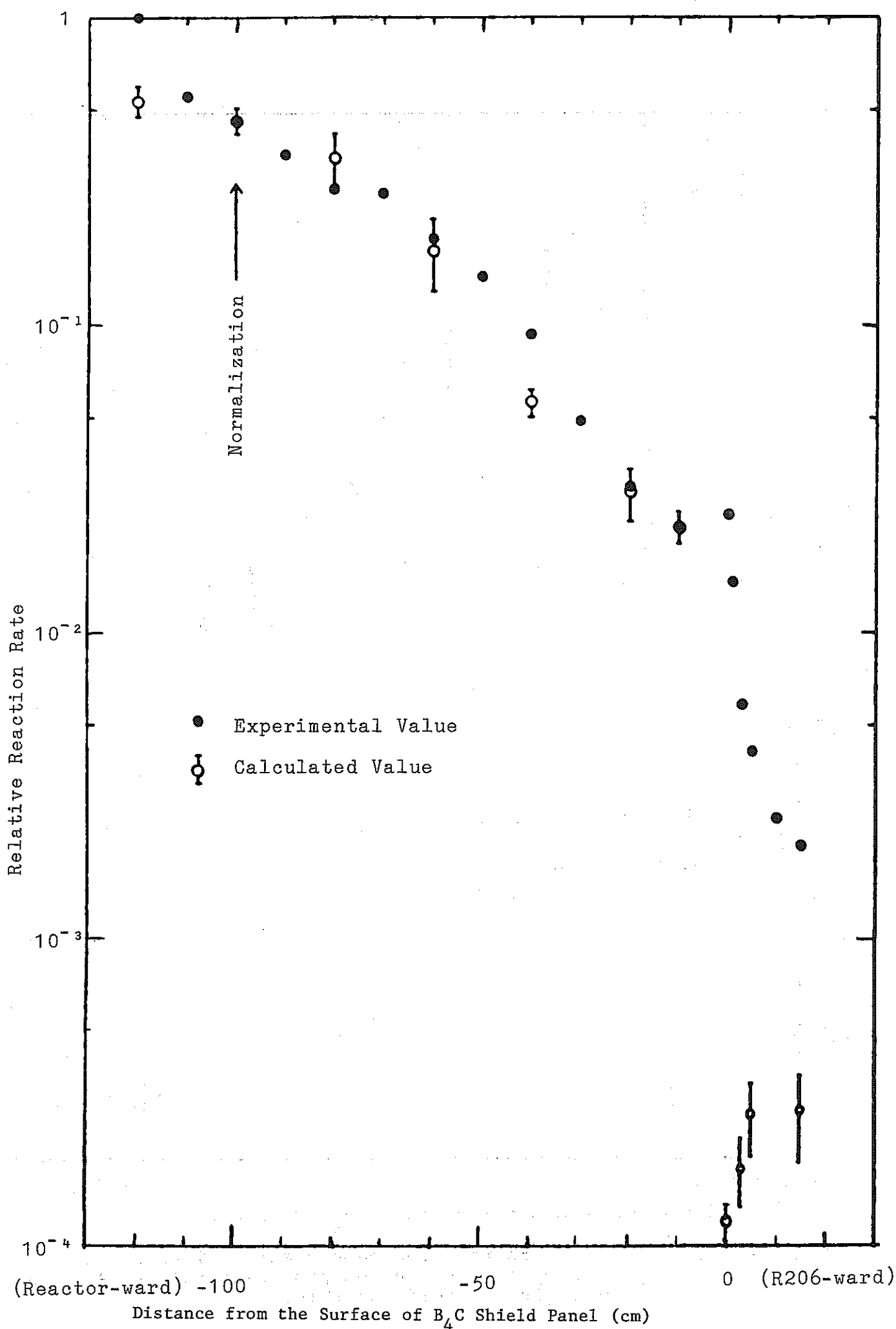


Fig. 3-3-10  $^{50}\text{Cr}(n,\gamma)^{51}\text{Cr}$  reaction rate distributions along the primary coolant outlet pipe penetration in the biological shield concrete.

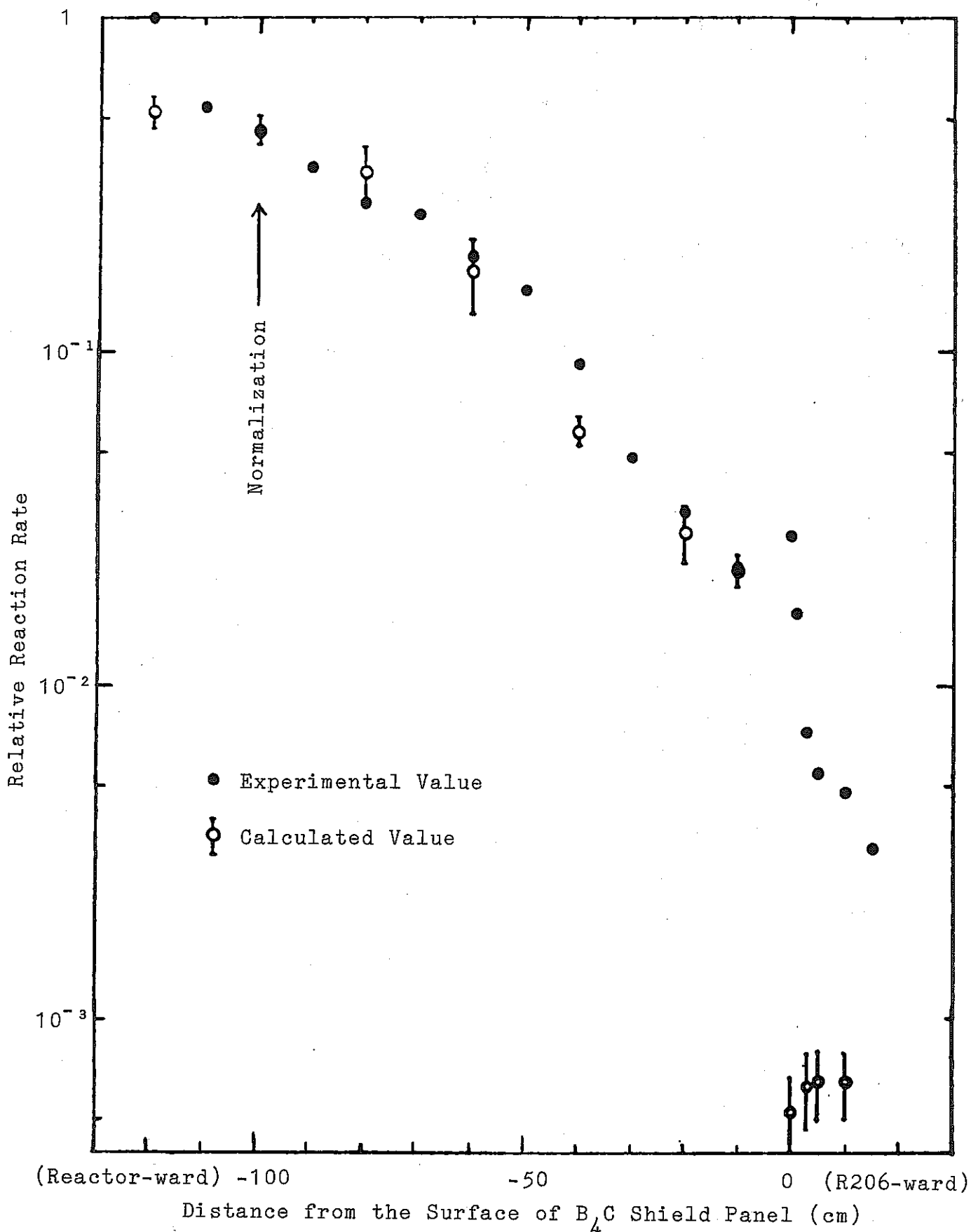


Fig. 3-3-11  $^{58}\text{Fe}(n, \gamma)^{59}\text{Fe}$  reaction rate distributions along the primary coolant outlet pipe penetration in the biological shield concrete.

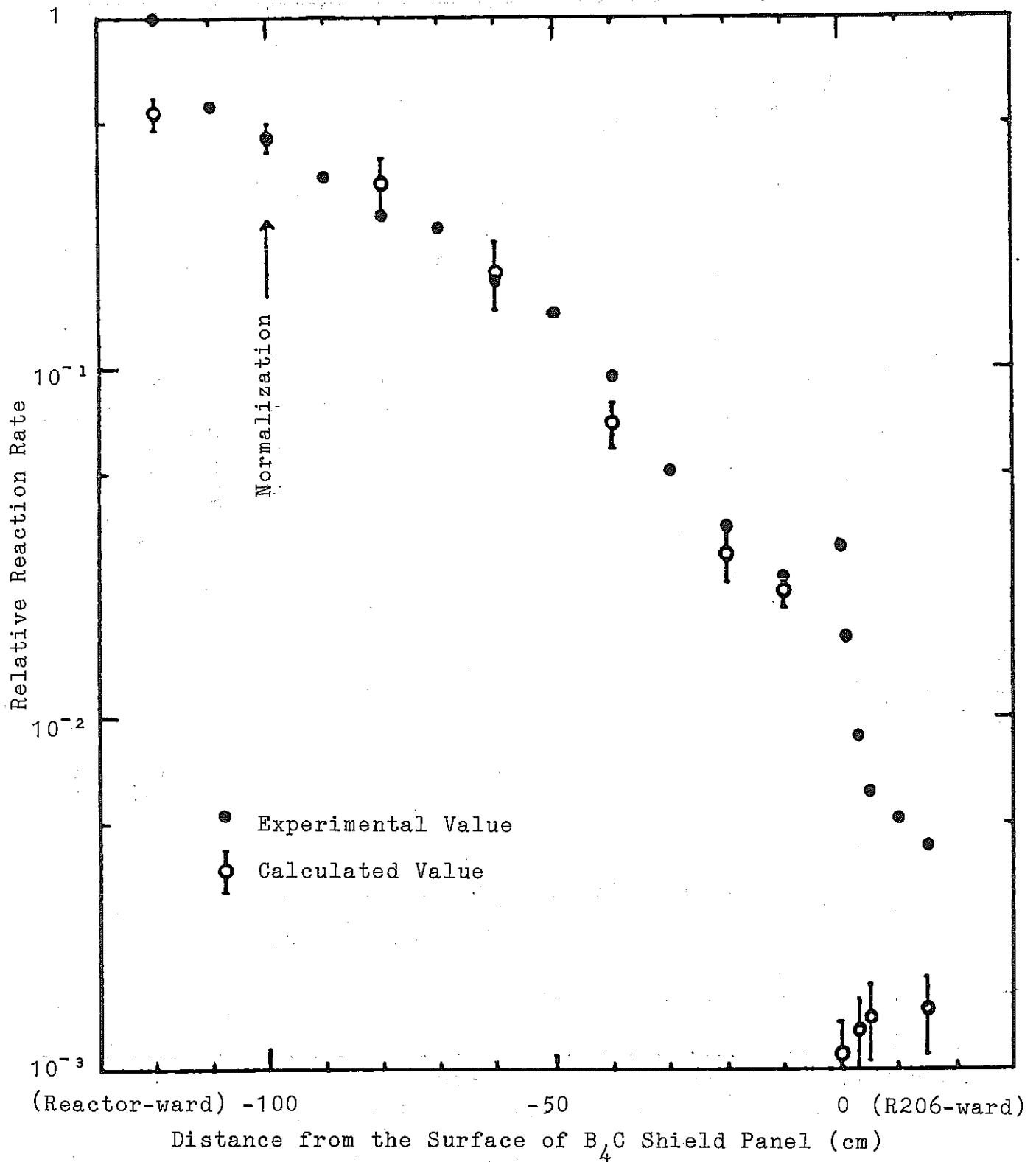


Fig. 3-3-12  $^{59}\text{Co}(n,\gamma)^{60}\text{Co}$  reaction rate distributions along the primary coolant outlet pipe penetration in the biological shield concrete.

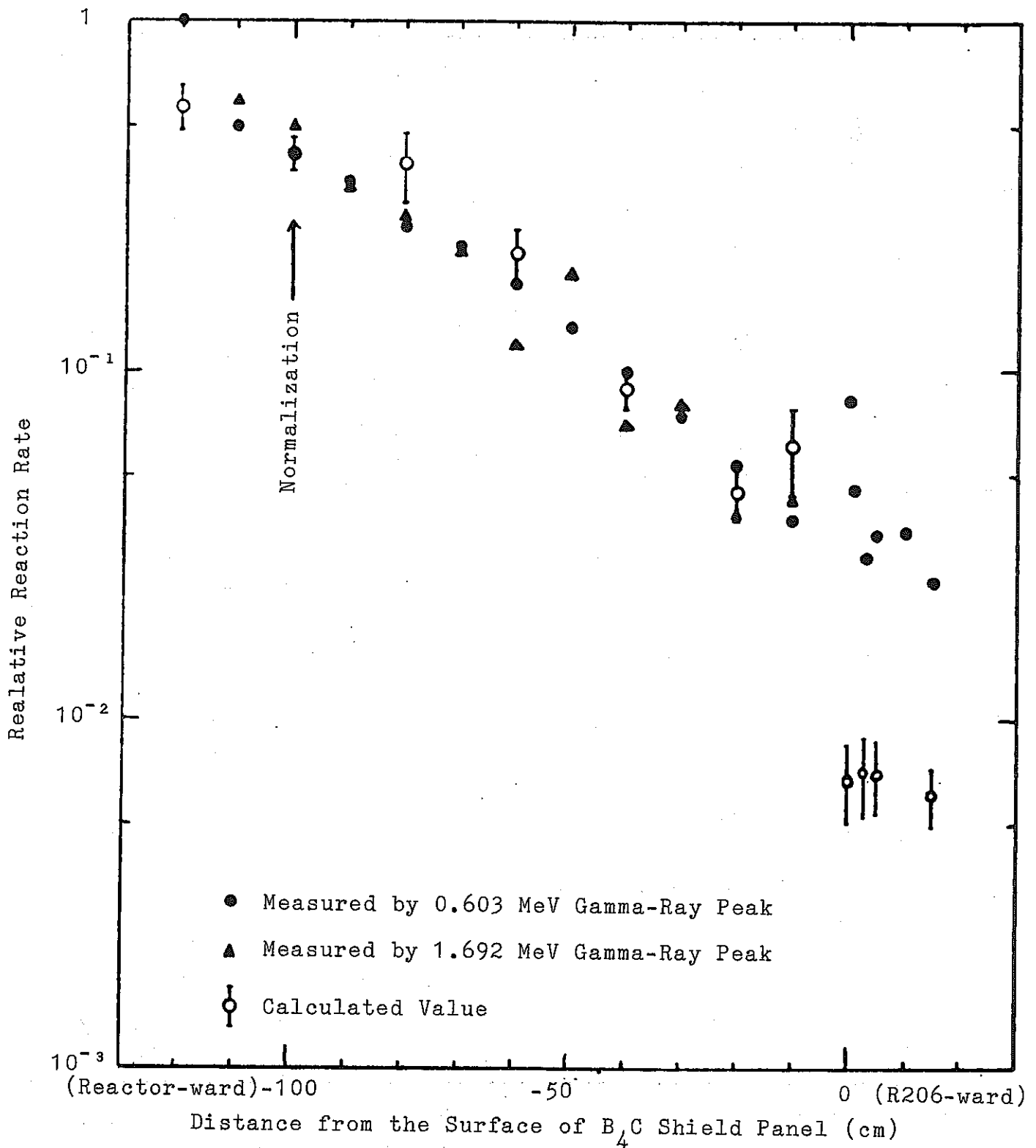


Fig. 3-3-13  $^{123}\text{Sb}(n,\gamma)^{124}\text{Sb}$  reaction rate distributions along the primary coolant outlet pipe penetration in the biological shield concrete.

### 3.4 Analysis of Neutron Behaviour in the Primary Pump Room

#### 3.4.1 Calculational Configuration

The primary pump room, R206, is located next to the reactor room as shown in Fig. 2-3-1. The configuration and the dimensions of the room are shown in Fig. 3-4-1. The pump room is a gigantic space about 11 meter high with about 40 square meters floor. Through the 1 meter thick biological shielding wall separating the reactor room, several penetrations are equipped. They are the penetration with 70 cm radius for the primary coolant outlet pipe, the one with 62.5 cm radius for the primary coolant inlet pipe, and two with 25 cm radius for the argon cover gas pipe and 19.25 cm radius for instrumentation cables, respectively. The cross sectional view of the penetrations were shown in Fig. 3-3-1. Rectangular openings, 1 meter wide by 1.8 meter in height for passing to the upper IHX room, 2 meter wide by 2 meter in height for leading the primary coolant pipe to the lower IHX room are equipped.

From the standpoint of the radiation shielding, these penetrations allow a lot of neutrons to leak from the reactor room, to cause the coolant pipes and primary pump activated and to enhance the background for the FFD/DN-method (fuel fracture detector counting delayed neutrons). Besides, neutrons in the primary pump room stream to the IHX room to activate the secondary coolant sodium. In order to estimate such neutrons,

detectors are installed<sup>6)</sup> making use of reactions such as  $^{235}\text{U}(n,f)$ ,  $^{238}\text{U}(n,f)$ ,  $^{232}\text{Th}(n,f)$ ,  $^{32}\text{S}(n,p)^{32}\text{P}$ ,  $^{109}\text{Ag}(n,\gamma)^{110\text{m}}\text{Ag}$ ,  $^{181}\text{Ta}(n,\gamma)^{182}\text{Ta}$  and  $^{191}\text{Ir}(n,\gamma)^{192}\text{Ir}$  in the pump room. The measurement locations and the detector types are summarized in Table 2-3-1.

#### 3.4.2 The Method and Conditions of the Calculation

The calculations were carried out with the albedo Monte Carlo code MORSE-ALB.<sup>7-11)</sup> The outline of the calculations are shown in Table 3-4-1. Elementary bodies constituting the calculational model are 13 right circular cylinders, 8 rectangular parallelepipeds, and a truncated right angle cone. The combinations of these bodies are shown in Fig. 3-4-2, Fig. 3-4-3 and Fig. 3-4-4. Regions which were used to define biasing conditions were summed up to 18 by combining bodies. Materials for cross sections and albedo media are summarized in Table 3-4-2. Albedo boundary was set on the surface of the concrete wall shown in Fig. 3-4-5, the polyethylene surface of FFD/DN-method, and the surface of the impeller of the primary pump shown in Fig. 3-4-4. A particle with sufficiently small weight which has been reduced due to many albedo reflections and real collisions receives the Russian Roulette kill or survival. These conditions are shown in Table 3-4-1.

The neutron source was obtained from the results of the preceding analysis described in Section 3.3. The neutron fluxes at the outside of the  $\text{B}_4\text{C}$  shields around the primary

coolant outlet pipe running from the reactor room to the pump room were converted into the source data for Monte Carlo calculation by the DOMINO-N code<sup>10)</sup>. The source spectrum is shown in Fig. 3-4-7.

Fifty-seven detectors consisting of 11 point detectors, 42 next event estimators<sup>11)</sup>, and 4 boundary crossing estimators were used. The arrangement of the detectors is shown in Fig. 3-4-8, and the detailed locations are summarized in Table 3-4-3. Point detectors were set not only at measurement points but around the primary pump and at the center of the room which is on the center line of the pump.

### 3.4.3 Calculational Result

#### A. Neutron flux distributions

Values obtained by the Monte Carlo calculation for detectors in the primary pump room are shown in Tables 3-4-4 through 3-4-7. In the vicinity of the neutron source, point detectors of No.1 and No.2 and next event estimators of No.53 are set right in front of the source. Point detectors of No.9 and No.10 are set 70 cm and 180 cm apart from it respectively. The fast neutron flux above 0.1 MeV is about  $10^3$  n/cm<sup>2</sup>/sec in the vicinity of the source, and rapidly decreases as the detector point gets farther from the source. Most of flux levels in the pump room become  $10^1 - 10^2$  n/cm<sup>2</sup>/sec. About two thirds of the fractional standard deviations (FSD) of the



scored neutron flux are within 20%, which means good convergence of Monte Carlo calculation. However, around the opening to the IHX room and on the side and bottom surface of FFD/DN-method where particles are unlikely to reach in small number of scatterings, larger values of FSD are seen.

On the other hand, most thermal neutron flux is  $10^3$  to  $10^4$  n/cm<sup>2</sup>/sec in the pump room, and even the value in the vicinity of the source is 2 to 3 times larger than the average thermal neutron flux. It is because thermal neutrons were generated mainly by the multiple scattering and the slowing down at the wall surface rather than streaming through the primary coolant pipe penetration from the reactor room. FSD is within 20% for more than 80% detectors. As for total neutron flux, it is about  $10^5$  to  $3 \times 10^5$  in the vicinity of the source, and  $3 \times 10^3$  to  $10^4$  on the average in the pump room. FSD is within 10% for about 60% detectors and is within 20% for about 90% detectors, which means good convergence of the calculation. Dose rate due to the neutrons is 0.5 to 1.5 rem/hour in the vicinity of the source, and 10 to 100 mrem/hour on the average in the pump room.

Fig. 3-4-9 shows the spatial distributions of the total neutron flux, thermal neutron flux, fast neutron flux above 0.1 MeV, and the neutron dose rate: vertical distribution scored by the detectors of No.47 through 50, 53 and horizontal distribution on the upper surface of FFD/DN scored by the detectors of No.20 and 26 (see Fig. 3-4-8). The ratios of the

values around the source to those in the other region are roughly 40, 4, 140 and 50 for total neutron flux, thermal neutron flux, fast neutron flux, and neutron dose rate respectively.

#### B. Neutron spectra

Fig. 3-4-10 shows the spectrum at three locations: the point 70 cm apart from the  $B_4C$  shields toward the pump, the center of the room, and the upper surface of FFD/DN-method. Every spectrum is flat below 10 keV as it is  $1/E$  shape in the low energy range, while it sharply drops in the high energy range as the energy becomes higher. The spectra resemble to the source spectrum shown in Fig. 3-4-7.

#### C. Comparison of calculated value with measured data

The reaction rates obtained by the calculation are compared with measured values<sup>6)</sup> in Table 3-4-8. Some problems may be included in the absolute values of the source, as was described before. Excluding the error of the neutron source, C/E values were normalized to those at position 1. Those relative C/E values are shown in Fig. 3-4-11 classifying them into three groups according to the dominant energy range of neutrons contributing to the reactions.

Relative C/E values distribute between 0.72 - 4.0 at the position 2 which is near to the source, 2.5 - 3.0 on the pump side surface, 0.76 - 2.8 on the upper surface of FFD/DN-method and 2.2 - 3.6 at the point 70 cm apart from the source toward

the primary pump. Although position 2 is close to the source, the relative C/E is not around 1.0. It is because position 1 and position 2 were so close to the disc source that flux scoring was much affected by the position of source neutron and the statistics of the calculation was not sufficient. On the other hand, the influence of source neutron position is not very large at the positions apart from the source and the calculated value was obtained with good statistics. As the primary coolant pipe was not taken into account, relative C/E values became a little larger than 1.0. Accordingly, results can be regarded reasonable enough.

With respect to the absolute C/E values for each reaction, obtained are 0.091 - 0.33 for  $^{109}\text{Ag}(n,\gamma)^{110\text{m}}\text{Ag}$  and  $^{181}\text{Ta}(n,\gamma)^{182}\text{Ta}$  that are mainly caused by slow neutrons, 0.066 - 0.11 for  $^{235}\text{U}(n,f)$  that is caused by overall energy neutrons. The C/E values for threshold reaction are small: 1/240 - 1/1040 for  $^{238}\text{U}(n,f)$ , 1/2000 - 1/13900 for  $^{232}\text{Th}(n,f)$  and 1/960 - 1/1140 for  $^{32}\text{S}(n,p)^{32}\text{P}$ . Small C/E values were obtained because source intensity was underestimated. C/E values for reactions caused by slow neutrons in the pump room are very close to those for reactions by slow neutrons especially to the values (0.092 through 0.18) for  $^{197}\text{Au}(n,\gamma)^{198}\text{Au}$  obtained in the streaming calculation through the primary coolant pipe penetration. This fact firmly suggests that the underestimation was caused because the hollow in the graphite shield for the primary coolant pipe was neglected in the Sn calculation<sup>1,2)</sup> executed inside the biological shielding concrete, and neutrons (especially fast component) arriving at

the inner surface of the concrete was underestimated.

D. Comparison with results obtained by the streaming calculation through the primary coolant pipe penetration

Table 3-4-9 shows the comparison of the calculated reaction rates on the surface of the  $B_4C$  shield between the calculation for the primary coolant pipe penetration and that for the primary pump room. Relative values normalized to the reaction rates for the detector of No. 8 are shown in parentheses under the calculated values.

As for results in the pump room, relative values of thermal neutron flux are 15.3 and 18.0, while those of  $(n,\gamma)$  reactions of  $^{197}Au$ ,  $^{50}Cr$ ,  $^{58}Fe$ ,  $^{59}Co$ ,  $^{123}Sb$ ,  $^{109}Ag$  and  $^{181}Ta$  which are caused by slow neutrons are 1.07 through 5.4. Relative values of  $^{235}U$   $(n,f)$  reaction rates caused by neutrons in overall energy range are 2.7 and 3.6.

The discrepancies brought about by the two calculations must have been caused by the wall scattering in the pump room, since the results of streaming calculation through the penetration include only neutrons that came through the penetration while those of the pump room calculation include neutrons scattered by the inner surface of the room. It is also suggested by the trend that the relative values of reaction rates in the pump room become larger as the neutron energy contributing to the reactions become smaller. Therefore, results around the opening to the pump room obtained in the primary coolant pipe penetration analysis may as well be corrected to take into account the wall scattering mentioned above. As for threshold reactions such

as  $^{238}\text{U}(n,f)$ ,  $^{232}\text{Th}(n,f)$ , and  $^{32}\text{S}(n,p) \rightarrow ^{32}\text{P}$ , the relative values of reaction rates obtained in the pump room calculation became 0.25 through 2.6. This means no evident difference due to the reflection exists in threshold reactions obtained by the two calculations and fast neutrons that reached at the opening of the penetration in the pump room must be almost those coming through the penetration.

Table 3-4-1 Input parameters of Monte Carlo calculation  
for primary pump room

Geometry ..... 22 bodies for the combinatory geometry<sup>17)</sup>  
(See Figs. 3-4-1, 3-4-2, 3-4-3 and 3-4-4.)  
18 Regions (See Figs. 3-4-4, 3-4-5 and  
3-4-6.)  
7 media including 3 albedo media

Cross section ..... P<sub>5</sub>, 21 groups (See Table 3-4-2.)

Neutron source ..... Circular disc source with 110 cm radius  
Energy-space-angle dependent  
Generated by DOMINO-N code<sup>10)</sup> from the  
results of JOYO primary coolant pipe  
penetration analysis (Monte Carlo  
calculation)

Flux estimator ..... 11 point detectors, 41 next event  
surface crossing estimators<sup>11)</sup> and 10  
boundary crossing estimators (See Table  
3-4-3 and Fig. 3-4-8.)

Importance sampling .. (1) Russian Roulette kill and survival

a) Case A (21-group-calculation)

for all region, energy group = ,	1 ~ 4	5 ~ 8	9 ~ 15	16 ~ 21
Weight killed	10 <sup>-7</sup>	10 <sup>-6</sup>	10 <sup>-4</sup>	10 <sup>-3</sup>
Weight survived	10 <sup>-6</sup>	10 <sup>-5</sup>	10 <sup>-3</sup>	10 <sup>-2</sup>

b) Case B (8-group-calculation)

Weight killed 10<sup>-8</sup>,  
weight survived 10<sup>-6</sup>

(2) Source energy biasing

(see Table 3-3-4.)

Histories ..... (1) Case A (21 groups) 8,000  
(2) Case B ( 8 groups) 20,000

Table 3-4-2 Cross section and albedo data for primary-pump room analysis

Cross section

Medium No.	Input No.	Medium	(binary ID)
1	1	Sodium	100
2	2	SS304 <sup>1)</sup>	200
3	3	Concrete (albedo)	400
4	4	Thermal insulator	600
5	5	Polyethylene (albedo)	700
6	6	Nitrogen gas	1000
7	2	SS304 (albedo)	200

Albedo

No.	Medium No.	Medium
1	3	Concrete with liner
2	7	SS304 (impeller)
3	5	Polyethylene

N.B. 1) Type 304 stainless steel.

Table 3-4-3 Detectors and locations

(1) Point detectors

No.	Coordinate (cm)			Comment
	X	Y	Z	
1	501.0	0.0	945.0	The opening of the primary coolant outlet pipe penetration (up)
2	501.0	0.0	815.0	The opening of the primary coolant outlet pipe penetration (down)
3	842.99	0.0	880.0	Outer surface of primary pump (front)
4	920.0	77.01	880.0	Outer surface of primary pump (left)
5	997.01	0.0	880.0	Outer surface of primary pump (back)
6	920.0	-77.01	880.0	Outer surface of primary pump (right)
7	641.125	70.0	364.01	Center of top surface of FFD
8	760.26	70.0	363.0	Lateral surface of FFD (near top surface)
9	570.0	45.44	880.0	70 cm from the opening for the outlet pipe
10	680.0	45.44	880.0	180 cm from the opening for the outlet pipe
11	920.0	0.0	530.0	Center of the room on the axis of primary pump

(2) Next event estimators

No.	Range (cm)						Comment
	X(-)	X(+)	Y(-)	Y(+)	Z(-)	Z(+)	
12	475.0	495.0	-363.3	-363.3	832.0	868.0	Passage to the IHX room
13	465.0	505.0	-363.3	-363.3	814.0	886.0	Passage to the IHX room
14	455.0	515.0	-363.3	-363.3	796.0	904.0	Passage to the IHX room
15	445.0	525.0	-363.3	-363.3	778.0	922.0	Passage to the IHX room
16	435.0	535.0	-363.3	-363.3	760.0	940.0	Passage to the IHX room
17	435.0	535.0	-263.3	-263.3	760.0	760.0	Upper exit from the pump room



Table 3-4-3 (continued)

No.	X(-)	X(+)	Y(-)	Y(+)	Z(-)	Z(+)	Comment	
18	820.0	1020.0	-363.3	-363.3	0.0	200.0	Passage to the lower IHX room	
19	820.0	1020.0	-263.3	-263.3	0.0	200.0	Lower exit from the pump room	
20	522.0	760.25	-45.0	185.0	364.01	364.01	Top surface of FFD	
21	760.26	760.26	-45.0	185.0	196.5	364.0	Lateral surface of FFD	
22	522.0	760.25	-45.01	-45.01	196.5	364.0	Lateral surface of FFD	
23	522.0	760.25	185.01	185.01	196.5	364.0	Lateral surface of FFD	
24	522.0	760.25	-45.0	185.0	196.49	196.49	Reverse surface of FFD	
25	522.0	760.25	185.0	415.0	364.0	364.0	Same height with FFD	
26	760.25	998.5	-45.0	185.0	364.0	364.0	Same height with FFD	
27	522.0	760.25	-263.3	-45.0	364.0	364.0	Same height with FFD	
No.	Coordinate of the center			Direction cosine of the normal			Radius	Comment
	X	Y	Z	u	v	w		
28	920.0	0.0	715.0	0.0	0.0	1.0	62.0	The Bottom of the Primary pump
29	920.0	0.0	0.0	0.0	0.0	1.0	62.0	Projection of the Bottom of the Primary Pump to the Floor
No.	X(-)	X(+)	Y(-)	Y(+)	Z(-)	Z(+)	Comment	
30	435.0	535.0	-263.29	-263.29	940.0	1026.0	Wall of IHX side	
31	535.0	635.0	-263.29	-263.29	760.0	940.0	Wall of IHX side	
32	635.0	735.0	-263.29	-263.29	760.0	940.0	Wall of IHX side	
33	735.0	835.0	-263.29	-263.29	760.0	940.0	Wall of IHX side	

Table 3-4-3 (continued)

No.	X(-)	X(+)	Y(-)	Y(+)	Z(-)	Z(+)	Comment			
34	835.0	935.0	-263.29	-263.29	760.0	940.0	Wall of IHX side			
35	935.0	1035.0	↑	↑	↑	↑				
36	1035.0	1135.0			760.0	940.0				
37	435.0	535.0			660.0	760.0				
38	↑	↑			560.0	660.0				
39					460.0	560.0				
40					360.0	460.0				
41	435.0	535.0			200.0	360.0				
42	820.0	1020.0			200.0	300.0				
43	↑	↑			300.0	400.0				
44					400.0	500.0				
45					500.0	600.0				
46	820.0	1020.0			-263.29	-263.29		600.0	760.0	Wall of reactor side
47	500.01	500.01			-45.0	185.0		364.0	464.0	
48	↑	↑			↑	↑		464.0	564.0	
49							564.0	664.0		
50	500.01	500.01	-45.0	185.0			664.0	764.0		
51	1020.0	1200.0	-263.29	-263.29			0.0	200.0	Wall of IHX side	
52	435.0	820.0	-263.29	-263.29	0.0	200.0				
No.	Coordinate of the center			Direction cosine of the normal			Radius	Comment		
	X	Y	Z	u	v	w				
53	500.2	0.0	880.0	1.0	0.0	0.0	110.0	Disc covering the source		

Table 3-4-3 (continued)

(3) Boundary crossing estimator

No.	Comment
54	Lateral surface of the primary pump
55	Bottom surface of the primary pump
56	Upper exit from the pump room
57	Lower exit from the pump room

Table 3-4-4 Estimated fast neutron fluxes above 0.1 MeV  
for detectors in the pump room

FAST NEUTRON FLUENCE ABOVE 0.1 MEV					The type of the detector
DETECTOR	FLUX	FSD (%)	MIN	MAX	
1	1.47E+03	25.0	1.10E+03	1.84E+03	Point
2	2.85E+03	40.7	1.69E+03	4.01E+03	
3	2.05E+02	4.4	1.95E+02	2.14E+02	
4	8.31E+01	6.8	7.75E+01	8.88E+01	
5	2.25E+01	9.7	2.04E+01	2.47E+01	
6	9.53E+01	12.4	8.35E+01	1.07E+02	
7	1.81E+01	2.0	1.77E+01	1.84E+01	
8	1.40E+01	2.6	1.37E+01	1.44E+01	
9	1.36E+03	4.1	1.30E+03	1.41E+03	
10	4.85E+02	3.0	4.70E+02	4.99E+02	
11	6.64E+01	2.5	6.48E+01	6.81E+01	
12	1.72E-01	98.4	2.80E-03	3.42E-01	Next event
13	2.26E+00	38.1	1.40E+00	3.12E+00	
14	2.43E+01	55.7	1.08E+01	3.77E+01	
15	1.55E+01	49.2	7.87E+00	2.31E+01	
16	1.55E+01	39.0	9.48E+00	2.16E+01	
17	3.58E+01	26.7	2.62E+01	4.54E+01	
18	1.58E+00	37.6	9.85E-01	2.17E+00	
19	3.67E+00	15.0	3.11E+00	4.22E+00	
20	1.75E+01	15.6	1.48E+01	2.03E+01	
21	5.98E+00	22.9	4.61E+00	7.35E+00	
22	4.04E+00	20.6	3.21E+00	4.87E+00	
23	3.23E+00	33.7	2.14E+00	4.32E+00	
24	5.42E-01	33.4	3.61E-01	7.23E-01	
25	1.47E+01	18.9	1.19E+01	1.75E+01	
26	3.01E+01	15.0	2.56E+01	3.46E+01	
27	1.82E+01	19.2	1.47E+01	2.17E+01	
28	2.27E+01	21.9	1.77E+01	2.77E+01	
29	3.67E+00	17.9	3.01E+00	4.32E+00	
30	1.51E+01	14.7	1.29E+01	1.73E+01	
31	7.11E+01	15.3	6.01E+01	8.20E+01	
32	1.02E+02	15.3	8.62E+01	1.17E+02	
33	1.12E+02	13.5	9.69E+01	1.27E+02	
34	1.40E+02	15.1	1.19E+02	1.61E+02	
35	1.18E+02	16.5	9.85E+01	1.38E+02	
36	1.40E+02	27.3	1.02E+02	1.78E+02	
37	2.63E+01	32.9	1.76E+01	3.49E+01	
38	1.30E+01	17.9	1.07E+01	1.53E+01	
39	9.04E+00	18.3	7.38E+00	1.07E+01	
40	7.05E+00	20.5	5.60E+00	8.49E+00	
41	5.77E+00	17.8	4.74E+00	6.80E+00	
42	1.97E+01	43.5	1.11E+01	2.82E+01	
43	1.52E+01	15.6	1.29E+01	1.76E+01	
44	3.44E+01	27.5	2.50E+01	4.39E+01	
45	4.96E+01	23.7	3.79E+01	6.13E+01	
46	8.56E+01	17.0	7.11E+01	1.00E+02	
47	1.02E+01	16.7	8.48E+00	1.19E+01	
48	1.19E+01	16.5	9.96E+00	1.39E+01	
49	1.94E+01	20.0	1.55E+01	2.33E+01	
50	2.27E+01	16.4	1.90E+01	2.65E+01	
51	2.09E+01	50.6	1.03E+01	3.14E+01	
52	6.56E+00	14.4	5.61E+00	7.51E+00	
53	2.74E+03	4.6	2.62E+03	2.87E+03	
54	1.00E+02	8.0	9.22E+01	1.08E+02	Boundary crossing
55	1.92E+01	29.0	1.36E+01	2.47E+01	
56	3.66E+01	27.0	2.68E+01	4.65E+01	
57	4.23E+00	14.8	3.60E+00	4.85E+00	

(n/cm<sup>2</sup>/sec)

Table 3-4-5 Estimated thermal neutron fluxes for detectors  
in the pump room

THERMAL FLUXES					The type of the detector
DETECTOR	FLUX	FSD (%)	MIN	MAX	
1	6.26E+03	7.8	5.77E+03	6.74E+03	Point
2	7.40E+03	43.3	4.19E+03	1.06E+04	
3	4.15E+03	6.3	3.89E+03	4.41E+03	
4	3.14E+03	15.2	2.66E+03	3.62E+03	
5	2.89E+03	13.5	2.50E+03	3.28E+03	
6	4.08E+03	23.7	3.11E+03	5.05E+03	
7	1.73E+03	2.8	1.68E+03	1.78E+03	
8	1.47E+03	11.4	1.30E+03	1.63E+03	
9	1.27E+04	5.5	1.20E+04	1.34E+04	
10	6.94E+03	3.1	6.72E+03	7.15E+03	
11	3.07E+03	1.6	3.02E+03	3.12E+03	
12	1.50E+02	66.3	5.06E+01	2.50E+02	Next event
13	8.40E+02	48.8	4.30E+02	1.25E+03	
14	7.35E+02	27.8	5.31E+02	9.40E+02	
15	7.04E+02	18.6	5.73E+02	8.35E+02	
16	7.69E+02	16.7	6.41E+02	8.98E+02	
17	3.54E+03	20.6	2.81E+03	4.26E+03	
18	4.52E+02	13.1	3.92E+02	5.11E+02	
19	1.03E+03	8.8	9.36E+02	1.12E+03	
20	3.98E+03	5.8	3.75E+03	4.21E+03	
21	2.40E+03	8.3	2.20E+03	2.60E+03	
22	2.26E+03	8.2	2.07E+03	2.44E+03	
23	1.74E+03	6.7	1.63E+03	1.86E+03	
24	6.60E+02	8.6	6.04E+02	7.17E+02	
25	2.77E+03	14.3	2.38E+03	3.17E+03	
26	2.58E+03	7.0	2.40E+03	2.76E+03	
27	2.34E+03	6.0	2.20E+03	2.49E+03	
28	8.76E+02	9.7	7.90E+02	9.61E+02	
29	1.74E+03	14.2	1.49E+03	1.98E+03	
30	2.18E+03	14.7	1.86E+03	2.50E+03	
31	4.78E+03	9.0	4.35E+03	5.21E+03	
32	5.61E+03	10.4	5.02E+03	6.20E+03	
33	4.29E+03	11.1	3.81E+03	4.76E+03	
34	5.39E+03	13.9	4.64E+03	6.14E+03	
35	3.56E+03	14.8	3.03E+03	4.09E+03	
36	2.30E+03	12.8	2.01E+03	2.60E+03	
37	3.03E+03	8.9	2.76E+03	3.30E+03	
38	2.08E+03	11.4	1.85E+03	2.32E+03	
39	1.72E+03	9.2	1.56E+03	1.88E+03	
40	3.62E+03	38.9	2.21E+03	5.03E+03	
41	1.97E+03	9.5	1.78E+03	2.15E+03	
42	1.49E+03	9.8	1.34E+03	1.64E+03	
43	2.14E+03	8.9	1.95E+03	2.33E+03	
44	3.05E+03	12.6	2.67E+03	3.43E+03	
45	2.35E+03	10.1	2.11E+03	2.58E+03	
46	3.67E+03	8.4	3.36E+03	3.98E+03	
47	3.41E+03	7.6	3.15E+03	3.67E+03	
48	3.02E+03	7.0	2.81E+03	3.23E+03	
49	3.53E+03	12.4	3.10E+03	3.97E+03	
50	3.37E+03	8.2	3.09E+03	3.65E+03	
51	1.43E+03	12.3	1.26E+03	1.61E+03	
52	1.49E+03	5.9	1.40E+03	1.58E+03	
53	2.04E+04	7.3	1.90E+04	2.19E+04	
54	3.34E+03	6.3	3.13E+03	3.55E+03	Boundary crossing
55	9.18E+02	14.8	7.82E+02	1.05E+03	
56	3.37E+03	22.1	2.63E+03	4.11E+03	
57	9.33E+02	7.5	8.63E+02	1.00E+03	

(n/cm<sup>2</sup>/sec)

Table 3-4-6 Estimated total neutron fluxes for detectors  
in the pump room

DETECTOR	TOTAL FLUXES FLUX	UNIT RESPONSE FOR ALL GROUPS			The type of the detector
		FSD (%)	MIN	MAX	
1	1.20E+05	16.4	1.00E+05	1.40E+05	Point
2	2.44E+05	39.7	1.47E+05	3.41E+05	
3	2.49E+04	14.2	2.14E+04	2.85E+04	
4	9.02E+03	7.6	8.34E+03	9.71E+03	
5	7.09E+03	10.1	6.37E+03	7.81E+03	
6	1.52E+04	21.1	1.20E+04	1.84E+04	
7	4.02E+03	1.8	3.95E+03	4.09E+03	
8	4.04E+03	16.1	3.39E+03	4.69E+03	
9	8.69E+04	1.7	8.54E+04	8.83E+04	
10	3.50E+04	1.1	3.46E+04	3.54E+04	
11	8.34E+03	.9	8.27E+03	8.42E+03	
12	2.35E+03	46.5	1.26E+03	3.45E+03	Next event
13	3.09E+03	25.4	2.31E+03	3.88E+03	
14	3.00E+03	15.0	2.55E+03	3.45E+03	
15	2.77E+03	11.0	2.46E+03	3.07E+03	
16	2.76E+03	10.7	2.47E+03	3.06E+03	
17	7.93E+03	10.1	7.12E+03	8.73E+03	
18	7.32E+02	10.0	6.59E+02	8.05E+02	
19	2.72E+03	18.2	2.23E+03	3.22E+03	
20	7.09E+03	4.2	6.80E+03	7.39E+03	
21	3.75E+03	6.5	3.51E+03	4.00E+03	
22	3.50E+03	6.7	3.26E+03	3.73E+03	
23	3.14E+03	8.6	2.87E+03	3.41E+03	
24	9.91E+02	8.6	9.06E+02	1.08E+03	
25	5.52E+03	8.1	5.07E+03	5.96E+03	
26	5.74E+03	4.4	5.49E+03	5.99E+03	
27	5.00E+03	4.0	4.79E+03	5.20E+03	
28	3.87E+03	9.9	3.49E+03	4.25E+03	
29	3.32E+03	9.7	3.00E+03	3.64E+03	
30	6.81E+03	8.6	6.22E+03	7.39E+03	
31	1.38E+04	5.3	1.31E+04	1.46E+04	
32	1.49E+04	6.8	1.39E+04	1.59E+04	
33	1.48E+04	5.6	1.40E+04	1.56E+04	
34	1.52E+04	6.3	1.43E+04	1.62E+04	
35	1.08E+04	6.7	1.01E+04	1.16E+04	
36	8.67E+03	7.1	8.06E+03	9.29E+03	
37	8.38E+03	7.2	7.78E+03	8.99E+03	
38	6.70E+03	9.2	6.09E+03	7.32E+03	
39	4.22E+03	10.3	3.79E+03	4.65E+03	
40	5.90E+03	25.1	4.42E+03	7.38E+03	
41	3.35E+03	8.1	3.08E+03	3.62E+03	
42	3.62E+03	10.5	3.24E+03	4.00E+03	
43	5.00E+03	7.2	4.64E+03	5.36E+03	
44	6.34E+03	8.4	5.81E+03	6.87E+03	
45	6.04E+03	8.8	5.51E+03	6.56E+03	
46	1.05E+04	4.6	1.00E+04	1.10E+04	
47	6.72E+03	10.5	6.01E+03	7.43E+03	
48	5.62E+03	5.7	5.30E+03	5.94E+03	
49	7.65E+03	15.5	6.46E+03	8.83E+03	
50	6.83E+03	7.2	6.34E+03	7.33E+03	
51	3.30E+03	8.1	3.03E+03	3.57E+03	
52	3.03E+03	4.9	2.88E+03	3.18E+03	
53	2.65E+05	3.4	2.56E+05	2.74E+05	
54	1.10E+04	3.1	1.07E+04	1.13E+04	Boundary crossing
55	3.59E+03	10.5	3.21E+03	3.97E+03	
56	7.77E+03	10.6	6.94E+03	8.59E+03	
57	2.85E+03	21.1	2.25E+03	3.46E+03	

(n/cm<sup>2</sup>/sec)

Table 3-4-7 Neutron dose rate for detectors in the  
pump room

NEUTRON DOSE CONVERSION 21G MREM/HR					The type of the detector
DETECTOR	DOSE RATE	FSD (%)	MIN	MAX	
1	6.19E+02	12.8	5.40E+02	6.99E+02	Point
2	1.43E+03	39.2	8.68E+02	1.99E+03	
3	1.61E+02	10.9	1.43E+02	1.78E+02	
4	5.06E+01	5.6	4.78E+01	5.35E+01	
5	3.56E+01	9.7	3.22E+01	3.91E+01	
6	8.76E+01	18.8	7.11E+01	1.04E+02	
7	2.01E+01	1.6	1.98E+01	2.04E+01	
8	1.95E+01	14.1	1.68E+01	2.23E+01	
9	6.15E+02	2.2	6.01E+02	6.28E+02	
10	2.46E+02	1.4	2.42E+02	2.49E+02	
11	4.79E+01	1.0	4.74E+01	4.84E+01	
12	1.03E+01	46.9	5.46E+00	1.51E+01	Next event
13	1.29E+01	25.3	9.67E+00	1.62E+01	
14	1.34E+01	14.7	1.15E+01	1.54E+01	
15	1.28E+01	11.3	1.14E+01	1.43E+01	
16	1.28E+01	10.3	1.15E+01	1.41E+01	
17	4.02E+01	10.0	3.62E+01	4.42E+01	
18	3.34E+00	11.5	2.96E+00	3.72E+00	
19	1.30E+01	16.2	1.09E+01	1.51E+01	
20	3.21E+01	4.3	3.07E+01	3.35E+01	
21	1.76E+01	7.5	1.63E+01	1.90E+01	
22	1.50E+01	7.1	1.40E+01	1.61E+01	
23	1.41E+01	9.5	1.28E+01	1.54E+01	
24	4.37E+00	9.6	3.95E+00	4.79E+00	
25	2.67E+01	7.2	2.47E+01	2.86E+01	
26	2.87E+01	4.9	2.73E+01	3.01E+01	
27	2.33E+01	4.4	2.23E+01	2.44E+01	
28	2.78E+01	28.1	2.00E+01	3.56E+01	
29	1.53E+01	10.6	1.36E+01	1.69E+01	
30	3.25E+01	9.4	2.95E+01	3.56E+01	
31	7.41E+01	5.8	6.98E+01	7.83E+01	
32	7.93E+01	6.9	7.39E+01	8.48E+01	
33	8.48E+01	7.0	7.89E+01	9.07E+01	
34	9.23E+01	6.7	8.61E+01	9.85E+01	
35	7.11E+01	9.1	6.47E+01	7.76E+01	
36	5.30E+01	8.3	4.86E+01	5.74E+01	
37	4.17E+01	8.7	3.81E+01	4.53E+01	
38	3.33E+01	10.3	2.99E+01	3.67E+01	
39	1.86E+01	10.4	1.67E+01	2.06E+01	
40	2.63E+01	22.8	2.03E+01	3.23E+01	
41	1.52E+01	8.6	1.39E+01	1.65E+01	
42	1.70E+01	10.3	1.53E+01	1.88E+01	
43	2.72E+01	9.4	2.47E+01	2.98E+01	
44	3.31E+01	9.3	3.00E+01	3.62E+01	
45	3.54E+01	10.2	3.18E+01	3.90E+01	
46	5.90E+01	5.1	5.60E+01	6.20E+01	
47	3.08E+01	10.7	2.76E+01	3.41E+01	
48	2.53E+01	6.2	2.37E+01	2.69E+01	
49	3.55E+01	13.4	3.08E+01	4.03E+01	
50	3.64E+01	8.1	3.35E+01	3.94E+01	
51	1.60E+01	8.7	1.46E+01	1.74E+01	
52	1.36E+01	5.6	1.29E+01	1.44E+01	
53	1.48E+03	2.8	1.44E+03	1.52E+03	
54	6.74E+01	3.9	6.48E+01	7.00E+01	Boundary crossing
55	1.81E+01	11.5	1.61E+01	2.02E+01	
56	3.99E+01	10.5	3.57E+01	4.40E+01	
57	1.37E+01	18.6	1.11E+01	1.62E+01	

(mrem/hour)

Table 3-4-8 Reaction Rates in the Pump Room

(Unit:  $\times 10^{-24}$  reactions/atom $\cdot$ sec $\cdot$ 50MW $_e$ )

Position	$^{235}\text{U}(n,f)$				$^{238}\text{U}(n,f)$				$^{232}\text{Th}(n,f)$			
	Exp.	Cal. 1) (fsd %)	Relative C/E	(Absolute) C/E	Exp.	Cal. 1) (fsd %)	Relative C/E	(Absolute) C/E	Exp.	Cal. 1) (fsd %)	Relative C/E	(Absolute) C/E
1. Upper pos. on the source	7.0+7	2.7+6 (5.4)	1.0	(0.039)	1.97+3	1.89+0 (18)	1.0	(1/1040)	1.2+3	1.2-1 (50)	1.0	(1/10000)
2. Lower pos. on the source	5.3+7	3.5+6 (22)	1.69	(0.066)	1.59+3	6.1+0 (66)	4.0	(1/260)	1.0+3	7.2-2 (15)	0.72	(1/13900)
3. Surface of the primary pump	1.74+7	1.80+6 (5.5)	2.6	(0.103)	1.59+2	3.78-1 (3.5)	2.5	(1/420)	1.0+2	2.49-2 (2.4)	2.5	(1/4020)
7. Top surface of FFD/DN	1.47+7	6.38+5 (2.5)	1.10	(0.043)	1.54+1	4.19-2 (1.7)	2.8	(1/370)	1.0+1	1.62-3 (2.1)	1.61	(1/6200)
8. Side surface of FFD/	5.2+6	5.7+5 (11)	2.8	(0.110)	6.6+0	2.77-2 (1.6)	4.3	(1/240)	4.0+0	1.55-3 (3.5)	3.8	(1/2600)

Position	$^{32}\text{S}(n,p)^{32}\text{P}$				$^{109}\text{Ag}(n,\gamma)^{110\text{m}}\text{Ag}$				$^{181}\text{Ta}(n,\gamma)^{182}\text{Ta}$			
	Exp.	Cal. 1) (fsd %)	Relative C/E	(Absolute) C/E	Exp. 2)	Cal. 1) (fsd %)	Relative C/E	(Absolute) C/E	Exp. 2)	Cal. 1) (fsd %)	Relative C/E	(Absolute) C/E
1. Upper pos. on the source	2.0+1	1.76-2 (15)	1.0	(1/1140)	1.193+6	1.45+5 (16)	1.0	(0.12)	2.158+7	2.39+6 (9.9)	1.0	(0.111)
2. Lower pos. on the source	1.6+1	1.66-2 (7.9)	1.19	(1/960)	1.214+6	2.0+5 (29)	1.33	(0.16)	2.378+7	3.5+6 (18)	1.32	(0.147)
3. Surface of the primary pump	-	6.43-3 (2.6)	-	-	3.520+5 3.540+5	1.09+5 (15)	2.6 2.6	(0.31) (0.31)	4.151+6 3.624+6	1.18+6 (13)	2.5 3.0	(0.28) (0.33)
7. Top surface of FFD/DN	-	3.90-4 (3.0)	-	-	1.831+5	1.66+4 (2.0)	0.76	(0.091)	1.634+6	1.590+5(1.8)	0.87	(0.097)
9. 70 cm from the B <sub>4</sub> C shield	-	3.42-2 (3.6)	-	-	8.847+5	2.37+5 (4.6)	2.2	(0.27)	1.131+7	2.66+6 (3.7)	2.2	(0.24)

N.B. 1) Calculated values for positions 3, 7, 8 and 9 are multiplied by a factor of 1.52 to take into account the component coming through the penetration for the primary coolant inlet pipe, for the argon cover gas pipe and the cable ducts.

2) Two detectors were set at the surface of the primary pump.



Table 3-4-9 Reaction Rates at the Opening of the Primary Coolant Outlet Pipe Penetration in the Primary Pump Room

(Unit:  $\times 10^{-24}$  reactions/atom $\cdot$ sec $\cdot$ 100MW<sub>t</sub>)

Reaction	Calculation in the duct for coolant pipe			Calculation in the pump room		Measurements	
	Detector 8	Detector 12	Detector 13	Detector 1	Detector 2		
Thermal flux.	4.1+2 <sup>a</sup> ) (50) (1.0)	7.5+2 (46) (1.83)	1.85+3 (49) (4.5)	6.26+3 (7.8) (15.3)	7.4+3 (43) (18.0)	-	-
<sup>197</sup> Au(n,γ)	6.0+6 (20) (1.0)	2.3+7 (17) (3.8)	5.7+6 (16) (0.95)	6.8+6 (16) (1.13)	8.9+6 (31) (1.48)	3.38+8 <sup>b</sup> )	-
[ <sup>197</sup> Au(n,γ)]Cd	6.0+6 (20) (1.0)	2.3+7 (17) (3.8)	5.5+6 (17) (0.92)	6.4+6 (17) (1.07)	8.3+6 (33) (1.38)	4.72+8 <sup>b</sup> )	-
<sup>50</sup> Cr(n,γ)	3.3+4 (14) (1.0)	8.6+4 (9.6) (2.6)	4.9+4 (27) (1.48)	1.29+5 (5.8) (3.9)	1.58+5 (29) (4.8)	1.76+8 <sup>b</sup> )	-
<sup>58</sup> Fe(n,γ)	8.2+3 (24) (1.0)	2.6+4 (24) (3.2)	8.0+3 (19) (0.98)	2.67+4 (6.4) (3.3)	4.44+4 (29) (5.4)	1.56+7 <sup>b</sup> )	-
<sup>59</sup> Co(n,γ)	8.0+5 (23) (1.0)	1.95+6 (33) (2.4)	7.7+5 (20) (0.96)	1.60+6 (9.3) (2.0)	1.67+6 (11) (2.3)	5.13+8 <sup>b</sup> )	-
<sup>123</sup> Sb(n,γ)	1.51+6 (26) (1.0)	3.7+6 (15) (2.5)	1.11+6 (18) (0.74)	1.61+6 (12) (1.07)	2.73+6 (25) (1.81)	-	-
<sup>109</sup> Ag(n,γ) <sup>110m</sup> Ag	2.6+5 (19) (1.0)	1.0+6 (16) (3.8)	2.5+5 (16) (0.96)	3.0+5 (16) (1.15)	4.0+5 (29) (1.54)	2,386+6 <sup>c</sup> )	2,428+6 <sup>d</sup> )
<sup>181</sup> Ta(n,γ)	4.1+6 (15) (1.0)	1.34+7 (12) (3.3)	3.5+6 (12) (0.85)	4.78+6 (9.9) (1.17)	6.96+6 (18) (1.70)	4.316+7 <sup>c</sup> )	4.756+6 <sup>d</sup> )
<sup>235</sup> U(n,f)	1.98+6 (14) (1.0)	5.2+6 (11) (2.6)	2.3+6 (19) (1.16)	5.35+6 (5.4) (2.7)	7.03+6 (22) (3.6)	1.40+8 <sup>c</sup> )	1.06+8 <sup>d</sup> )
<sup>238</sup> U(n,f)	4.7+0 (9.4) (1.0)	9.7+0 (7.4) (2.1)	4.5+0 (12) (0.96)	3.8+0 (18) (0.81)	1.2+1 (66) (2.6)	3.94+3 <sup>c</sup> )	3.18+3 <sup>d</sup> )
<sup>232</sup> Th(n,f)	4.1-1 (16) (1.0)	6.7-1 (11) (1.63)	3.1-1 (7.9) (0.76)	2.4-1 (50) (0.59)	1.4-1 (15) (0.34)	2.4+3 <sup>c</sup> )	2.0+3 <sup>d</sup> )
<sup>32</sup> S(n,p)	1.33-1 (14) (1.0)	1.59-1 (20) (1.20)	1.05-1 (8.4) (0.79)	3.5-2 (15) (0.26)	3.3-2 (7.9) (0.25)	4.0+1 <sup>c</sup> )	3.2+1 <sup>d</sup> )

N.B. a) Read as  $4.1 \times 10^2$  n/cm<sup>2</sup>·sec·100MW<sub>th</sub>. b) ST 21 experiments<sup>5)</sup>.  
c,d) ST11 experiemnts<sup>6)</sup>. Upper and lower positions, respectively.

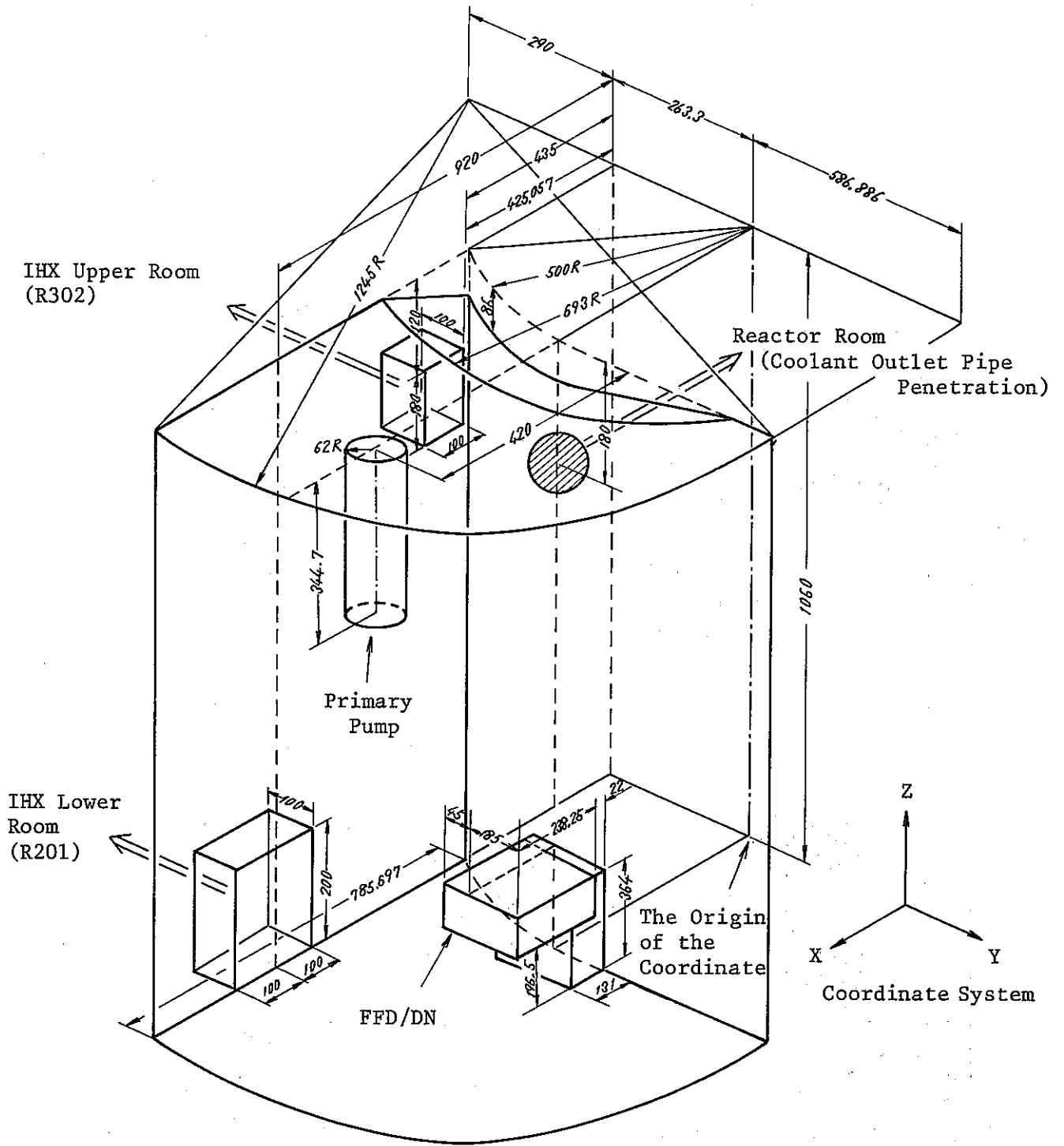


Fig. 3-4-1 Dimensions of pump room

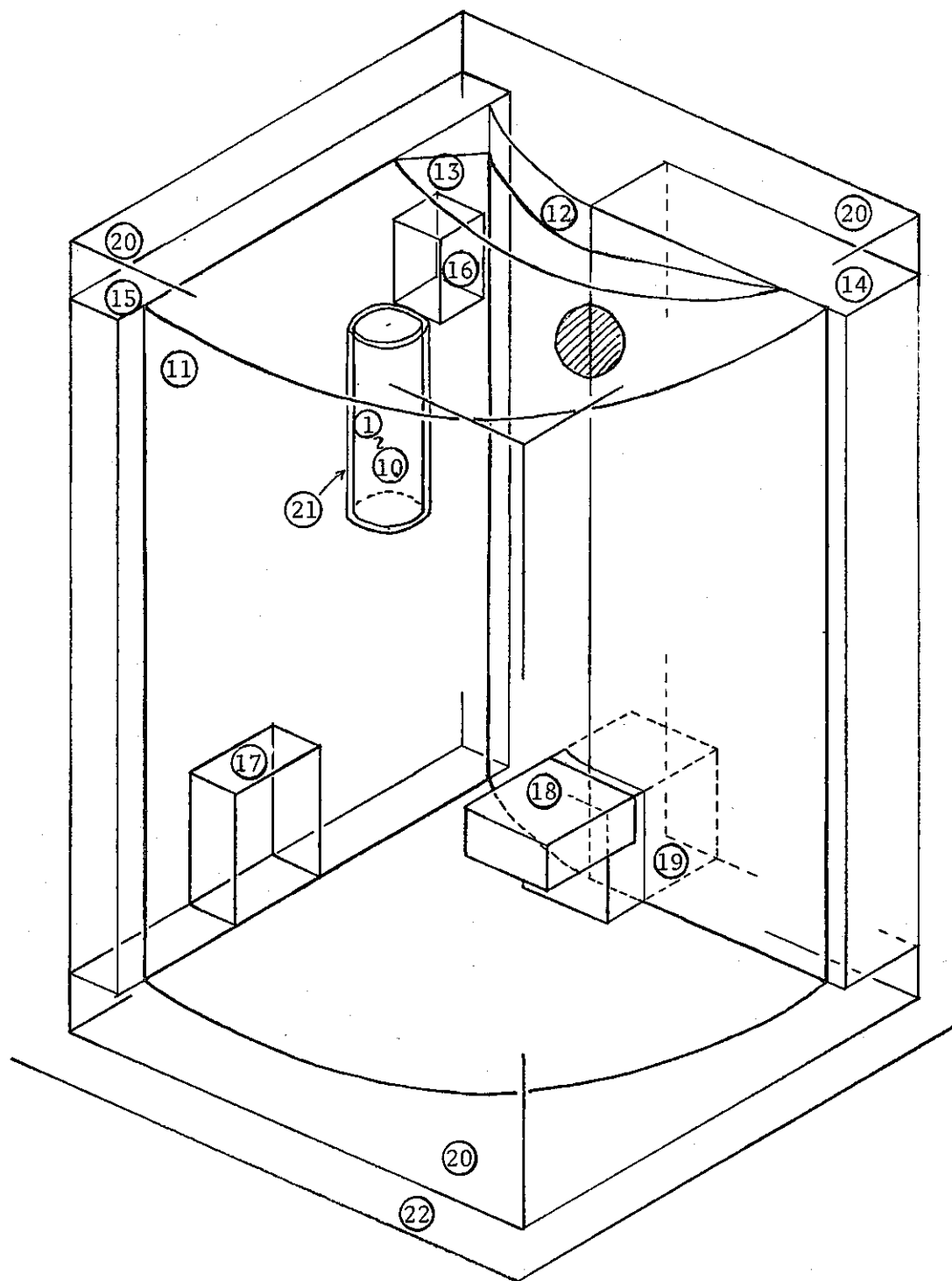


Fig. 3-4-2 Arrangement of bodies constituting the pump room

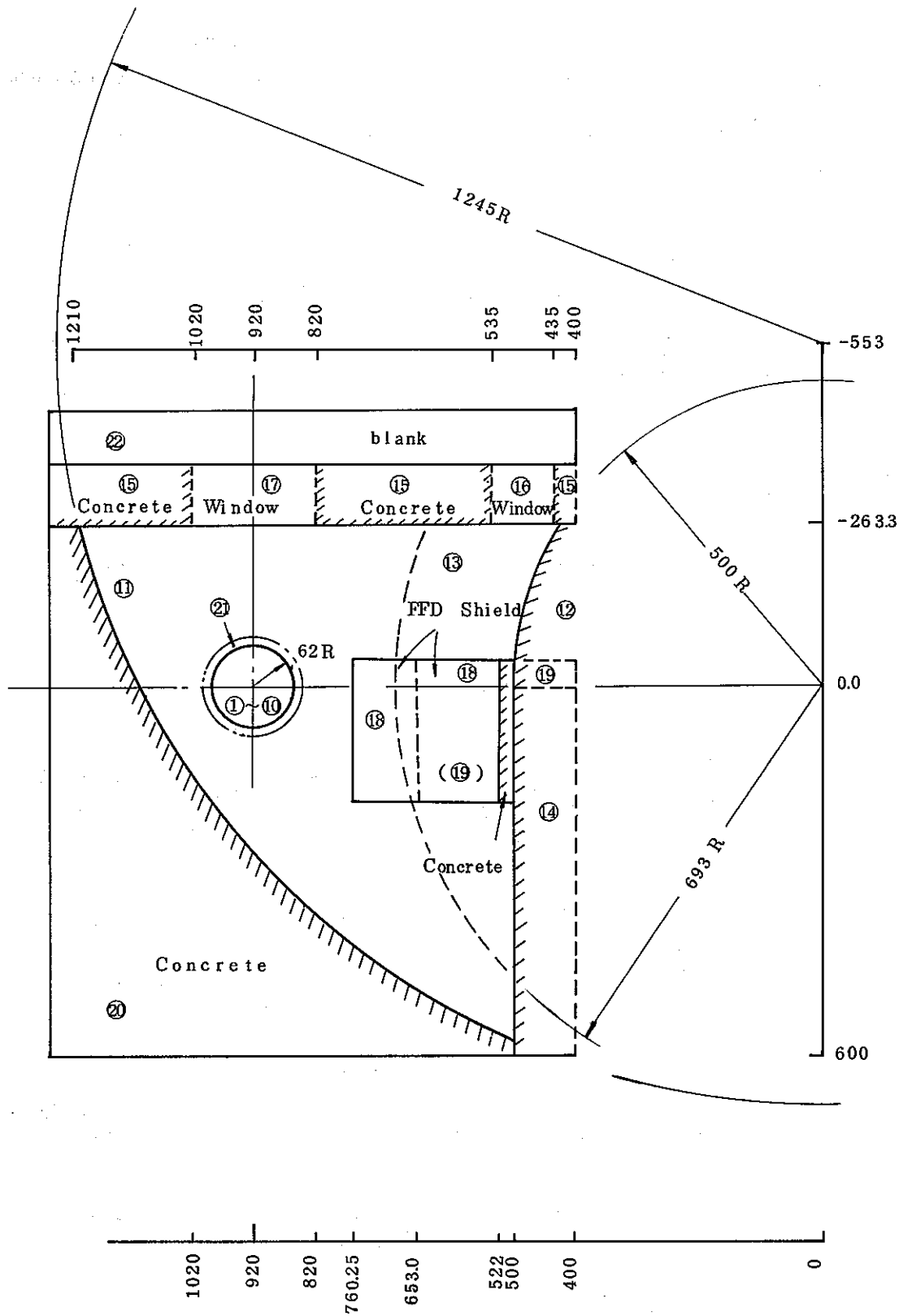


Fig. 3-4-3 Horizontal scheme of pump room with body numbers  
(Unit: cm)

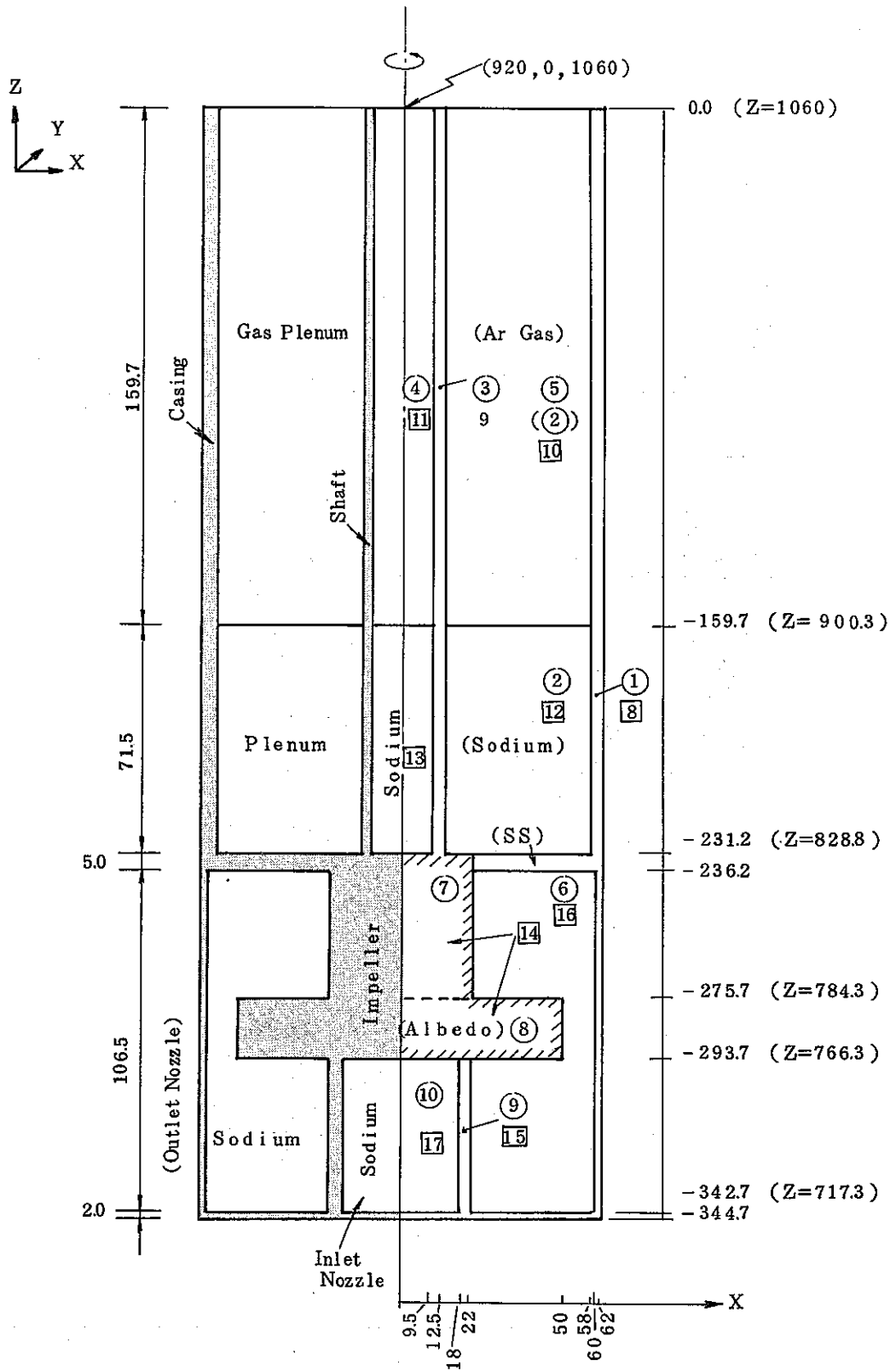


Fig. 3-4-4 Body arrangements in the calculational model of primary pump (Unit: cm)

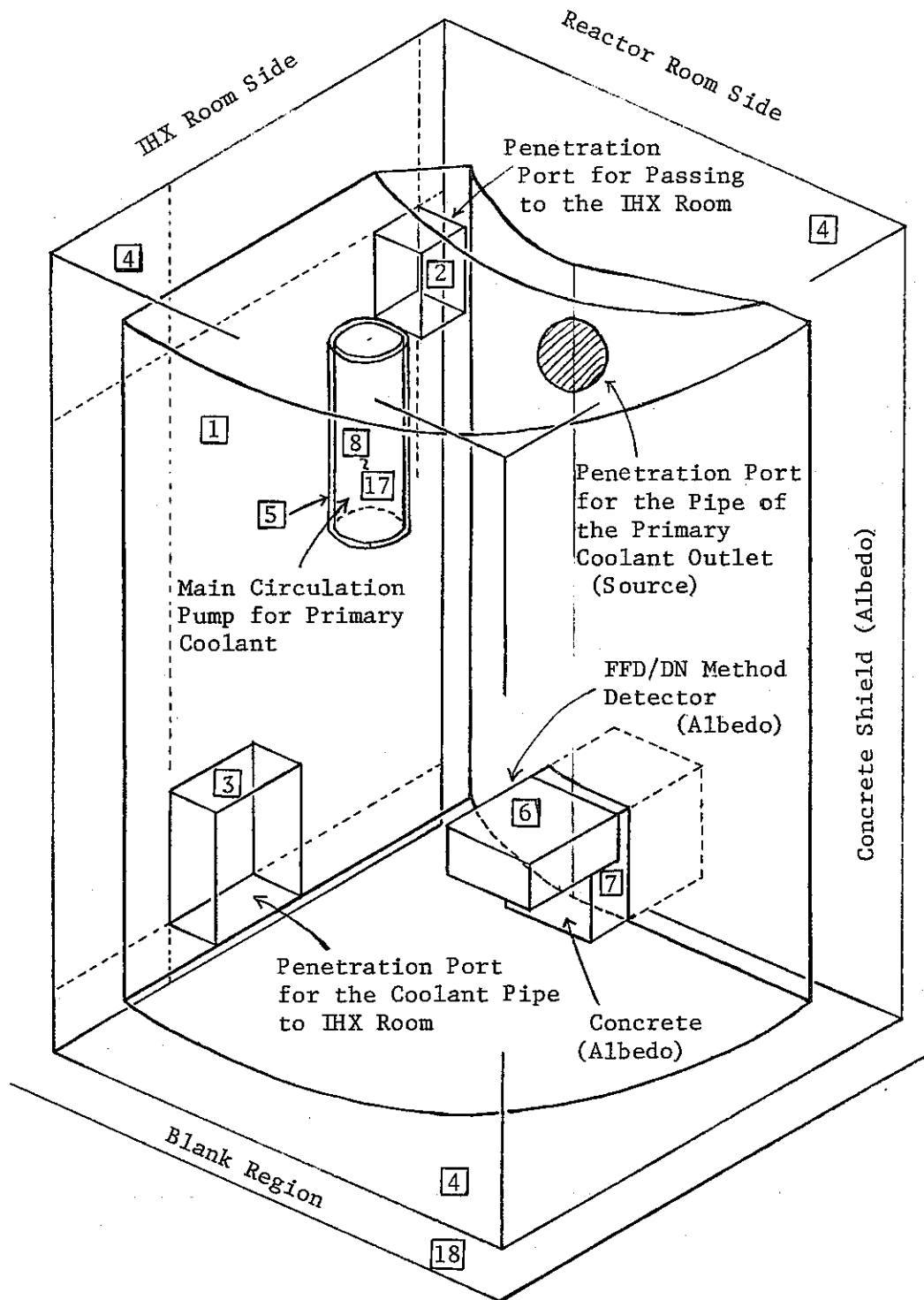


Fig.3-4-5 Regions for the calculation of the pump room

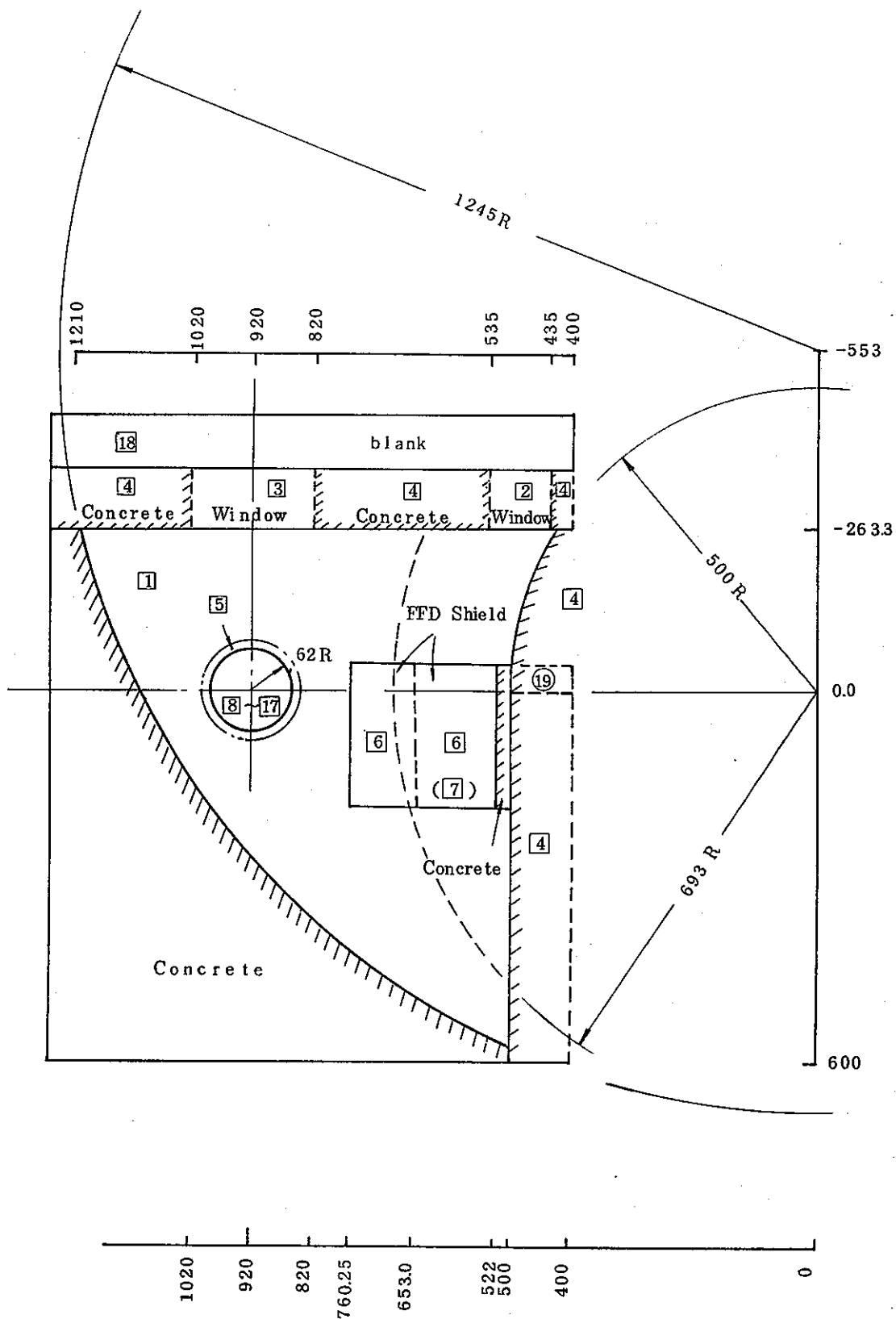


Fig. 3-4-6 Horizontal scheme of pump room with region numbers  
(Unit: cm)

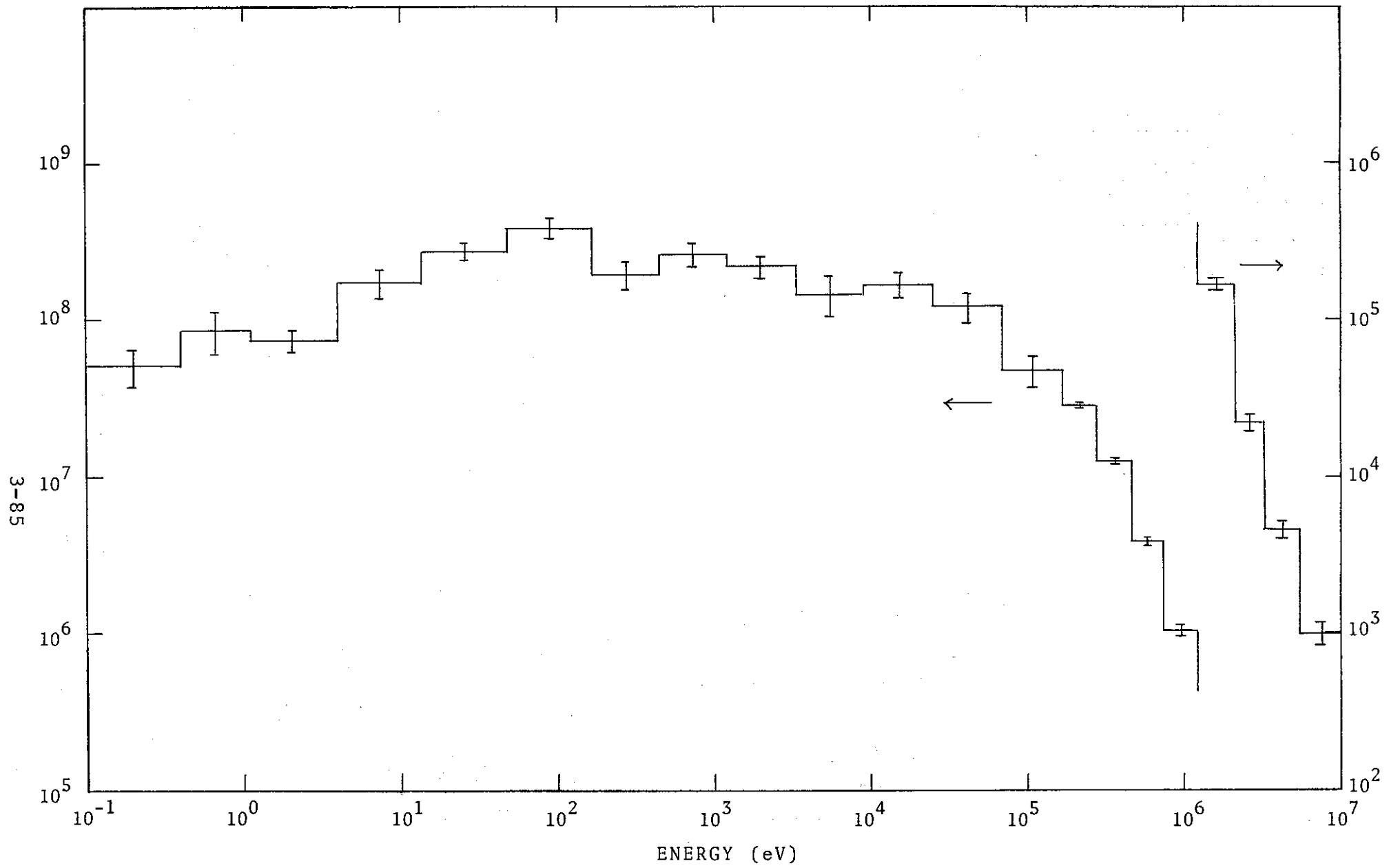
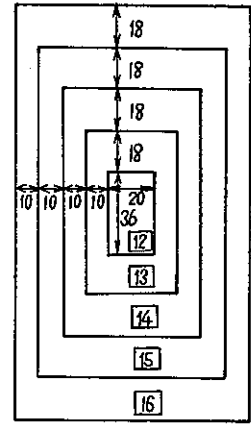
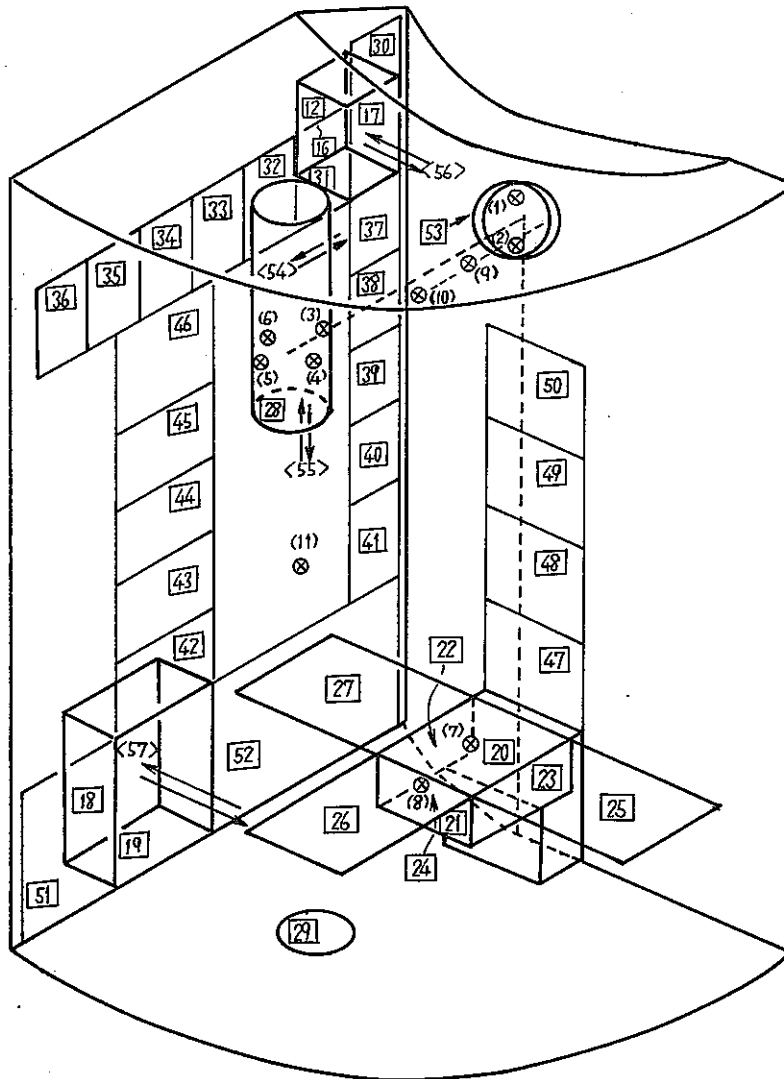


Fig.3-4-7 Source spectrum for primary pump room neutron analysis





unit:cm  
 Next Event Estimators at  
 the Opening to the IHX  
 Room



- (1)~(11) Point Detector
- 12 ~ 52 Next Event Estimator
- <53>~<60> Boundary Crossing Estimator

Fig. 3-4-8 Flux estimators used for the calculation  
 in the pump room

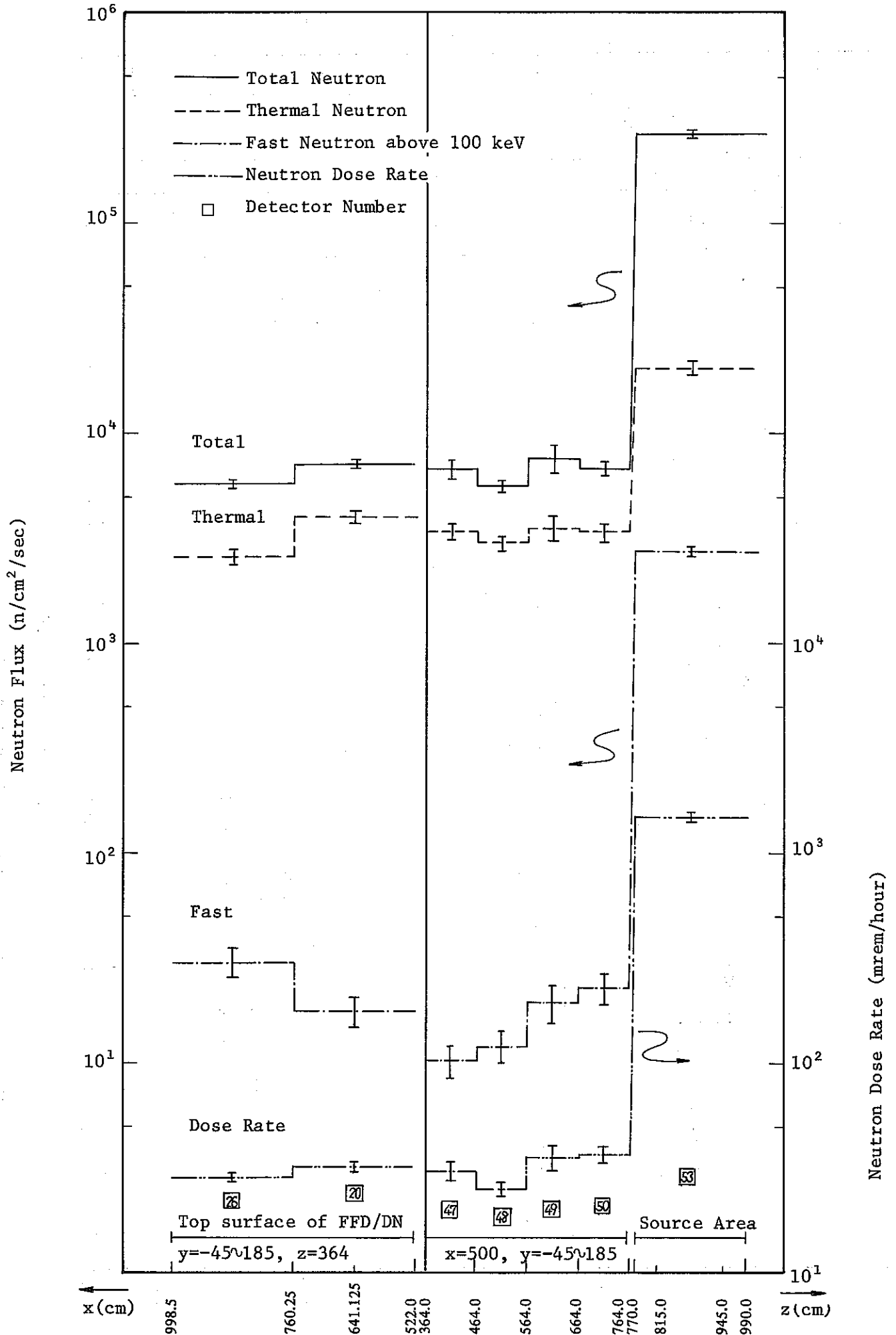


Fig. 3-4-9 Neutron flux and dose rate distributions on the FFD/DN and downward from the source in the pump room

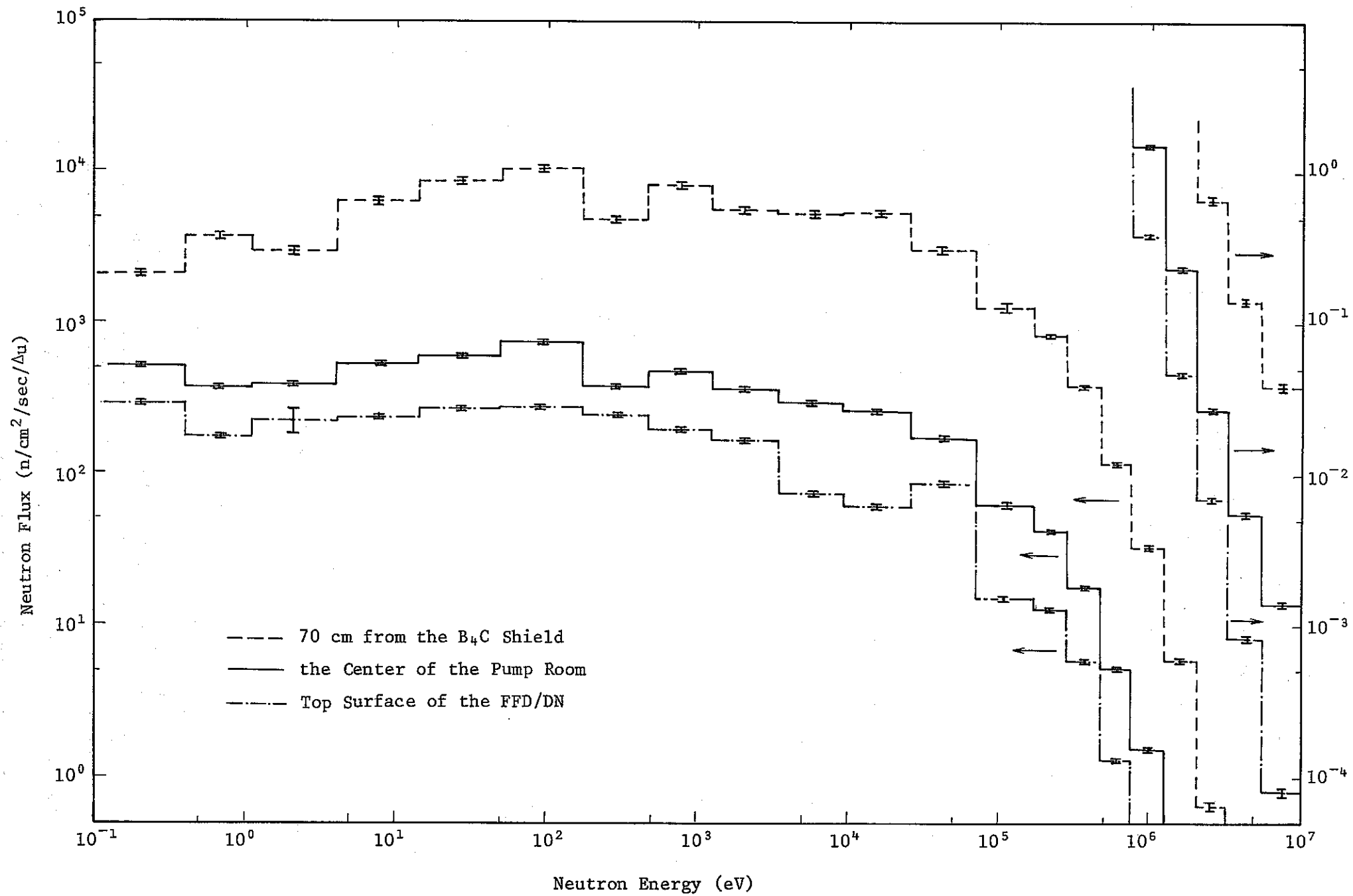


Fig. 3-4-10 Neutron spectra in the pump room

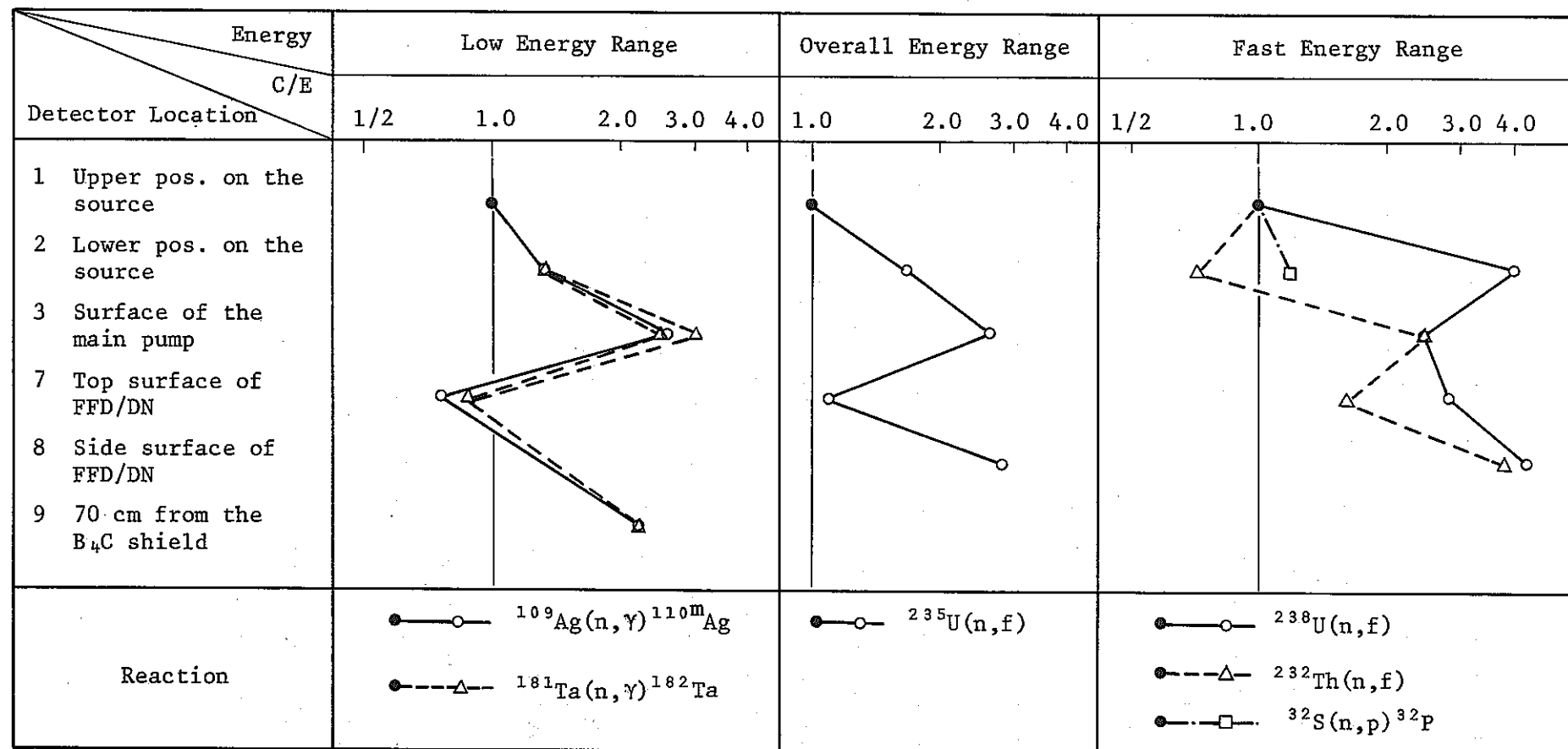


Fig. 3-4-11 C/E values for various reactions at several locations in the pump room

### 3.5 Neutron Streaming Analysis for the IHX Room

Cross sectional view of the IHX room (R302, A-loop) is shown in Fig. 2-3-1 and Fig. 2-4-1. Neutron streaming passes to IHX room are ducts of argon cover-gas pipe and sodium overflow pipe penetrating the biological concrete shield and a passage way, 1 m wide by 1.8 m in height, to the primary pump room. Neutron current flowing into the IHX room from the pump room was  $5.32 \times 10^7$  n/sec/100MW<sub>t</sub> according to the neutron distribution analysis in the pump room. On the other hand, neutron current from the argon cover-gas pipe duct was estimated at  $2.75 \times 10^9$  n/sec/100MW<sub>t</sub> by Monte Carlo method. Therefore neutrons streaming through the ducts give a main contribution to the neutron flux in the IHX room. In the present analysis, neutron distribution in the IHX room was calculated with only the source due to the duct of argon cover-gas pipe and the values obtained by Monte Carlo calculation were doubled since the two ducts have the same radius and are close to each other.

The analysis was performed in two steps with albedo Monte Carlo code MORSE-ALB<sup>7 ~ 11</sup>). In the first step, neutron streaming through the duct of argon cover-gas pipe was calculated and in the second step neutron behaviour in the IHX room was analyzed.

### 3.5.1 Neutron Streaming Calculation through the Argon Cover-gas Pipe Duct (source calculation)

The argon cover-gas duct has a diameter of 85 cm and its axis is located at the height of 396 cm from mid-core level. A calculational model is shown in Fig. 3-5-1. The biological concrete shield was treated by albedo boundary, which was taken at the depth of 5 cm from the concrete surface. Atomic number density of each component is shown in Table 3-3-1. SS304 (stainless steel of type 304) was diluted by a factor of 0.06046 for the bellows.

Neutron source to this duct was edited by the DOMINO-N code<sup>10)</sup> from results of DOT3.5 calculation which has been performed as "Radiation shielding analyses of JOYO"<sup>1,2)</sup>. In the edition, the fluxes between  $z=346$  cm and  $446$  cm at  $r=382.9$  cm were used, and isotropic angular distribution was assumed. The disc source with the radius of 50 cm obtained by the DOMINO-N code was located at  $z=-1.5$  cm as shown in Fig. 3-5-1. The source preserves axial flux distribution and azimuthal curvature in DOT3.5 R-Z calculation. Source intensity is  $3.294 \times 10^{11}$  n/sec/100 MW<sub>t</sub>, and its spectrum and biasing factors in Monte Carlo calculation are shown in Table 3-5-1.

Detector locations are shown in Table 3-5-2 and Fig. 3-5-2. Detectors with numbers 6 to 10 are used for neutron source calculation to IHX room and are located at the outside of the B<sub>4</sub>C shield panel.

Two cases of Monte Carlo calculation were executed using biasing parameters shown in Table 3-5-3. One is the calculation for whole energy neutron with 15,000 histories, and another is for fast neutron (1st through 8th group) with 20,000 histories. Computer times were 37 minutes and 13 minutes on FACOM M200, respectively.

The results from two cases were summarized. Table 3-3-4 shows total neutron fluxes, fast neutron fluxes above 0.1 Mev, thermal neutron fluxes and neutron dose rates. Figure 3-5-3 shows attenuation curves of the quantities mentioned above in the argon cover-gas pipe. Neutrons decrease by about two orders of magnitude from the duct mouth to the exit.

As for the detectors with numbers 6 to 10 whose results were used for the source to IHX room, neutron fluxes have an anisotropy of  $\bar{\mu}$  ranging from 0.6 to 0.9, where  $\bar{\mu}$  is the value of direction cosine (to IHX room) averaged over the neutron angular fluxes. The results by detectors from No.6 to No.10 are edited into a disc neutron source with radius of 70 cm for IHX room by the DOMINO-N code<sup>10</sup>). The contribution of the flux scored by the detector of No.10 which has a cylindrical geometry (see Fig. 3-5-2) was added to the flux in the outermost angle obtained by the detector of No.9 to make the source for the IHX room calculation. Obtained neutron current coming out of argon cover-gas pipe duct to IHX room was  $2.75 \times 10^9$  n/sec/100MW<sub>t</sub> (+4.6%). Neutron spectrum shown in Fig. 3-5-4 has an accuracy of 10 ~ 20% for each group and has an 1/E shape

in energy range of 10 keV ~ 1eV. In the figure, flux reduction for slow neutron due to absorption by the  $B_4C$  shield panels is prominent.

### 3.5.2. Calculational Model and Conditions for the IHX Room

Calculational geometry is shown in Fig. 3-5-5. Concrete surface of the room was treated as albedo boundary. IHX was divided into two regions at primary coolant level. Atomic number densities of the materials are shown in Table 3-1-1.

A disc neutron source of 70 cm radius was located at the exit of the argon cover-gas pipe duct with a distance of 19.86 cm away from the biological concrete shield. The source energy biasing factors are shown in Table 3-5-1. Other parameters for the present calculations are listed in Table 3-5-5.

Detector type and locations are shown in Table 3-5-6 and Fig. 3-5-6. In order to reduce computer time consumed by random walks in the IHX, path stretching bias was employed so that particles pointing outwards were strengthened in the IHX and thermal insulation region. The biasing factors and conditions of Russian roulette kill are shown in Table 3-5-7.

Calculations were performed for overall energy neutrons up to 10,000 histories and for fast neutrons (1st through 8th group) up to 20,000 histories. Computer times were 35 minutes and 16 minutes on FACOM-M200 respectively.



### 3.5.3 Results and Comparison with Measured Data

Fluxes obtained for the 1st through the 8-th group from whole energy calculation were replaced with results of fast neutron calculation. The following numerical values were obtained on the basis of the neutron intensity  $2.75 \times 10^9$  n/sec/100MW<sub>t</sub> from the argon cover-gas pipe duct. They do not include contribution from overflow pipe duct through the biological concrete shield. Deviations in source distribution are not taken into account in the calculated values.

Table 3-5-8 shows total, fast and thermal neutron fluxes and neutron dose rate. At the source position, neutron flux is  $4.9 \times 10^3$  n/sec/cm<sup>2</sup> for fast neutron and  $1.2 \times 10^5$  n/sec/cm<sup>2</sup> for thermal neutron. Fast neutrons decrease by a decade and thermal neutrons by a factor of 4 to 8 from the source position to the front surface of the IHX (detector No.4). The fast and thermal neutron fluxes at the back surface of the IHX (detector No.5) are 1/40 and 1/5 of the fluxes at the front, respectively. A change of neutron fluxes in axial direction on the surface of the IHX are small.

An average neutron flux on the whole surface of the IHX was estimated at  $1.3 \times 10^2$  n/sec/cm<sup>2</sup> for fast neutron and  $4.2 \times 10^3$  n/sec/cm<sup>2</sup> for thermal neutron. A volume-averaged thermal neutron flux which was obtained by track length estimator was  $7.2 \times 10^2$  n/sec/cm<sup>2</sup> ( $\pm 10\%$ ) in the upper part of the IHX (region No.7) and  $7.7 \times 10^2$  n/sec/cm<sup>2</sup> ( $\pm 8\%$ ) in the lower part (region No.8).

Neutron spectra at the source position and the IHX surface are shown in Fig. 3-5-7. Neutron spectrum at the front of the IHX is similar to that for source position except thermal neutron. A spectrum at the rear of the IHX is soft and fast neutron component is very small.

Table 3-5-9 shows comparison of calculated reaction rate with measured data<sup>6)</sup> for reactions such as  $^{235}\text{U}(n,f)$ ,  $^{238}\text{U}(n,f)$ ,  $^{232}\text{Th}(n,f)$ ,  $^{32}\text{S}(n,p)^{32}\text{P}$ ,  $^{109}\text{Ag}(n,\gamma)^{110}\text{Ag}$  and  $^{181}\text{Ta}(n,\gamma)^{182}\text{Ta}$ . Positions are shown in Fig. 2.4.1. Two measured values for Ag and Ta are shown in Table 2-4-1 and were averaged for the comparison. Calculated values by Monte Carlo method mentioned above were doubled to include contribution from overflow pipe duct. But the results at the source position (location No.2 and 5) were used without doubling process.

Since neutron distributions were not measured in the argon cover-gas pipe duct, C/E values were normalized to those at the duct exit (location No.2). Absolute and relative values of C/E are shown in Table 3-5-9. Changes of the relative C/E values with detector positions are shown in Fig. 3-5-8. The following discussions were made concerning the relative C/E values.

The C/E values for  $^{32}\text{S}(s,p)^{32}\text{P}$ ,  $^{232}\text{Th}(n,f)$  and  $^{238}\text{U}(n,f)$  reactions which are caused by fast neutron are 0.34 ~ 0.71 at the front of the IHX (location No.4) and 2.6 ~ 5.9 at the rear (location No.3). The C/E value of  $^{235}\text{U}(n,f)$  reaction which

is sensitive to thermal and the other energy range is 1.6 at the front of the IHX and 2.9 at the rear, that is, calculated values agree with experimental data within a factor of 3. As for  $^{109}\text{Ag}(n,\gamma)^{110\text{m}}\text{Ag}$  and  $^{181}\text{Ta}(n,\gamma)^{182}\text{Ta}$  reactions which are very sensitive to low energy neutron, agreement is better: the C/E values are  $0.79 \sim 1.21$  at the front and  $1.15 \sim 1.26$  at the rear. It is found from Fig. 3-5-8 that calculation generally underestimated neutron fluxes at the front of the IHX and overestimated them at the rear. This tendency is more conspicuous for high energy range. These discrepancies must have been caused by the neglect of the pipes in the IHX room or by the approximation of albedo scattering.

As for the absolute C/E values, Table 3-5-9 shows good agreement between calculation and experiment in the low energy range. However, C/E values for fast neutron are very small. It is supposed that the fast neutron flux at the inner surface of the biological concrete shield was underestimated<sup>1,2)</sup> by the DOT-3.5 code<sup>12)</sup> and was used for source calculation of the present analysis. In the two-dimensional calculation by DOT3.5 code, hollow part in the graphite shield designed to lead the argon cover-gas pipe were not considered, and neutrons that stream through this void region toward the argon cover-gas pipe duct must have been neglected.

Neutron streaming-passes which make a large contribution to neutron source in the IHX room were also examined taking account of C/E values. Nominal value of neutron current from

ducts in the biological concrete shield was 103 times larger than that from the pump room as mentioned at the beginning of this subsection and shown in Table 3-5-10. As a result of analyses, absolute C/E values in the pump room described in the section 3.4 turned out to be smaller than that in the IHX room, which means neutron current from the pump room was underestimated more than that from the ducts. Besides, spectra of neutrons flowing into the IHX room from two sides resemble to each other as shown in Fig. 3-5-9. Therefore, the ratio of neutron current from two sides were corrected using the C/E values, and the results are shown in Table 3-5-10. It is found that neutron intensity from ducts are larger than that from the pump room by a factor of 6 to 10 even if the neutron current ratio is normalized by C/E value.

Table 3-5-1 Source energy distribution for argon cover-gas duct streaming calculation

Energy group	Original source distribution <sup>1)</sup>	Biasing factor	Biased source distribution
1	0.247-7 <sup>2)</sup>	30000.0	0.250-3
2	0.626-7	16000.0	0.337-3
3	0.342-6	5000.0	0.573-3
4	0.261-5	1200.0	0.106-2
5	0.165-4	245.0	0.135-2
6	0.626-4	126.0	0.266-2
7	0.248-3	63.6	0.527-2
8	0.634-3	39.8	0.850-2
9	0.358-2	16.8	0.203-1
10	0.916-2	10.5	0.324-1
11	0.114-1	9.34	0.353-1
12	0.174-1	7.62	0.450-1
13	0.203-1	7.06	0.490-1
14	0.259-1	6.26	0.540-1
15	0.303-1	5.82	0.590-1
16	0.490-1	4.55	0.750-1
17	0.650-1	3.94	0.870-1
18	0.790-1	3.58	0.950-1
19	0.830-1	3.50	0.970-1
20	0.590-1	4.13	0.830-1
21	0.546+0	1.35	0.248+0

N.B. 1) Output of DOMINO code.

2) Read as  $0.247 \times 10^{-7}$ .

Table 3-5-2 Detectors for argon cover-gas duct streaming calculation

No.	Detector type <sup>1)</sup>	Coordinate (cm)			Base vector			Radius		Comment
		X	Y	Z	U	V	W	Inner	Outer	
1	Ring	0.0	0.0	1.0	0.0	0.0	1.0	0.0	21.6	Attenuation in the argon gas pipe
2	Ring	0.0	0.0	30.0	0.0	0.0	1.0	0.0	5.315	
3	Ring	0.0	0.0	70.0	0.0	0.0	1.0	0.0	5.315	
4	Ring	0.0	0.0	99.0	0.0	0.0	1.0	0.0	5.315	
5	Ring	0.0	0.0	119.86	0.0	0.0	1.0	0.0	5.315	
6	Ring	0.0	0.0	119.86	0.0	0.0	1.0	0.0	7.5	Source for IHX room
7	Ring	0.0	0.0	119.86	0.0	0.0	1.0	7.5	21.0	
8	Ring	0.0	0.0	119.86	0.0	0.0	1.0	21.0	50.0	
9	Ring	0.0	0.0	119.86	0.0	0.0	1.0	50.0	70.0	
10	Cylinder	0.0	0.0	100.0	0.0	0.0	1.0	70.0	19.86	Flux around the bellows (duct exit)
11	Ring	0.0	0.0	99.0	0.0	0.0	1.0	32.73	42.5	
12	Ring	0.0	0.0	-1.4	0.0	0.0	1.0	0.0	50.0	Flux at the source
13	Point	35.0	0.0	119.86	0.0	0.0	1.0	-	-	Flux behind the B <sub>4</sub> C shield
14	Point	-35.0	0.0	119.86	0.0	0.0	1.0	-	-	

N.B. 1) Ring and cylinder detectors are next event surface crossing estimators.

Table 3-5-3 Path stretching and Russian Roulette kill condition for argon cover-gas duct streaming calculation

Region No.	Direction of path stretching <sup>1)</sup>				Weight of Russian Roulette kill				
	2) Type	U (R)	V (Z)	W -	1 <sup>4</sup> g	5 <sup>8</sup> g	9 <sup>15</sup> g	16 <sup>20</sup> g	21g
1	1	0.0	0.0	1.0	1.0-7 <sup>3)</sup>	1.0-6	1.0-5	1.0-4	1.0-3
2	1	0.0	0.0	1.0	1.0-7	1.0-6	1.0-5	1.0-4	1.0-3
3	1	0.0	0.0	1.0	1.0-7	1.0-6	1.0-5	1.0-4	1.0-3
4	1	0.0	0.0	1.0	1.0-7	1.0-6	1.0-5	1.0-4	1.0-3
5	1	0.0	0.0	1.0	1.0-7	1.0-6	1.0-5	1.0-4	1.0-3
6	1	0.0	0.0	1.0	1.0-7	1.0-6	1.0-5	1.0-4	1.0-3
7	1	0.0	0.0	1.0	1.0-7	1.0-6	1.0-5	1.0-4	1.0-3
8	1	0.0	0.0	1.0	1.0-7	1.0-6	1.0-5	1.0-4	1.0-3
9	1	0.0	0.0	1.0	1.0-7	1.0-6	1.0-5	1.0-4	1.0-3
10	1	0.0	0.0	1.0	1.0-7	1.0-6	1.0-5	1.0-4	1.0-3
11	1	0.0	0.0	1.0	1.0-7	1.0-6	1.0-5	1.0-4	1.0-3
12	1	0.0	0.0	1.0	1.0-7	1.0-6	1.0-5	1.0-4	1.0-3
13	1	0.0	0.0	1.0	1.0-7	1.0-6	1.0-5	1.0-4	1.0-3
14	1	0.0	0.0	1.0	1.0-7	1.0-6	1.0-5	1.0-4	1.0-3
15	1	0.0	0.0	1.0	1.0-7	1.0-6	1.0-5	1.0-4	1.0-3
16	1	0.0	0.0	1.0	1.0-7	1.0-6	1.0-5	1.0-4	1.0-3
17	2	-0.70711	0.70711	-	1.0-7	1.0-6	1.0-5	1.0-4	1.0-3
18	2	-0.70711	0.70711	-	1.0-5	1.0-4	1.0-3	1.0-2	5.0-2
19	2	-0.70711	0.70711	-	1.0-5	1.0-4	1.0-3	1.0-2	5.0-2
20	2	-0.70711	0.70711	-	1.0-5	1.0-4	1.0-3	1.0-2	5.0-2
21	0	-	-	-	-	-	-	-	-
22	1	0.0	0.0	1.0	1.0-5	1.0-4	1.0-3	1.0-2	5.0-2
23	1	0.0	0.0	1.0	1.0-7	1.0-6	1.0-5	1.0-4	1.0-2
24	1	0.0	0.0	1.0	1.0-7	1.0-6	1.0-5	1.0-4	1.0-2
25	1	0.0	0.0	1.0	1.0-7	1.0-6	1.0-5	1.0-4	1.0-2
26	1	0.0	0.0	1.0	1.0-7	1.0-6	1.0-5	1.0-4	1.0-2
27	1	0.0	0.0	1.0	1.0-7	1.0-6	1.0-5	1.0-4	1.0-2
28	1	0.0	0.0	1.0	1.0-7	1.0-6	1.0-5	1.0-4	1.0-2
29	1	0.0	0.0	1.0	1.0-7	1.0-6	1.0-5	1.0-4	1.0-2
30	1	0.0	0.0	1.0	1.0-7	1.0-6	1.0-5	1.0-4	1.0-2
31	1	0.0	0.0	1.0	1.0-7	1.0-6	1.0-5	1.0-4	1.0-2
32	1	0.0	0.0	1.0	1.0-7	1.0-6	1.0-5	1.0-4	1.0-2
33	1	0.0	0.0	1.0	1.0-7	1.0-6	1.0-5	1.0-4	1.0-2
34	0	-	-	-	-	-	-	-	-

N.B. 1) Bias parameter PATH = 0.5. See Ref. 10.

2) Type = 1 : (X,Y,Z) Coordinate system  
 2 : (R,Z) Coordinate system  
 0 : No-bias

3) Read as  $1.0 \times 10^{-7}$ .

Table 3-5-4 Neutron flux and dose rate distribution in and around the argon cover-gas duct

TOTAL FLUXES		UNIT RESPONSE FOR ALL GROUPS				FAST NEUTRON FLUENCE ABOVE 0.1 MEV			
DETECTOR	FLUX	FSD	MIN	MAX	DETECTOR	FLUX	FSD	MIN	MAX
1	9.7754E+07	.032	9.4607E+07	1.0090E+08	1	2.8565E+05	.099	2.5734E+05	3.1396E+05
2	2.6446E+07	.111	2.3499E+07	2.9393E+07	2	1.8563E+05	.748	4.6746E+04	3.2452E+05
3	8.5555E+06	.147	7.3003E+06	9.8107E+06	3	9.0603E+03	.192	7.3225E+03	1.0798E+04
4	3.4979E+06	.299	2.4536E+06	4.5422E+06	4	7.3895E+03	.334	4.9200E+03	9.8589E+03
5	5.4204E+05	.244	4.0972E+05	6.7436E+05	5	2.1838E+03	.296	1.5377E+03	2.8300E+03
6	3.3430E+05	.207	2.6518E+05	4.0342E+05	6	1.8597E+03	.208	1.4731E+03	2.2463E+03
7	1.8242E+05	.377	1.1360E+05	2.5123E+05	7	2.4272E+03	.114	2.1502E+03	2.7041E+03
8	2.1151E+05	.071	1.9556E+05	2.2647E+05	8	6.8586E+03	.168	5.7057E+03	8.0116E+03
9	2.4501E+05	.112	2.1760E+05	2.7241E+05	9	1.1939E+03	.280	8.6018E+02	1.5276E+03
10	7.9655E+04	.102	7.1547E+04	8.7764E+04	10	2.8971E+02	.284	2.0734E+02	3.7209E+02
11	2.5095E+06	.057	2.3675E+06	2.6515E+06	11	1.2619E+04	.184	1.0301E+04	1.4936E+04
12	1.3208E+08	.019	1.2953E+08	1.3464E+08	12	3.6469E+05	.087	3.3308E+05	3.9631E+05
13	1.8605E+05	.050	1.7753E+05	1.9617E+05	13	5.6662E+03	.129	4.9367E+03	6.3958E+03
14	1.7062E+05	.038	1.6411E+05	1.7712E+05	14	5.3650E+03	.090	4.8806E+03	5.8493E+03

(n/sec/cm<sup>2</sup>)

(n/sec/cm<sup>2</sup>)

THERMAL FLUXES		NEUTRON DOSE CONVERSION 21G MREM/HR				NEUTRON DOSE CONVERSION 21G MREM/HR			
DETECTOR	FLUX	FSD	MIN	MAX	DETECTOR	DOSE RATE	FSD	MIN	MAX
1	4.8045E+07	.047	4.5780E+07	5.0311E+07	1	4.6935E+05	.031	4.5468E+05	4.8401E+05
2	1.0372E+07	.188	8.4183E+06	1.2325E+07	2	1.2956E+05	.117	1.1442E+05	1.4469E+05
3	3.6842E+06	.251	2.7582E+06	4.6101E+06	3	4.7015E+04	.179	3.8591E+04	5.5439E+04
4	6.1882E+05	.276	4.4832E+05	7.8931E+05	4	4.6718E+04	.720	1.3099E+04	8.0338E+04
5	1.0257E+05	.389	6.2714E+04	1.4243E+05	5	2.6944E+03	.229	2.0771E+03	3.3117E+03
6	1.882E+04	.331	4.1385E+04	8.2379E+04	6	1.7622E+03	.192	1.4231E+03	2.1012E+03
7	2.228E+03	.405	1.3227E+03	3.1229E+03	7	1.5654E+03	.315	1.0723E+03	2.0586E+03
8	1.0755E-03	.938	6.5684E-05	2.0840E-03	8	1.6523E+03	.089	1.5050E+03	1.7987E+03
9	3.8820E+04	.114	3.4409E+04	4.3230E+04	9	1.4934E+03	.130	1.2994E+03	1.6873E+03
10	2.2610E+04	.215	1.7758E+04	2.7461E+04	10	4.3761E+02	.183	3.5788E+02	5.1754E+02
11	6.1722E+05	.093	5.5990E+05	6.7453E+05	11	1.3846E+04	.072	1.2849E+04	1.4842E+04
12	7.1258E+07	.032	6.8947E+07	7.3569E+07	12	6.2872E+05	.018	6.1711E+05	6.4032E+05
13	1.5689E+02	.632	5.7790E+01	2.5594E+02	13	1.6394E+03	.067	1.5304E+03	1.7485E+03
14	3.9526E+02	.659	1.3461E+02	6.5591E+02	14	1.4107E+03	.042	1.3515E+03	1.4699E+03

(n/sec/cm<sup>2</sup>)

(mrem/hour)



Table 3-5-5 Description of input parameters of Monte Carlo calculation for the IHX room

Geometry .....	11 bodies with combinatory geometry <sup>17)</sup> . 11 regions (see Fig. 3-5-5). 9 media including 3 albedo medium.
Cross section .....	P <sub>5</sub> , 21 groups.
Neutron source .....	Circular disc source with 70 cm radius. Energy-space-angle dependent. Generated by DOMINO-N code <sup>10)</sup> from the results of Ar cover gas duct streaming analysis.
Flux estimator .....	10 point, 5 next event surface crossing <sup>11)</sup> and 4 boundary crossing estimators (see Table 3-5-6, Fig. 3-5-6).
Importance sampling ..	Russian Roulette kill and survival (see Table 3-5-7). Source energy biasing. Exponential transform (see Table 3-5-7).
Histories .....	10,000 for 1 ~ 21 group analysis. 20,000 for 1 ~ 8 group analysis.

Table 3-5-6 Detectors of Monte Carlo calculation for the IHX room

(1) Point detectors

No.	Coordinate (cm)			Comment
	X	Y	Z	
1	190.7	269.9	150.0	} 1 cm away from the source (front of the B <sub>4</sub> C shield)
2	225.7	209.3	150.0	
3	113.83	185.1	150.0	110 cm away from the B <sub>4</sub> C shield
4	82.03	94.27	150.0	Surface of IHX (r=125 cm, front)
5	-82.03	-94.27	150.0	Surface of IHX (r=125 cm, back)
6	9.13	124.67	150.0	Surface of IHX (r=125 cm)
7	94.27	-83.03	150.0	Surface of IHX (r=125 cm, 90 deg. from No.4)
8	-94.27	82.03	150.0	Surface of IHX (r=125 cm, 90 deg. from No.5)
9	82.03	94.27	1.0	Surface of IHX (r=125 cm, near floor)
10	82.03	94.27	299.0	Surface of IHX (r=125 cm, near ceiling)

(2) Next event surface crossing estimators

No.	Ring center (cm)			Direction cosine			Radius (cm)		Comment
	X	Y	Z	U	V	W	Inner	Outer	
11	208.2	239.6	150.0	-0.8660	-0.5000	0.0	0.0	70.0	1 cm away from the source

No.	Rhomboid range (cm)						Comment
	X(-)	X(+)	Y(-)	Y(+)	Z(-)	Z(+)	
12	296.0	296.0	-35.0	65.0	0.0	90.0	Outlet to the pump room
13	296.0	296.0	-35.0	65.0	90.0	180.0	Outlet to the pump room
14	396.0	396.0	-35.0	65.0	0.0	90.0	Outlet to the pump room
15	396.0	396.0	-35.0	65.0	90.0	180.0	Outlet to the pump room

Table 3-5-6 (continued)

(3) Boundary crossing estimators

No.	Region number		Comment
	from	to	
16	1	6	Surface of thermal insulation of IHX
17	6	7	Surface of IHX (r=95 cm, upper)
18	6	8	Surface of IHX (r=95 cm, lower)
19	1	5	Outlet to the pump room

Table 3-5-7 Path stretching and Russian Roulette kill condition of Monte Carlo calculation for the IHX room

Region No.	Direction of path stretching <sup>1)</sup>		Weight of Russian Roulette kill			
	R	Z	1 ~ 4g	5 ~ 8g	9 ~ 15g	16 ~ 21g
1	(no bias)		1.0-7 <sup>2)</sup>	1.0-6	1.0-4	1.0-3
2	_____				_____	
3	_____				_____	
4	_____				_____	
5	(no bias)		1.0-7	1.0-6	1.0-4	1.0-3
6	1.0	0.0	1.0-7	1.0-6	1.0-4	1.0-3
7	1.0	0.0	1.0-7	1.0-6	1.0-4	1.0-3
8	1.0	0.0	1.0-7	1.0-6	1.0-4	1.0-3

N.B. 1) Bias parameter PATH=0.5. See Ref. 10.

2) Read as  $1.0 \times 10^{-7}$ .

Table 3-5-8 Neutron flux and dose rate distribution in the IHX room

TOTAL FLUXES

UNIT RESPONSE FOR ALL GROUPS

FAST NEUTRON FLUENCE ABOVE 0.1 MEV

DETECTOR	FLUX	FSD	MIN	MAX
1	5.3397E+05	.272	3.8878E+05	6.7917E+05
2	3.3314E+05	.257	2.4752E+05	4.1877E+05
3	8.2306E+04	.009	8.1536E+04	8.3076E+04
4	5.1024E+04	.017	5.0144E+04	5.1905E+04
5	4.9682E+03	.047	4.7326E+03	5.2038E+03
6	4.1469E+04	.016	4.0817E+04	4.2121E+04
7	1.5829E+04	.024	1.5453E+04	1.6205E+04
8	2.4446E+04	.018	2.3998E+04	2.4894E+04
9	4.0769E+04	.123	3.5773E+04	4.5766E+04
10	3.5783E+04	.091	3.2539E+04	3.9027E+04
11	5.8758E+05	.031	5.6924E+05	6.0593E+05
12	1.7387E+04	.069	1.6189E+04	1.8585E+04
13	2.1141E+04	.071	1.9636E+04	2.2646E+04
14	3.8987E+03	.123	3.4203E+03	4.3770E+03
15	3.5170E+03	.100	3.1638E+03	3.8703E+03
16	2.0466E+04	.017	2.0127E+04	2.0806E+04
17	1.3548E+04	.038	1.3035E+04	1.4060E+04
18	1.7178E+04	.037	1.6549E+04	1.7808E+04
19	1.8713E+04	.052	1.7747E+04	1.9679E+04

(n/sec/cm<sup>2</sup>)

DETECTOR	FLUX	FSD	MIN	MAX
1	4.8548E+03	.441	2.7146E+03	6.9949E+03
2	2.3366E+03	.244	1.7673E+03	2.9059E+03
3	1.5138E+03	.021	1.4820E+03	1.5457E+03
4	6.6170E+02	.022	6.4708E+02	6.7632E+02
5	1.7348E+01	.032	1.6788E+01	1.7908E+01
6	5.2887E+02	.029	5.1331E+02	5.4442E+02
7	1.5191E+02	.027	1.4780E+02	1.5601E+02
8	2.6032E+02	.025	2.5372E+02	2.6691E+02
9	4.5921E+02	.172	3.8024E+02	5.3817E+02
10	6.1381E+02	.325	4.1445E+02	8.1317E+02
11	4.8705E+03	.037	4.6926E+03	5.0484E+03
12	6.8664E+01	.138	5.9199E+01	7.8128E+01
13	7.1886E+01	.169	5.9735E+01	8.4036E+01
14	9.9341E+00	.127	8.6746E+00	1.1194E+01
15	1.3950E+01	.175	1.1511E+01	1.6390E+01
16	2.0020E+02	.050	1.9022E+02	2.1019E+02
17	1.1523E+02	.077	1.0635E+02	1.2412E+02
18	1.4161E+02	.086	1.2942E+02	1.5380E+02
19	6.7502E+01	.120	5.9393E+01	7.5610E+01

(n/sec/cm<sup>2</sup>)

THERMAL FLUXES

NEUTRON DOSE CONVERSION · 21G MREM/HR

DETECTOR	FLUX	FSD	MIN	MAX
1	6.1307E+04	.078	5.6500E+04	6.6114E+04
2	5.6949E+04	.068	5.3064E+04	6.0834E+04
3	1.6882E+04	.022	1.6515E+04	1.7249E+04
4	1.4627E+04	.038	1.4064E+04	1.5190E+04
5	3.0766E+03	.075	2.8473E+03	3.3059E+03
6	1.2591E+04	.036	1.2140E+04	1.3042E+04
7	5.7800E+03	.050	5.4915E+03	6.0686E+03
8	8.9682E+03	.034	8.6618E+03	9.2745E+03
9	9.5272E+03	.085	8.7209E+03	1.0333E+04
10	1.3498E+04	.223	1.0487E+04	1.6509E+04
11	1.1623E+05	.099	1.0476E+05	1.2770E+05
12	7.2500E+03	.115	6.4168E+03	8.0832E+03
13	7.2893E+03	.136	6.2987E+03	8.2798E+03
14	2.2244E+03	.193	1.7960E+03	2.6528E+03
15	1.7401E+03	.161	1.4601E+03	2.0201E+03
16	7.0239E+03	.024	6.8527E+03	7.1951E+03
17	3.8208E+03	.075	3.5344E+03	4.1072E+03
18	4.4801E+03	.046	4.2757E+03	4.6846E+03
19	6.6648E+03	.089	6.0740E+03	7.2557E+03

(n/sec/cm<sup>2</sup>)

DETECTOR	DOSE RATE	FSD	MIN	MAX
1	3.1633E+03	.258	2.3481E+03	3.9785E+03
2	1.6754E+03	.190	1.3572E+03	1.9936E+03
3	5.2780E+02	.011	5.2213E+02	5.3346E+02
4	2.9738E+02	.016	2.9277E+02	3.0199E+02
5	2.2987E+01	.041	2.2055E+01	2.3919E+01
6	2.4188E+02	.015	2.3822E+02	2.4554E+02
7	8.8541E+01	.019	8.6836E+01	9.0245E+01
8	1.3728E+02	.017	1.3501E+02	1.3955E+02
9	2.2569E+02	.098	2.0347E+02	2.4792E+02
10	2.1277E+02	.076	1.9659E+02	2.2895E+02
11	3.5458E+03	.030	3.4400E+03	3.6516E+03
12	8.2256E+01	.074	7.6188E+01	8.8324E+01
13	1.1570E+02	.082	1.0627E+02	1.2513E+02
14	1.7094E+01	.115	1.5130E+01	1.9058E+01
15	1.7781E+01	.106	1.5891E+01	1.9670E+01
16	1.1511E+02	.021	1.1269E+02	1.1752E+02
17	7.4395E+01	.038	7.1595E+01	7.7195E+01
18	9.1884E+01	.034	8.8724E+01	9.5043E+01
19	9.6077E+01	.059	9.0376E+01	1.0178E+02

(mrem/hour)

Table 3-5-9 Comparison of calculated reaction rate with the measured value in the IHX room

(Unit: reactions/10<sup>24</sup> atom/sec/50MW<sub>t</sub>)

1) Location	<sup>235</sup> U(n,f)				<sup>238</sup> U(n,f)				<sup>232</sup> Th(n,f)			
	Exp.	Calc. <sup>3)</sup> (fsd %)	Relative (Absolute) C/E (C/E)		Exp.	Calc. (fsd %)	Relative (Absolute) C/E (C/E)		Exp.	Calc. (fsd %)	Relative (Absolute) C/E (C/E)	
1	-	9.08+6 (1.8)	—		-	2.89+0 (1.5)	—		-	1.22-1 (2.8)	—	
2	4.42+7 <sup>2)</sup>	1.58+7 (5.9)	1.0 (0.36)		7.91+2	2.43+0 (13)	1.0 (1/330)		2.5+2	8.52-2 (44)	1.0 (1/2900)	
3	1.38+6	1.44+6 (7.1)	2.9 (1.04)		1.8+0	3.24-2 (7.9)	5.9 (1/56)		5-1	4.54-4 (8.2)	2.6 (1/1100)	
4	1.34+7	7.47+6 (3.4)	1.6 (0.56)		6.64+2	1.32+0 (2.6)	0.66 (1/500)		2.0+2	4.91-2 (3.1)	0.71 (1/4100)	

Location	<sup>32</sup> S(n,p) <sup>32</sup> P				<sup>109</sup> Ag(n,γ) <sup>110m</sup> Ag				<sup>181</sup> Ta(n,γ) <sup>182</sup> Ta			
	Exp.	Calc. (fsd %)	Relative (Absolute) C/E (C/E)		Exp.	Calc. (fsd %)	Relative (Absolute) C/E (C/E)		Exp.	Calc. (fsd %)	Relative (Absolute) C/E (C/E)	
1	-	3.23-2 (3.0)	—		5.54+5	5.64+5 (2.7)	0.64 (1.02)		7.01+6	5.59+6 (2.4)	0.73 (0.80)	
2	1.70+1	4.56-2 (62)	1.0 (1/370)		5.42+5	8.64+5 (5.0)	1.0 (1.59)		7.91+6	8.60+6 (6.5)	1.0 (1.09)	
3	-	1.03-4 (20)	—		1.45+4	2.66+4 (4.7)	1.15 (1.83)		1.60+5	2.19+5 (4.3)	1.26 (1.37)	
4	1.42+1	1.25-2 (3.1)	0.34 (1/1100)		2.65+5	3.31+5 (3.1)	0.79 (1.25)		2.44+6	3.21+6 (2.8)	1.21 (1.32)	
5	-	1.33-2 (47)	—		7.41+5	9.59+5 (8.1)	0.81 (1.29)		1.55+7	1.09+7 (16)	0.64 (0.70)	

N.B. 1) See Fig. 2-4-1.

2) Read as 4.42 × 10<sup>7</sup>.

3) Calculated values are multiplied by a factor of 2 to include sodium over-flow duct contribution (except for location 2 and 5).

Table 3-5-10 Comparison of incident current from reactor side with that from primary pump room.

(I) Calculated results from present analyses (nominal value)

- Ⓐ Current from reactor side :  $5.50 \times 10^9$
- Ⓑ Current from primary pump room:  $5.32 \times 10^7$
- Ⓓ Ratio of current ( Ⓐ / Ⓑ ) : 103

(II) Corrected current ratio by C/E

Used reaction	C/E		Ⓗ . Maximum Ratio of C/E ( Ⓕ / Ⓖ )	Ⓘ . Corrected Current ratio <sup>1)</sup> ( Ⓓ / Ⓗ )
	Ⓕ Ar-duct exit	Ⓖ Pump room		
$^{235}\text{U}(n,f)$	0.36	0.039 } 0.110	9.2	11
$^{109}\text{Ag}(n,\gamma)^{110\text{m}}\text{Ag}$	1.59	0.091 } 0.31	17	6.1
$^{181}\text{Ta}(n,\gamma)^{182}\text{Ta}$	1.09	0.097 } 0.33	11	9.4

N.B. 1)  $\text{Ⓘ} = \frac{\text{Ⓓ}}{\text{Ⓗ}} = \frac{5.50 \times 10^9}{5.32 \times 10^7 \times \text{Ⓗ}}$

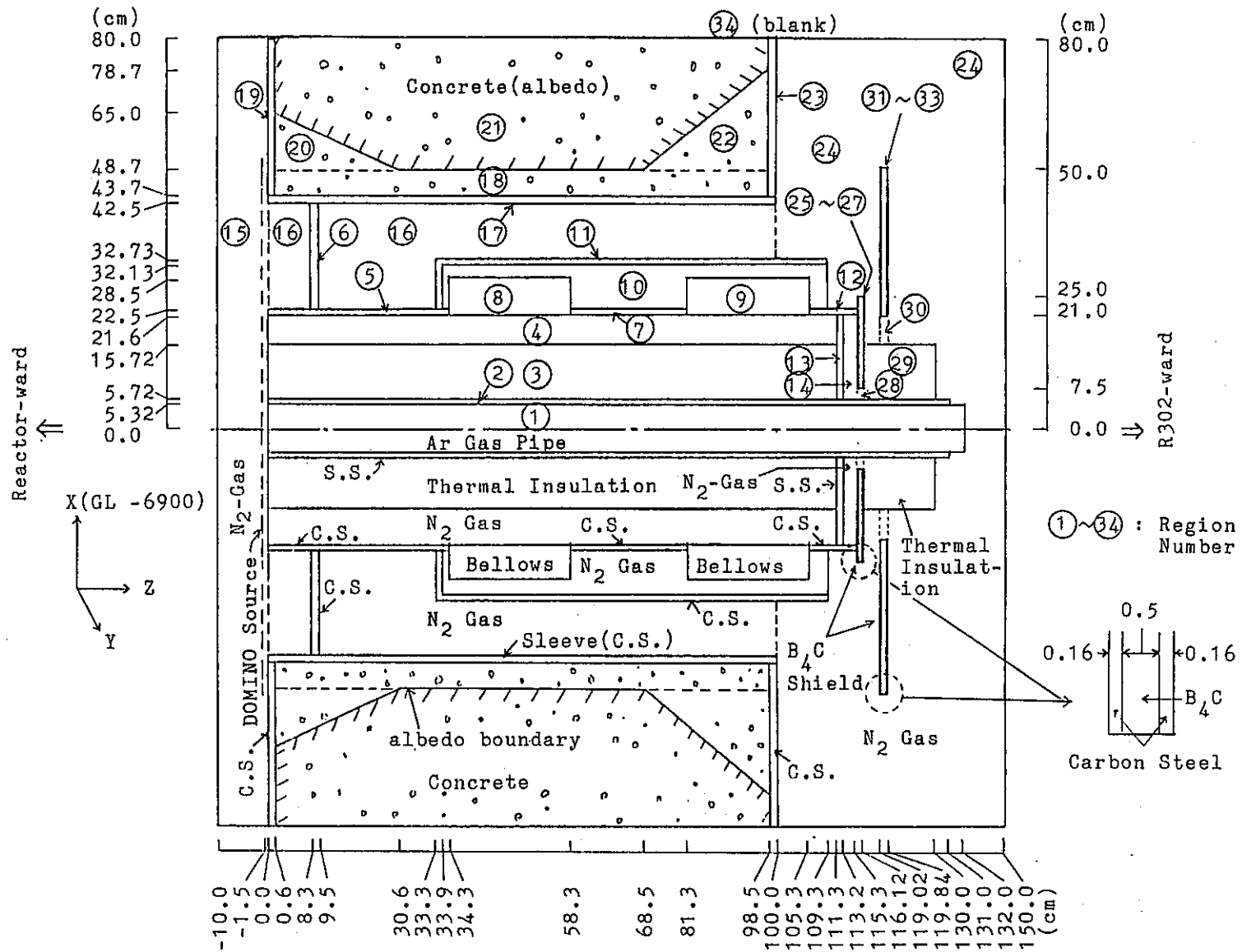


Fig. 3-5-1 Calculational model of argon cover-gas pipe duct.

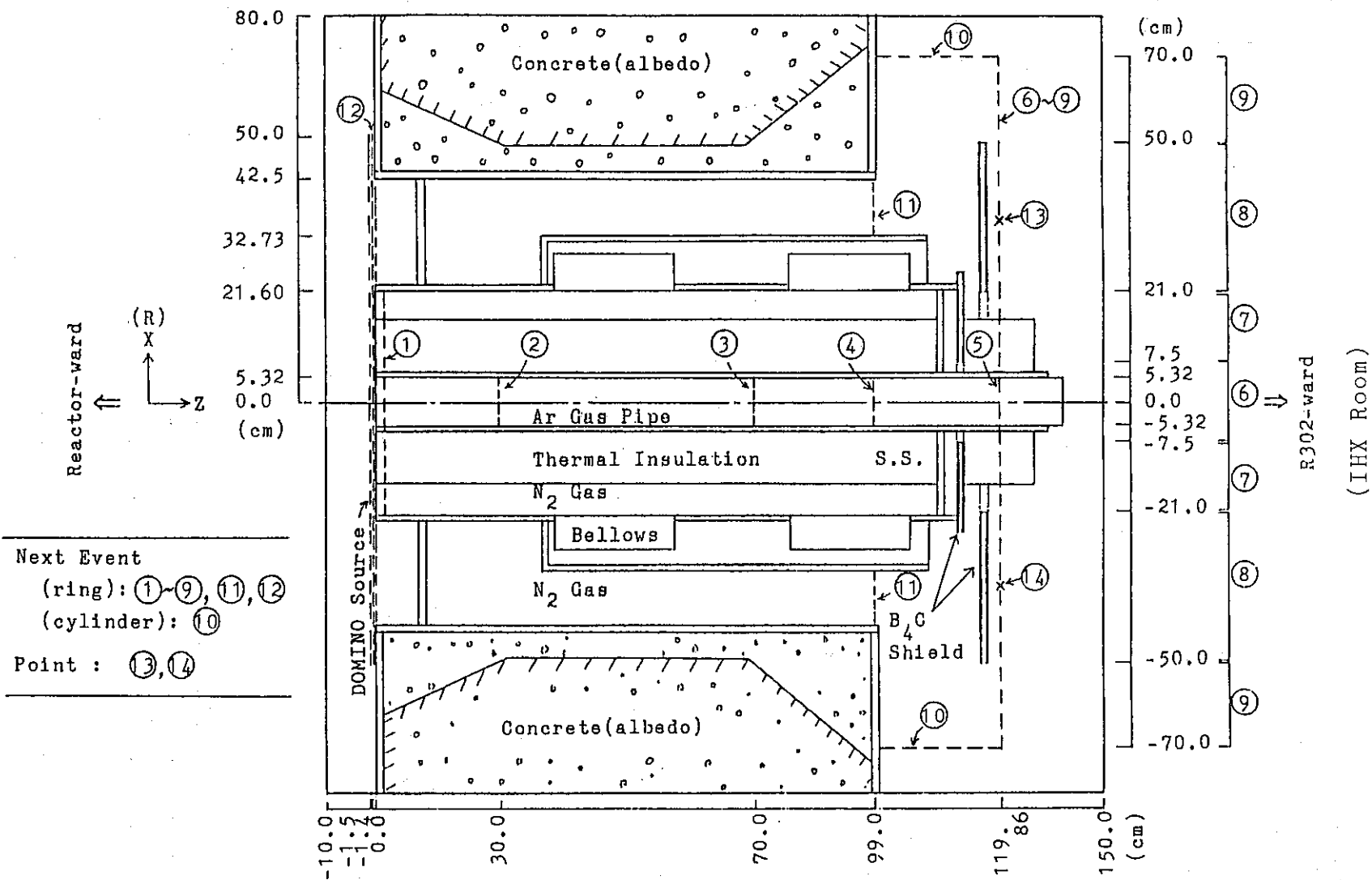


Fig. 3-5-2 Detector locations for neutron streaming calculation through the argon cover-gas duct.



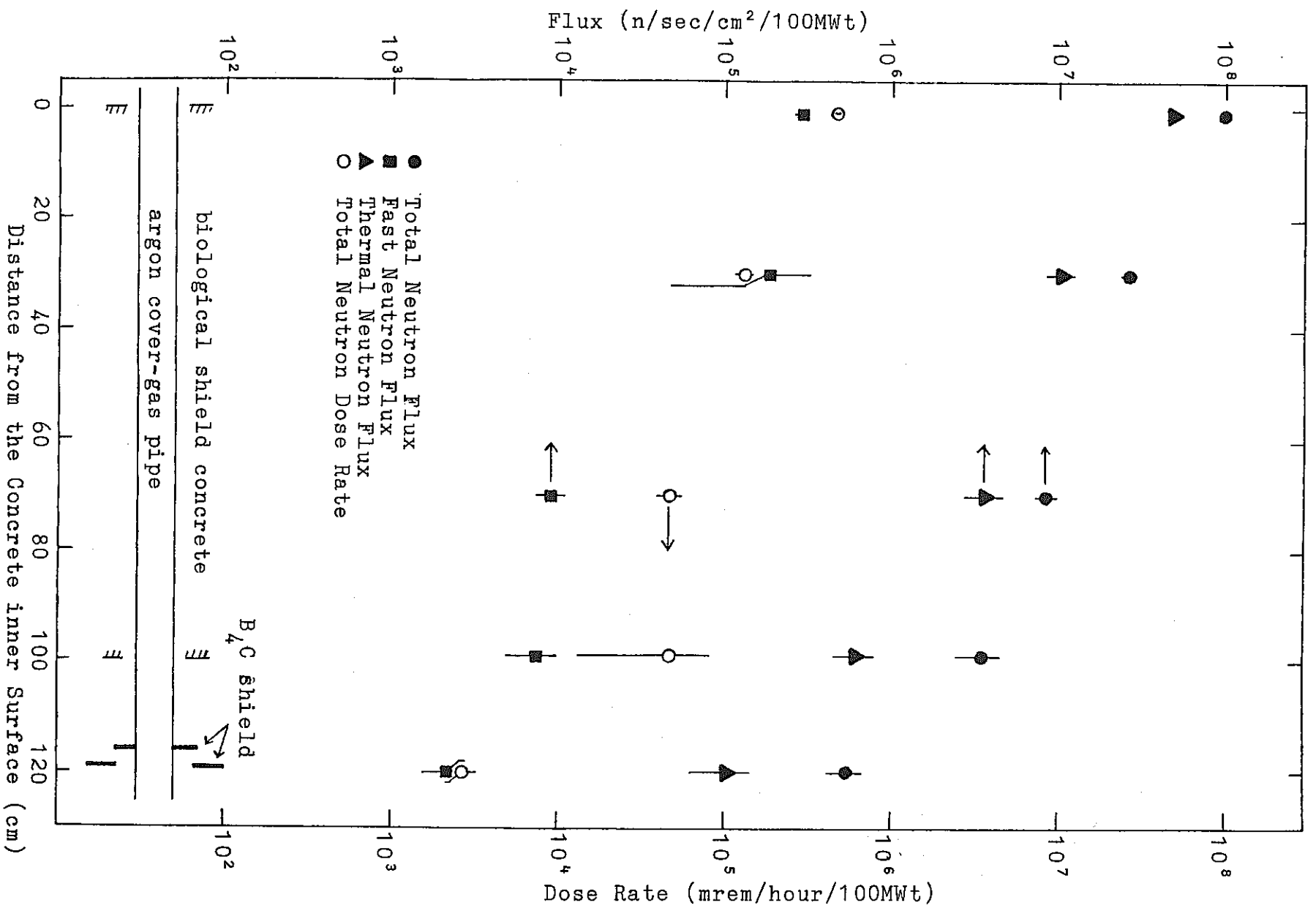


Fig. 3-5-3 Neutron flux and dose rate distribution in the argon cover-gas pipe.  
3-110

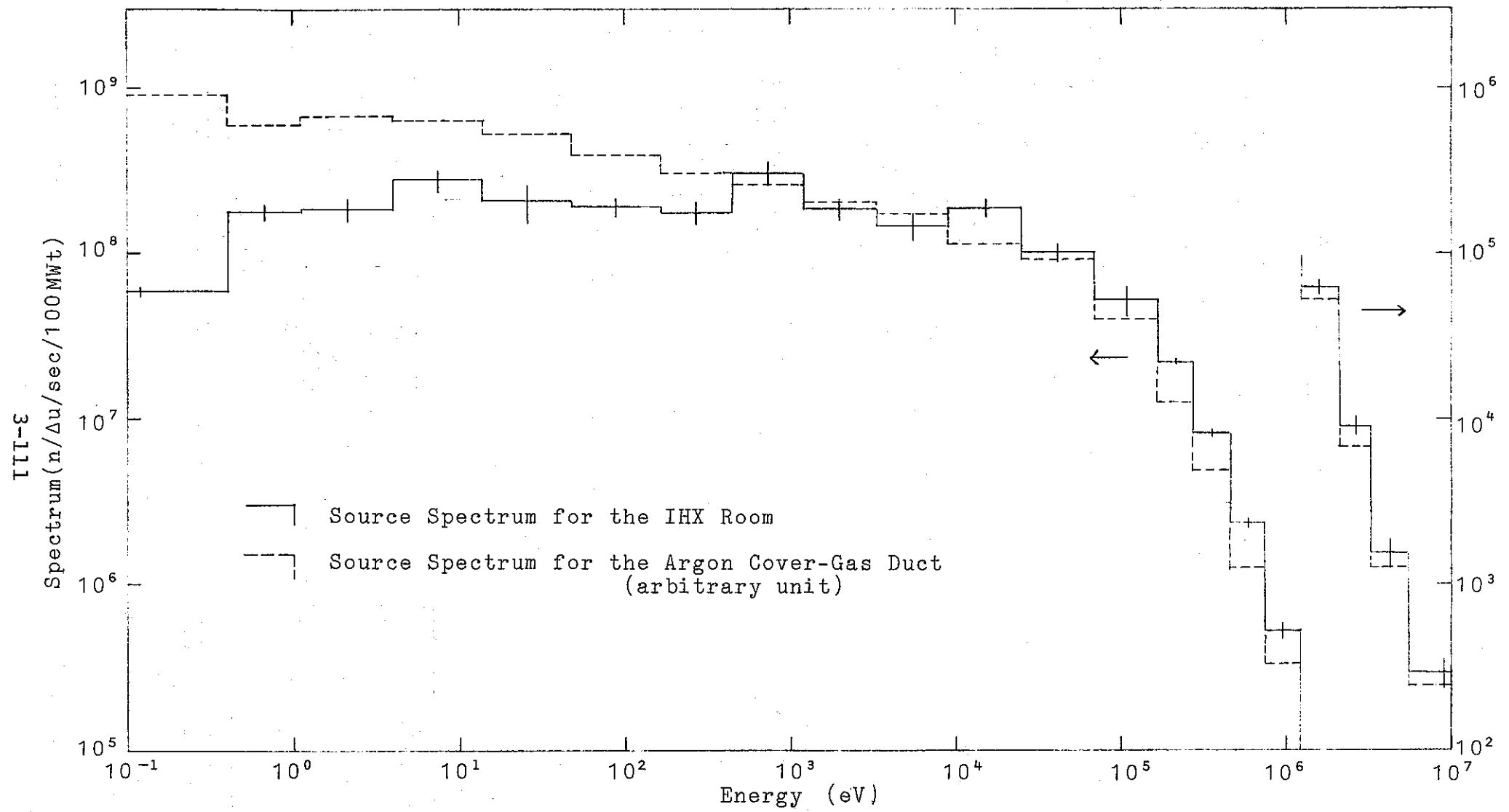


Fig. 3-5-4 Source spectrum for the neutron distribution analysis in the IHX room.

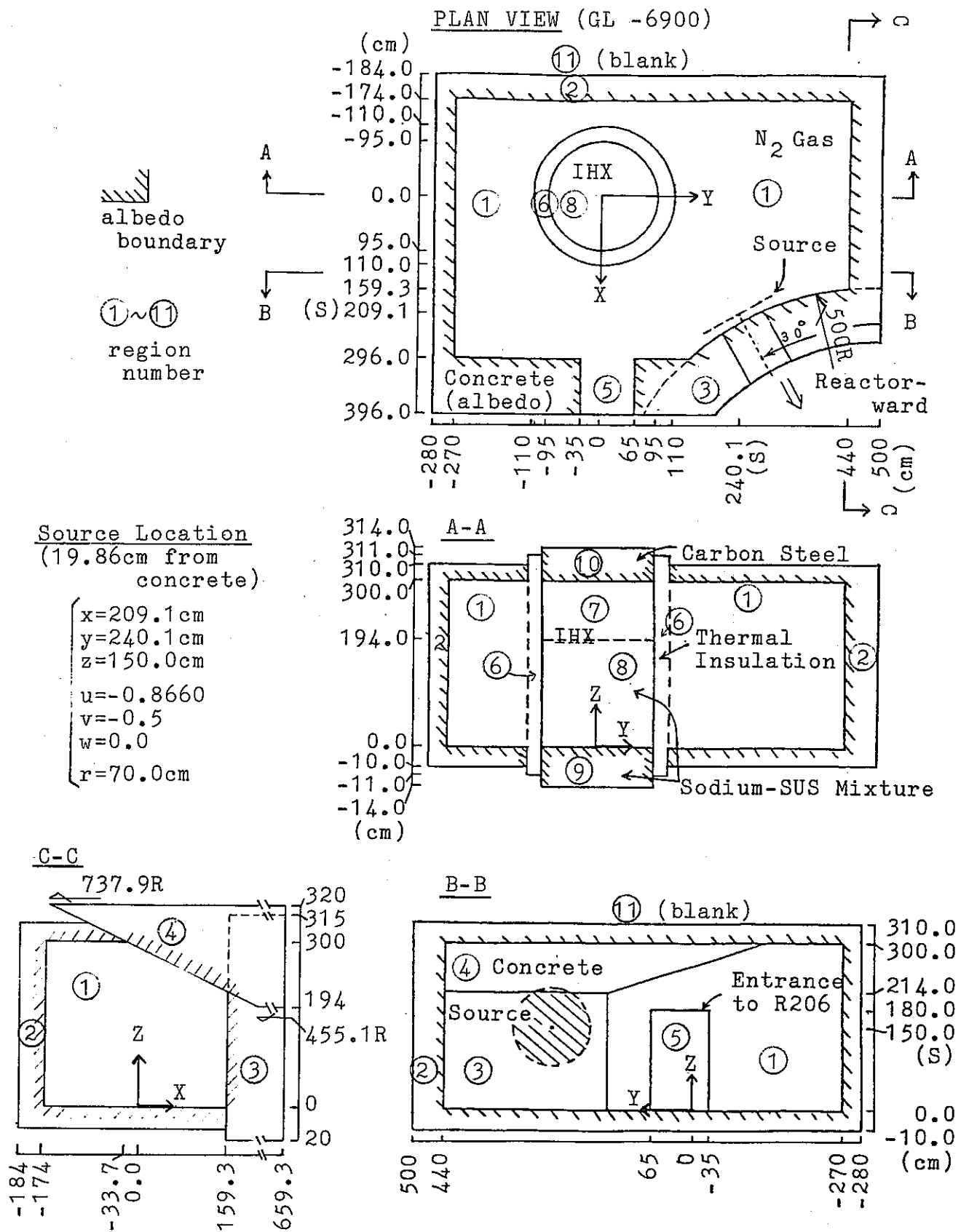
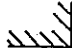
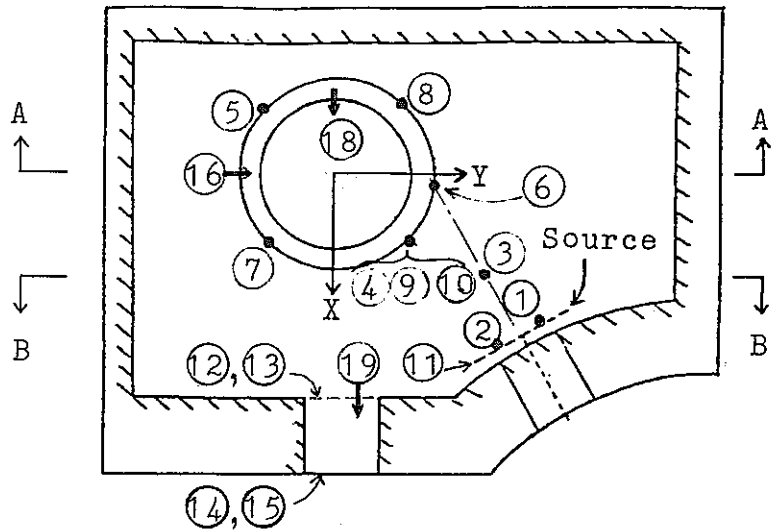


Fig. 3-5-5 Calculational model of the IHX room

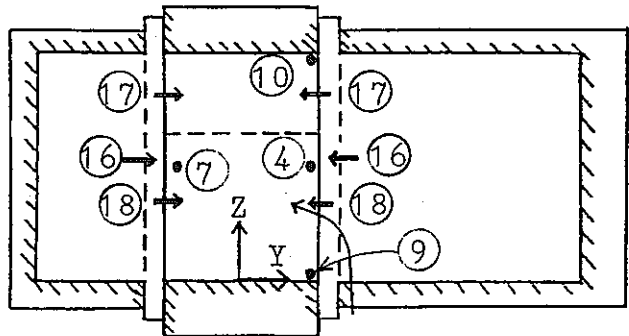
PLAN VIEW (GL -6900)

 albedo boundary



- ①~⑩ : Point
- ⑪ : Ring
- ⑫~⑮ : Rhomboid
- ⑯~⑲ : Boundary

A-A



B-B

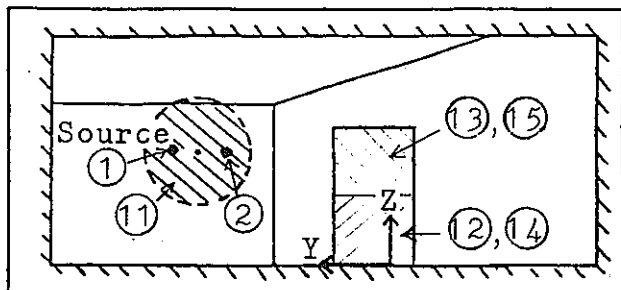


Fig. 3-5-6 Detector locations for neutron distribution analysis in the IHX room.

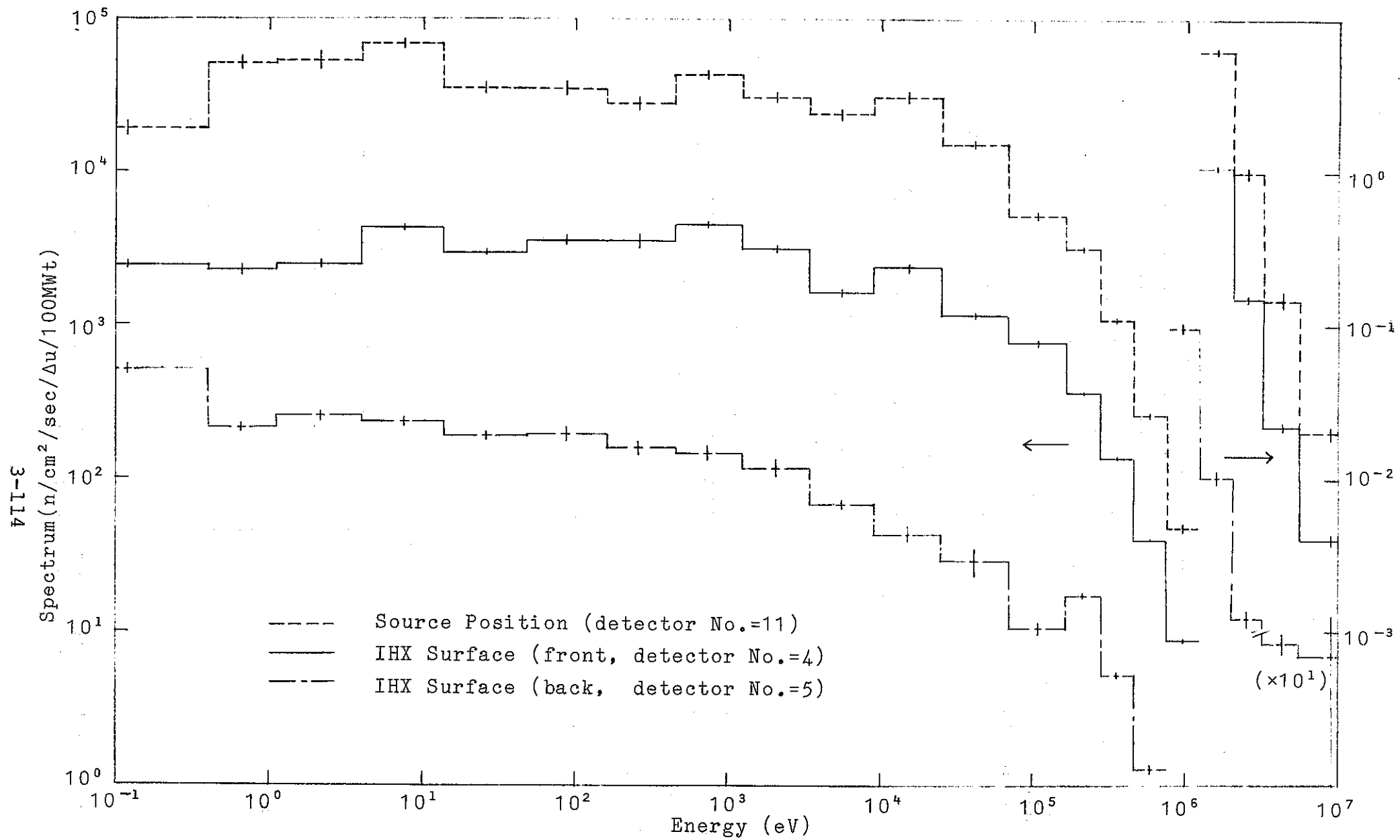


Fig. 3-5-7 Neutron spectrum at the source and IHX surface( $r=125cm$ ).

Energy C/E	Low Energy Range				Overall Energy Range				Fast Energy Range					
	1/2	1	2	4	1/2	1	2	4	1/4	1/2	1	2	4	8
Detector location														
2. Source Position (right)														
5. Source Position (left)														
1. Intermediate Position of Source-IHX														
4. IHX Surface(front)														
3. IHX Surface(back)														
Reaction	○ $^{109}\text{Ag}(n, \gamma)^{110\text{m}}\text{Ag}$ △ $^{181}\text{Ta}(n, \gamma)^{182}\text{Ta}$				$^{235}\text{U}(n, f)$				○ $^{232}\text{Th}(n, f)$ △ $^{238}\text{U}(n, f)$ × $^{32}\text{S}(n, p)^{32}\text{P}$					

Fig. 3-5-8 C/E values for various reactions at several locations in the IHX room.

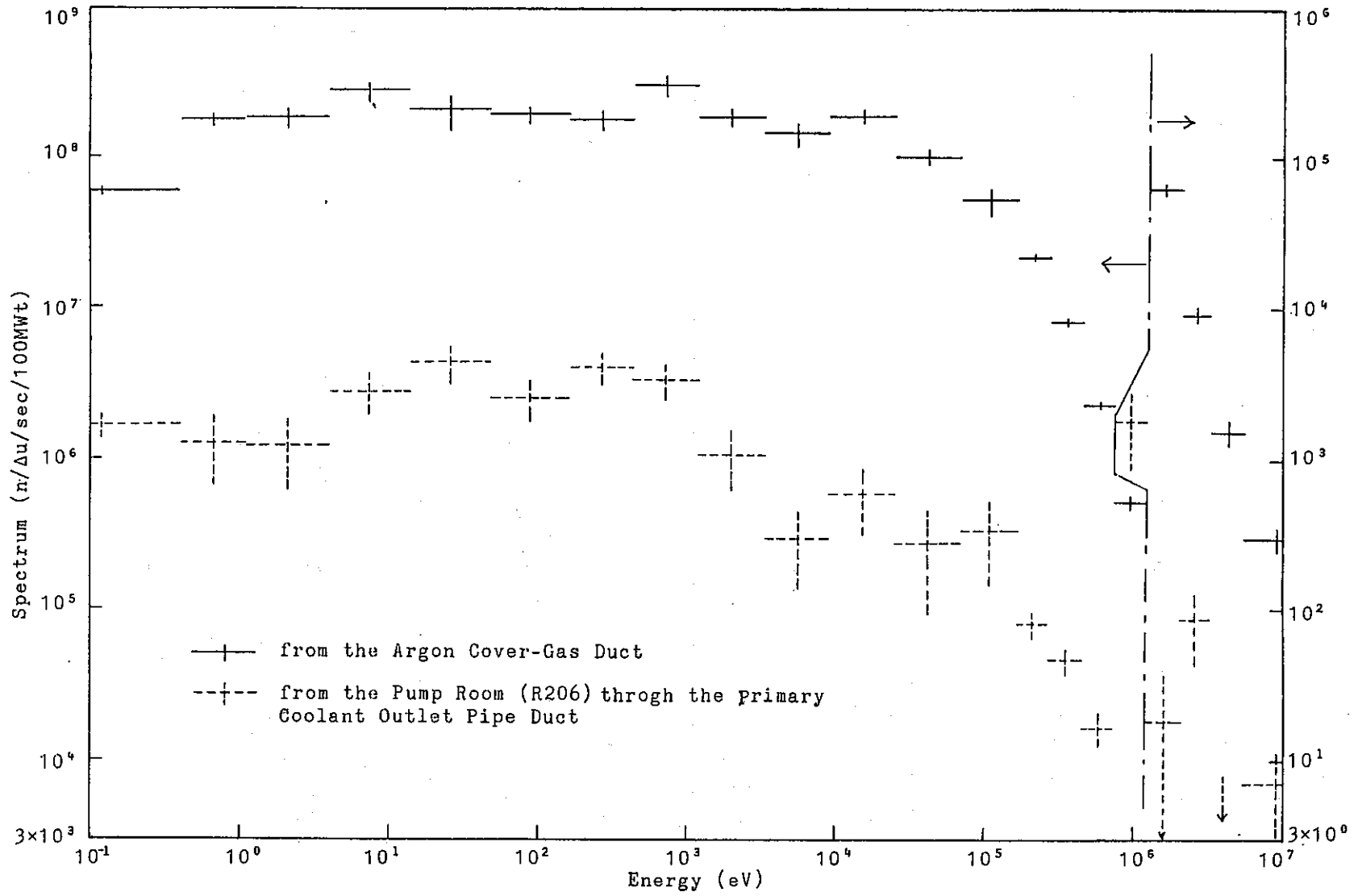


Fig. 3-5-9 Neutron spectra flowing into the IHX room.

### 3.6 Discussion

Albedo Monte Carlo calculation was performed, on the basis of the results obtained by the 2 dimensional Sn transport calculation<sup>1,2)</sup> for in-vessel and enclosure shield system of "JOYO". As compared with the experimental data<sup>2,4-6)</sup> concerning the neutron streaming, the absolute C/E values of reaction rate for intermediate energy and slow neutron show a factor of 4 in the Channel A, 0.4 - 1.8 in the IHX room, 1/20 - 1/5 in the penetration for the primary coolant pipe, and 1/25 - 1/3 in the primary pump room, respectively. It should be noted that the penetration for the primary coolant pipe is followed by the primary pump room and that the C/E values for the former and for the latter are nearly equal. Accordingly, it is considered that the present albedo Monte Carlo calculation well described the neutron streaming.

On the other hand, absolute C/E values for threshold detector reactions such as  $^{238}\text{U}(n,f)$  measured in the primary pump room and the IHX room were remarkably underestimated as described in Sections 3.4 and 3.5. The measured reaction rates are as large as, or even larger than the values calculated from neutron flux obtained at the reactor side mouth of the penetration that lead to the pump room or the IHX room. This suggests that some problems exists with respect to the source used in the albedo Monte Carlo calculation and they should be especially focused on the fast neutron spectrum.



The C/E values of reaction rates for intermediate energy and slow neutrons decrease according as the order of Channel A, IHX room, primary coolant pipe penetration and primary pump room. As described in the section 3.5, the principal neutron source for the IHX room is made by the penetration for argon cover gas pipe and overflowed sodium pipe 30 cm upper of the primary coolant pipe penetration. The trend observed in the above C/E values must be deeply related to the height of the penetration location and the height of the top of the graphite shield. The relative location is shown in Fig. 3-0-2, and it is understood that the source for Channel A seemed to be reasonable as the Channel A is open to the cavity above the graphite shield. On the other hand, the center line of the penetrations for argon cover gas and primary coolant pipes are 20 cm and 50 cm lower than the top of the graphite shield respectively. Especially, since the primary pipe has a large diameter of 50 cm and is surrounded by thick insulator, the hollow in the graphite shield is fairly large. Lots of neutrons stream through the hollow from the core, but the streaming effect was not taken into account in the present work. That is why calculational results became much lower. The neutron streaming through the hollow has the larger effect on fast neutrons at the mouth of the penetration.

Neutrons coming directly from the reactor to the IHX room through the argon cover gas and the overflowed sodium pipe penetration were larger by an order of magnitude than the

contribution from the other penetrations in the IHX room, as described in Section 3.6.

It is difficult problem to evaluate the neutron flux near the duct mouth as noted in the above discussions. However, the applicability of the albedo Monte Carlo method can be studied sufficiently through the relative C/E values which are not likely influenced by an ambiguity of the source used for the calculation. In the following section, the calculational accuracy of the present Monte Carlo method is described with the discussion concerning the distribution of relative values.

### 3.7 Summary of Streaming Analyses by Albedo Monte Carlo Method

The shielding performance data<sup>2,4 ~6)</sup> concerning neutron streaming in JOYO were analyzed by the albedo Monte Carlo method.<sup>7 ~11)</sup>

The computing time for each case is shown as follows:

Streaming path	Energy group	C.P.U.Time (histories)	Computer system
Channel A in Pedestal	1 - 2lg	13 min. (5,000)	CYBER 176
Primary Coolant Outlet	1 - 2lg	73 min. (7,500)	FACOM M200
Pipe Penetration	1 - 8g	48 min. (20,000)	FACOM M200
Primary Pump Room	1 - 2lg	76 min. (8,000)	FACOM M190
	1 - 8g	18 min. (20,000)	FACOM M200
Argon Cover Gas Pipe	1 - 2lg	37 min. (15,000)	FACOM M200
Penetration	1 - 8g	13 min. (20,000)	FACOM M200
IHX Room	1 - 2lg	35 min. (10,000)	FACOM M200
	1 - 8g	16 min. (20,000)	FACOM M200

As the neutron sources used for this analysis has an ambiguity, the absolute values of C/E did not always concentrate to 1.0. The values for the intermediate energy and thermal neutron are listed as follows:

Channel A: C/E = 3.2 ~ 9.7

(Sn results without streaming effect: C/E =  $5.6 \times 10^{-3}$  ~ 3.1)

Primary Coolant Pipe Penetration: C/E = 1/20 ~ 1/5

Primary Pump Room : C/E = 1/25 ~ 1/3

IHX Room : C/E = 0.4 ~ 1.8

In the Channel A, the neutron streaming effect through the detector guide tube was very high. The present albedo Monte Carlo method estimated well the effect, which the two-dimensional Sn calculation<sup>1,2)</sup> did not estimate well.

It should be noticed that the absolute C/E values in the primary coolant pipe penetration are similar to those in the primary pump room where the streaming neutrons through the former make a source of the latter. This result means that the present albedo Monte Carlo method could describe well the neutron behaviours in the primary coolant pipe penetration and the primary pump room.

The C/E values were normalized to those near the neutron source for each streaming path in order to eliminate the ambiguity in the neutron source and the results are listed in Tables 3-7-1 through 3-7-3.

The relative C/E values are summarized as follows:  
For thermal and intermediate energy neutron ,

Streaming path	Relative C/E	Quantities
Channel A	0.77 ~ 2.65	Thermal neutron flux, $^{10}\text{B}(n,\gamma)$
Primary coolant pipe penetration	0.53 ~ 1.61	Thermal neutron flux, $^{197}\text{Au}(n,\gamma)$ $^{50}\text{Cr}(n,\gamma)$ , $^{58}\text{Fe}(n,\gamma)$ $^{59}\text{Co}(n,\gamma)$ , $^{123}\text{Sb}(n,\gamma)$
Primary pump room	0.76 ~ 3.0	$^{109}\text{Ag}(n,\gamma)$ , $^{181}\text{Ta}(n,\gamma)$
IHX room	0.64 ~ 1.26	$^{109}\text{Ag}(n,\gamma)$ , $^{181}\text{Ta}(n,\gamma)$

It is found from the present results that the albedo Monte Carlo method could describe the slow-neutron streaming through each path with accuracy within a factor of 2.

For the  $^{235}\text{U}$  fission rate which has response to the neutrons in the wide energy region, the normalized C/E values were obtained as follows:

---

Channel A : C/E = 0.45 (Normalized to the Sn result  
at the core mid-plane)

Primary pump room: C/E = 1.00 ~ 2.8 (Normalized to the value  
at the duct mouth)

IHX room : C/E = 1.00 ~ 2.9 (ditto)

---

Besides, the threshold reaction rates of  $^{238}\text{U}(n,f)$ ,  $^{232}\text{Th}(n,f)$  and  $^{32}\text{S}(n,p)$   $^{32}\text{P}$  were measured in the primary pump room and the IHX room and were estimated within a factor of 6 as follows:

---

Primary pump room : C/E = 0.72 ~ 4.3 (Normalized to the value at the  
duct mouth)

IHX room : C/E = 0.66 ~ 5.9 (ditto)

---

An agreement of threshold reaction rate between the calculation and the experiments was worse than those of capture rates and  $^{235}\text{U}$  fission rate. The neglect of sodium pipe in the calculational model for the primary pump and the IHX room must have made neutron flux overestimated at the position shaded by the pipe in the room. The shield effect of the pipe upon the threshold reaction seems to be larger, and it is the first reason. Another reason is the difference of the source

neutron spectrum between the calculation and the actual one. Consequently, the better modeling and source distribution must improve the agreements between the calculations and the experiments. The remaining problems are the uncertainties of the group constants and the differential albedo data.

It can be summarized that the present albedo Monte Carlo method can evaluate the neutron streaming through penetrations and the behaviours in the vacancy with accuracy within a factor of 2 ~ 3.

Table 3-7-1 Summary of C/E values in the Channel A

Position <sup>1)</sup> (cm)	Normalized C/E values (Sn results)			
	$\phi_{th}$ by $^{10}\text{B}(n,\alpha)$	$\phi_{th}$ by TLD	$^{10}\text{B}$ counter	$^{10}\text{B}$ counter (Cd covered)
Core-war				
500 <sup>2)</sup>	1.0 (1.0)	1.0 (1.0)	1.0	1.0
550	0.77 (4.7-2) <sup>3)</sup>	—	0.91	1.63
600	0.95 (9.1-3)	1.46 (1.43-3)	1.17	2.56
650	2.00 (1.76-3)	—	2.65	4.71

N.B. 1) Distance from the bottom of the pedestal through the channel.

2) Normalization point.

3) Read as  $4.7 \times 10^{-2}$ .

Table 3-7-2 Summary of C/E values in the primary coolant pipe duct

Position <sup>1)</sup> (cm)	Normalized C/E values							
	$\phi_{\text{thermal}}$	$^{197}\text{Au}(n,\gamma)$	$^{197}\text{Au}(n,\gamma)/\text{Cd}$	Cd ratio(Au) <sup>3)</sup>	$^{50}\text{Cr}(n,\gamma)$	$^{58}\text{Fe}(n,\gamma)$	$^{59}\text{Co}(n,\gamma)$	$^{123}\text{Sb}(n,\gamma)$
Core-ward								
-120	0.71	0.81	0.92	1.18	0.54	0.53	0.54	0.57
-100 <sup>2)</sup>	1.00	1.00	1.00	1.14	1.00	1.00	1.00	1.00
-80	1.05	1.61	2.2	0.99	1.24	1.23	1.23	1.53
-60	0.73	1.39	2.1	0.89	0.90	0.90	1.04	1.23
-40	0.63	0.91	1.17	1.04	0.60	0.63	0.73	0.90
-20	0.80	1.61	2.4	0.91	0.94	0.88	0.83	0.83
-10	-	-	-	0.94	0.98	0.98	0.91	1.64

N.B. 1) Distance from the outer surface of B<sub>4</sub>C shield.

2) Normalization point.

3) Unnormalized C/E.



Table 3-7-3 Summary of C/E values in the pump room and the IHX room

Detector position		Normalized C/E values					
		$^{235}\text{U}(n,f)$	$^{238}\text{U}(n,f)$	$^{232}\text{Th}(n,f)$	$^{32}\text{S}(n,p)$ $^{32}\text{S}$	$^{109}\text{Ag}(n,\gamma)$ $^{110m}\text{Ag}$	$^{181}\text{Ta}(n,\gamma)$ $^{182}\text{Ta}$
In the pump room	1. Source position (upper surface of pipe)	1.0	1.0	1.0	1.0	1.0	1.0
	2. Source position (lower surface of pipe) <sup>1)</sup>	1.69	4.0	0.72	1.19	1.33	1.32
	3. Main pump surface	2.6	2.5	2.5	-	2.6	2.5, 3.0
	7. On the top of FFD/DN	1.10	2.8	1.61	-	0.76	0.87
	8. At the side of FFD/DN	2.8	4.3	3.8	-	-	-
	9. 70 cm from source toward pump	-	-	-	-	2.2	2.2
In the IHX room	1. 110 cm from source toward IHX	-	-	-	-	0.64	0.73
	2. Source position (right-hand of pipe) <sup>1)</sup>	1.00	1.00	1.00	1.00	1.00	1.00
	3. Back of IHX	2.89	5.89	2.64	-	1.15	1.26
	4. Front of IHX	1.56	0.66	0.71	0.34	0.79	1.21
	5. Source position (left-hand of pipe)	-	-	-	-	0.81	0.64

N.B. 1) Normalization point

#### 4. CONCLUSION

In the analyses<sup>1,2)</sup> on the in-vessel and enclosure shield system of JOYO formerly conducted as a part of activities of the Specialists' Committee on Shielding Calculation, it was cleared that the shielding measurement data taken in the head access area could be estimated by the two dimensional Sn transport calculation with accuracy within an order of magnitude.

In the present work, analyzed by the albedo Monte Carlo method<sup>7-11)</sup> were the following subjects:

- (1) the effect upon the measured neutron reaction rates of detector guide tube through the "JOYO" pedestal (Channel A) that was left to be a problem in the former analyses.
- (2) the neutron behaviour in the primary coolant pipe penetration, in the primary pump room, in the argon cover gas pipe penetration from the reactor vessel to the IHX room, and in the IHX room.
- (3) comparison of the calculated reaction rates in the cavities mentioned above with the measured data, all of which had been left unanalyzed.

Group constants used in the calculation were obtained by collapsing 100-group neutron effective macroscopic cross sections into 21 groups. The cross sections were made by RADHEAT-V3.5 code system<sup>15)</sup> from ENDF/B-IV and include scattering kernels up to P<sub>5</sub>. Differential Albedo data of the

concrete covered with liner was calculated by one dimensional Sn transport code ANISN-N<sup>7)</sup> (revised version of ANISN in NAIG), and the other albedo data for single layer were obtained by SLDN code<sup>8,9)</sup> based on the one dimensional invariant imbedding method. The source for the Monte Carlo calculation through the penetration of the biological shielding concrete was obtained by DOMINO code<sup>13)</sup> (revised version<sup>10)</sup> in NAIG) based on the result of the two-dimensional Sn transport calculation<sup>1,2)</sup> conducted in the committee. Sources for the calculation in the primary pump room and IHX room were calculated on the basis of the Monte Carlo calculation results through the penetration in the biological shielding concrete. That is to say, the former is the Sn - Monte Carlo coupling method, and the latter is the Monte Carlo - Monte Carlo coupling method. Though the statistical error is included in the source distribution of the latter, the propagation of the error was neglected. As for importance sampling, source energy biasing, path length stretching by exponential transformation, and Russian Roulette kill and survival were used. The Monte Carlo calculation for fast neutrons down to 8th group (above 165 keV) was carried out as well as the calculation for overall energy groups.

The calculational result was compared with the measured data<sup>2,4~6)</sup>, and the following relative C/E values of the reaction rates were obtained for intermediate energy and slow neutrons taking off the uncertainty of the source used for the present calculation:

Channel A .....	0.8 ~ 2.7
(underestimated by 3 orders of magnitude in Sn calculation <sup>1,2</sup> )	
Penetration for the primary coolant outlet pipe .....	0.53 ~ 2.4
Primary pump room .....	0.76 ~ 3.0
IHX room .....	0.64 ~ 1.26

The reaction rate of  $^{235}\text{U}(n,f)$  of which cross section is fairly high in extensive energy range from thermal through fast region were measured in Channel A, primary pump room, and IHX room. Calculated values agreed with measured values within a factor of 3 as follows:

Channel A .....	2.0
Primary pump room .....	1.00 ~ 2.8
IHX room .....	1.00 ~ 2.9

Following result was obtained as to C/E values of threshold detector reactions for fast neutrons:

Primary pump room .....	0.72 ~ 4.3
IHX room .....	0.66 ~ 5.9

Fast neutrons are likely to be scattered and shielded by sodium pipe and structural materials. In the present analysis, the primary pump, the FFD/DN detector, and the IHX having large volume were taken into account, but the sodium pipes connecting those installations were neglected. The neglect must have increased the discrepancy between calculated and measured

values. In addition, uncertainty in the source spectra used for the present calculation might have increased the discrepancy. However, the discrepancy must be of the kind to be reduced, provided both systems mentioned above are modeled exactly.

In the present analysis, it was confirmed that albedo Monte Carlo method could generally estimate the shielding data concerning the neutron streaming within a factor of 3. It turned out that the neutron streaming through the hollow in the uppermost part of the graphite shielding for the primary coolant pipe and argon cover gas pipe has fairly large influence upon the analysis.

## Acknowledgement

The authors wish to highly appreciate N. Ohtani of FBR Reactor Physics Section, Power Reactor and Nuclear Fuel Development Corporation (PNC) for his fruitful discussions and advices regarding the Monte Carlo calculation.

They are also grateful to S. Suzuki of "JOYO", O-arai Engineering Center of PNC for the presentation of "JOYO" shield performance as well as a lot of data and suggestions to device the calculational model. The aid by M. Sasaki of the same section to use the computer should be appreciated as well.

## References

- 1) PNC Specialists' Committee for Shielding Calculation  
"Radiation Shielding Analyses of JOYO" (in Japanese),  
SN253 79-02 (July, 1979)
- 2) PNC, Toshiba, Hitachi, MAPI, KHI,  
"Radiation Shielding Analyses of JOYO",  
SN241 81-29 (November, 1981)
- 3) W.E. Ford, III, "The POPOP4 Library of Neutron-Induced  
Secondary Gamma-Ray Yield and Cross Section Data." CTC-42.  
(September, 1970)/RSIC DLC-12.
- 4) Y.Sekiguchi, S.Suzuki, M.Kawashima et al.: "Start-up Test  
of Experimental Fast Reactor "JOYO", Shielding Test (ST-11)"  
(in Japanese), PNC Report N941 80-179 (October, 1980)
- 5) Y.Sekiguchi, S.Suzuki, M.Kawashima et al., "Start-up Test  
of Experimental Fast Reactor "JOYO", Shielding Test (ST-21)"  
(in Japanese), PNC Report SN941 79-111 (July, 1979)
- 6) K.Bingo, T.Numakunai and N.Itoh, "Measurement of Neutron  
Dose Rate of Experimental Fast Reactor "JOYO" (in Japanese),  
JAERI-memo 8052 (January, 1979)

- 7) M. Kawai, M.Yamauchi, I.Komatsu and Y.Sato,  
"A Study on Method for the Calculation of Neutron Streaming through a Sodium Duct in Shielding Materials" (in Japanese), PNC Report SJ201 76-06 (March, 1976).
- 8) M.Kawai, M.Yamauchi, I.Komatsu and Y.Sato,  
"A Study on Method for the Calculation of Neutron Streaming through a Sodium Duct in Shielding Materials (II)" (in Japanese), PNC Report SJ201 77-22 (February, 1977).
- 9) M.Kawai, M.Yamauchi, H.Kadotani, and I.Suzuki,  
"A Study of Applicability of an Albedo Monte Carlo Method for Neutron Streaming Calculation", Proc. of Fifth Int. Conf. on Reactor Shielding, Knoxville, P.636 (April, 1977).
- 10) M.Kawai, Y.Hayashida and M.Nakai, "Improvement of Streaming Analysis Technique with Monte Carlo Method" (in Japanese), PNC Report SJ201 79-09 (February, 1979).
- 11) M.Kawai, Y.Hayashida and M.Nakai, "Development of Neutron Streaming Calculation Technique with Adjoint Monte Carlo Method" (in Japanese), PNC Report SJ201 81-02 (February, 1981).
- 12) W.A.Rhodes, "DOT-3.5, Two Dimensional Discrete Ordinates Radiation Transport Code", RSIC CCC-276 (July, 1975).



- 13) M.B.Emmett, C.E.Burgart and T.J.Hoffman, "DOMINO-A General Purpose Code for Coupling Discrete Ordinates and Monte Carlo Radiation Transport Calculations", ORNL-4853 (1973).
- 14) O.Kawaguchi, H.Yokobori, Z.Suzuki, K.Tada and T.Kawakita, "Supplement to Analyses of Radiation shielding Analyses of JOYO-(B)", SJ206 82-06 (February, 1982).
- 15) K.Koyama, K.Minami, Y.Taji and S.Miyasaka, "RADHEAT-V3, A Code System for Generating Coupled Neutron and Gamma-Ray Group Constants and Analyzing Radiation Transport", JAERI-M 7155 (1977); K.Koyama (Private Communication)
- 16) K.Koyama, Y.Okumura, K.Furuta and S.Miyasaka, "Multi-Group Cross Section Sets for Shielding Materials-100 Neutron Groups and 20 Gamma-Ray Groups in  $P_5$  Approximation" (in Japanese), JAERI-M 6978 (January, 1977).
- 17) E.A.Straker, W.H.Scott, Jr. and N.R.Bynn, "The MORSE Code with Combinatory Geometry", DNA 2860T (May, 1972).